Resources Needed for Entangling Two Qubits through an Intermediate Mesoscopic System

by

Maryam Sadat Mirkamali

A thesis
presented to the University of Waterloo
in fulfillment of the
thesis requirement for the degree of
Doctor of Philosophy
in
Physics

Waterloo, Ontario, Canada, 2019

Examining Committee Membership

The following served on the Examining Committee for this thesis. The decision of the Examining Committee is by majority vote.

External Examiner:	Dr. Michel Pioro-Ladrière Professor, Dép. de physique, Université de Sherbrooke
Supervisor(s):	Dr. David G. Cory Professor, Dept. of Chemistry, University of Waterloo
Internal Member:	Dr. Kevin Resch Professor, Dept. of Physics and Astronomy, University of Waterloo
Internal-External Member:	Dr. Joseph Emerson Associate Professor, Dept. of Applied Mathematics, University of Waterloo
Other Member(s):	Dr. Matteo Mariantoni Assistant Professor, Dept. of Physics and Astronomy, University of Waterloo

Author's Declaration

I hereby declare that I am the sole author of this thesis. This is a true copy of the thesis, including any required final revisions, as accepted by my examiners.

I understand that my thesis may be made electronically available to the public.

Abstract

One of the main challenges in designing large scale quantum processors is connecting separated qubits. In this thesis, we explore new opportunities that mesoscopic many-body systems provide for creating quantum correlation between isolated quantum systems. In particular, we study entangling two non-interacting qubits through an intermediate mesoscopic system consisting of identical two-level systems. Two uncoupled qubits can be entangled either by projectively measuring a joint property of them or by creating an indirect interaction between them. The focus of this thesis is on procedures that are based on joint measurement on the qubits.

We propose a new method for entangling two non-interacting qubits by measuring their parity indirectly through an intermediate mesoscopic system. Indirect joint measurement scheme benefits from coherent magnification of the target qubits' state in the collective state of the mesoscopic system; such that a low-resolution measurement on the mesoscopic system suffices to prepare post-selected entanglement on the target qubits. The protocol is designed to require only global control and course-grained collective measurement of the mesoscopic system along with local interactions between the target qubits and mesoscopic system. A generalization of the method measures the hamming weight of the qubits' state and probabilistically produces an entangled state by post-selecting on hamming weight one. Our technique provides a new design element that can be integrated into quantum processor architectures and quantum measurement devices.

We quantify the resources required for implementing the indirect joint measurement technique when the intermediate mesoscopic system consists of spin-1/2 particles with internal dipolar coupling. A mesoscopic spin system consisting of two non-interacting halves, each coupled to one of the target qubits is proved to provide a helpful geometry that allows implementing the coherent magnification process with experimentally available control tools. We show that the requirements on the amplified state of the target qubits and the mesoscopic spin system perfectly maps to the specifications of micro-macro entanglement between each target qubit and its nearby half of the mesoscopic spin system. In the light of this equivalence, the effects of experimental imperfections are explored; in particular, bipartite entanglement between the target qubits is shown to be robust to imperfect preparation of the mesoscopic spin system. Our analysis provides a new approach for using an intermediate spin system for connecting separated qubits. It also opens a new path in exploring entanglement between microscopic and mesoscopic spin systems.

Acknowledgements

My merciful Lord, All praises truly belong to you.

I would like to express deepest gratitude to my supervisor Dr. David Cory for his guidance and support during my PhD study. His vast knowledge and scientific intuition have always been admirable. I learned a lot from him both on doing research and on properly presenting it to the community. I am also incredibly grateful to Dr. Joseph Emerson for all he taught me on open quantum systems and his insightful comments in the early stages of my project. Special thanks to other members of my PhD advisory committee, Dr. Kevin Resch and Dr. Matteo Mariantoni and to the external examiner of my defence session Dr. Michel Pioro-Ladrière.

I was fortunate to work with brilliant scientists during the course of my PhD. I am especially grateful to Osama Moussa who taught me a lot about the NV lab, both the confocal microscope and the spin control. I would like to thank my past and present colleagues in Cory Group, Madelaine Liddy, Razieh Annabestani, Ian Hincks, Fei Wang, Hamid Reza Mohebbi, Jiahui Chen, Holger Haas, Troy Borneman, Mohamad Niknam, Rahul Deshpande, Dusan Sarenac, Joachim Nsofini, Ivar Taminiau, Andrew Stasiuk, Lane Gunderman, Chris Wood, Chris Granade and Sara Sheldon.

I am incredibly thankful to my parents who always believe in me and encourage me to move forward in my path and who have been the first and the best role models for me. Special thanks to my siblings, parents-in-law and siblings-in-law. Many thanks to my husband and best friend, Mehdi. Thank you for motivating me the most. Thank you for helping me manage family life along with the intense PhD study and research. Thank you for your constant love. Final thanks to our little son, Hossein. The joy you brought to our life can not be measured or described.

Dedication

To my hero uncles, Shahid Mostafa and Shahid Mojtaba

Table of Contents

List of Figures

Chapter 1

Introduction

This thesis explores the use of a mesoscopic system as a tool for creating quantum correlations between separated quantum systems. In particular, we evaluate the resources required for entangling two non-interacting qubits by measuring their joint state through an intermediate mesoscopic ensemble of two-level systems e.g., spin half particles. Our study brings new insights into the opportunities that mesoscopic systems provide for connecting separated quantum systems as well as the challenges on the way.

Following developments in addressing and controlling atomic and molecular scale quantum systems such as dopants in solids [1, 2, 3, 4, 5, 6], a crucial step forward towards a scalable quantum architecture is connecting these localized separated qubits. Mesoscopic systems, that are intermediate size many-body systems with collective quantum characteristics [7, 8, 9, 10, 11, 12, 13], provide natural candidates for this purpose. They are extended in space, interact locally with the separated qubits, and can be integrated into solid-state structures through nano-fabrication techniques.

In this thesis, we study entangling two non-interacting qubits through an intermediate mesoscopic system consisting of many two-level systems that can be controlled and measured collectively and interacts locally with the qubits. A reasonable level of control is collective control of the mesoscopic system, local control over each qubit and local interaction between each qubit and a nearby spin within the mesoscopic system. We evaluate the resources required for creating post-selected entanglement between the target qubits by measuring a joint property of them through the mesoscopic system.

Two main schemes are discussed and the required resources of each are identified. The resources that are examined are the purity of the initial state, size, control and internal

dynamics of the mesoscopic system. The requirements on the measurement and the mesoscopic system's robustness to noise are also discussed. We start with a simple analyzable procedure that enables entangling the qubits by applying two successive high-resolution projective collective measurements on the mesoscopic system including and excluding the two spins that are connected to the target qubits. This approach is discussed in chapter 3. We show that the success of this method solely relies on the power of the projective measurements and there are minimum requirements on the other resources including state preparation, control, size, etc. We build on this analysis by introducing *indirect joint measurement* on the qubits that benefits from amplification of the target qubits' state in the collective states of the mesoscopic system and needs only a low-resolution collective measurement on the mesoscopic system to generate post-selected entanglement on the target qubits. Indirect joint measurement scheme is introduced in chapter 4 and its implementation with a mesoscopic *spin* system consisting of spin half particles with internal magnetic dipole coupling is evaluated in chapter 5. In particular, creating micro-macro entanglement between the target qubits and the mesoscopic spin system is identified as a robust and implementable strategy for amplifying the target qubits' state in the collective magnetization of the mesoscopic spin system. The sensitivity of indirect joint measurement procedure to the experimental imperfections is analyzed; particularly it is proved to be robust to limited initial polarization of the mesoscopic spin system.

This thesis complements the ongoing efforts towards using mesoscopic systems as coherent control elements to connect localized separated qubits. Previous schemes propose generating an *indirect interaction* between the qubits via an intermediate mesoscopic system. It has been proposed to use a mesoscopic conductor to engineer an effective interaction Hamiltonian between two Rydberg atoms [14]. Floating metallic gates [15, 16] and quantum Hall edge states [17, 18] have been suggested for creating an effective interaction Hamiltonian between two otherwise uncoupled quantum dot based qubits. A mesoscopic ferromagnet was considered to mediate interaction between separated spin qubits [19].

Another approach to connecting localized qubits via an intermediate system is *quantum state transfer*. There are extensive theoretical studies in transferring quantum states between separated qubits through a hypothetical 1D spin chain [20, 21, 22, 23, 24, 25, 26, 27, 28, 29]. In Chapter 5, we argue that indirect joint measurement meshes better with the experimentally available resources. It does not require addressing individual spins in the chain or engineering the interaction between them and needs only available dipolar coupling and collective control. It is not restricted to a 1D geometry; in fact, it is expected to respond significantly faster with mesoscopic systems in 2D and 3D structure. Moreover, it is robust to limited polarization of the mesoscopic system's initial state.

It is worth mentioning that the three approaches to connecting non-interacting qubits

through an intermediate many-body system; namely, engineering an indirect interaction capable of performing a CNOT gate, quantum state transfer and entangling by indirect joint measurement, are equivalent up to local operations and classical communications. Bipartite entanglement between separated qubits is equivalent to quantum state transfer because an entangled pair of qubits can be used to transfer a quantum state applying quantum teleportation protocols (1) [30, 31]. On the other hand, two separated qubits can be entangled by first entangling one of them with a nearby ancilla qubit with local operations; then transferring the state of the ancilla to the second qubit through quantum state transfer (2) [20, 32]. A CNOT gate, either direct or indirect, creates maximum entanglement between two qubits given that the control and the target qubits are respectively prepared in an equal superposition state and a polarized state (3). Moreover, quantum state transfer combined with a local CNOT gate provides an indirect CNOT gate between uncoupled qubits (4). Overall, as the schematic graph in figure 1.1 shows, all the three schemes are equivalent up to local operations and classical communications [33].

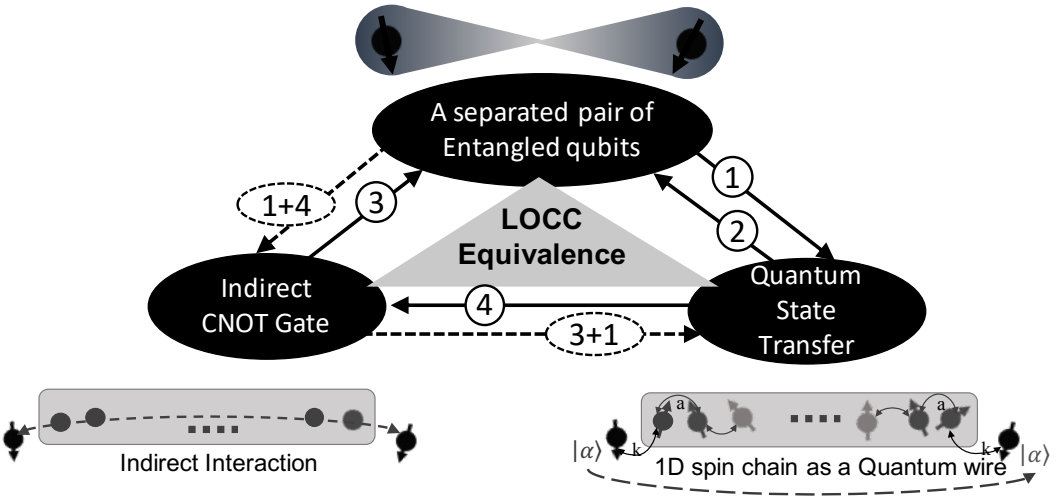

Figure 1.1: The equivalent ways of connecting separated qubits

Studying the many-body dynamics of a mesoscopic system is challenging because full quantum simulation is not possible due to the large size of the Hilbert space and semi-classical methods might not capture all the interesting features. We have different approaches to overcome these challenges. We start with evaluating the collective analyzable dynamics of the mesoscopic system (in chapters 3 and 4), then (in chapter 5) we simulate the full quantum dynamics of a spin system with internal magnetic dipolar interaction

and collective control for small sizes (up to 2×20 spins) based on Krylov approximation method [34]. Consistent collective behaviours are extracted and extrapolated to bigger sizes of the mesoscopic system.

Acknowledgement of Contributions

- Chapter 3 contains results published as a patent in [35] with additional unpublished results of the author.
- Chapter 4 contains results published in [36]. This work was done in collaboration with David G. Cory and Joseph Emerson.
- Chapter 5 contains results of the author that are not published yet.

Chapter 2

Quantum Processes and Entanglement

This chapter gives a short overview of the analysis of quantum processes directed towards their application in the rest of the thesis. Moreover, it provides formal definitions of entangled states and presents measures to quantify bipartite entanglement.

From an operational point of view, quantum processes are divided into three: preparation, transformation, and measurement. The first four sections are devoted to brief mathematical descriptions of these processes. Section 2.1 discusses the representation of quantum states and the preparation process. The transformations of closed and open quantum systems are covered in sections 2.2 and 2.4. The measurement process is discussed in section 2.3. For a more comprehensive review of quantum processes, see [37, 38]. The last section of this chapter, 2.5, reviews multiple measures for quantifying bipartite entanglement, both between two qubits and between one qubit and a mesoscopic system. A thorough survey on entanglement and its measures can be found in reference [39].

2.1 Preparation and Quantum States

2.1.1 Hilbert space and pure states

Any quantum system is associated with a *Hilbert space*, $\mathcal{H}$, that is a complex vector space with an inner product and is complete in the norm. A preparation procedure is ideally

described by a *pure state* which can be represented by a unit vector, called a *state vector*, in the system's Hilbert space.

Dirac notation provides a convenient representation of state vectors and their inner product: A state vector $\psi \in \mathcal{H}$ is represented by a *ket* $|\psi\rangle$ and the inner product of two vectors ψ and ϕ is: $\langle\psi|\phi\rangle := \langle\psi|\,|\phi\rangle$, where *bra* $\langle\psi|$ represents the conjugate transpose of the ket $|\psi\rangle$, $\langle\psi| = |\psi\rangle^\dagger$ and belongs to the dual Hilbert space.

For instance, a qubit, the simplest quantum system with two levels, is associated with a two-dimensional Hilbert space $\mathcal{H}_q = \mathbb{C}^2$. A convenient choice of basis for $\mathcal{H}_q$ is $\{|0\rangle = \begin{pmatrix}1\\0\end{pmatrix}, |1\rangle = \begin{pmatrix}0\\1\end{pmatrix}\}$ called the *computational basis*. An arbitrary normalized pure state of a qubit can be represented as,

$$|\psi\rangle = a\,|0\rangle + b\,|1\rangle \tag{2.1}$$

where a and b are complex numbers satisfying the normalization condition $|a|^2 + |b|^2 = 1$. For $|a| = |b| = \frac{1}{\sqrt{2}}$, the state $|\psi\rangle$ is called an *equal superposition state*.

A pure state of a qubit can be represented[1] geometrically by a point on a sphere with unit radius, called the *Bloch sphere*. The north and south poles of the Bloch sphere represent states $|0\rangle$ and $|1\rangle$, respectively. Any other point represent a superposition between $|0\rangle$ and $|1\rangle$,

$$|\psi\rangle = \cos(\theta/2)\,|0\rangle + \sin(\theta/2)e^{i\phi}\,|1\rangle \tag{2.2}$$

where θ is the polar angle and ϕ is the azimuthal angle as shown in figure 2.1.

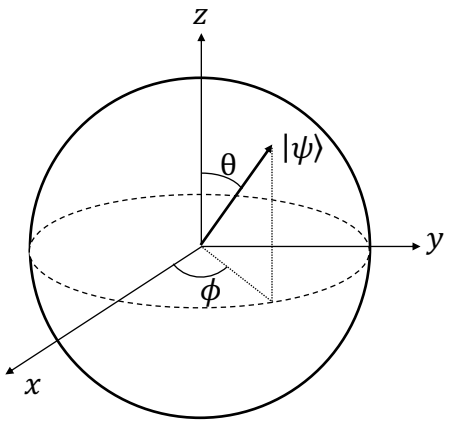

Figure 2.1: The Bloch sphere representation of an arbitrary pure state of a qubit.

[1] Up to a physically unobservable global phase.

Composite Systems

Given a quantum system A, with Hilbert space $\mathcal{H}_A$, and a quantum system B, with Hilbert space $\mathcal{H}_B$, any ideal preparation of the composite system AB belongs to the composite Hilbert space,

$$\mathcal{H}_{AB} = \mathcal{H}_A \otimes \mathcal{H}_B \tag{2.3}$$

An orthonormal basis for $\mathcal{H}_{AB}$ can be constructed by tensor product of two orthonormal bases of $\mathcal{H}_{q_A}$ and $\mathcal{H}_{q_B}$: $\{|a_i\rangle \otimes |b_j\rangle\}$ where $\{|a_i\rangle\}$, $i = 1, 2, ..., dim(\mathcal{H}_A)$ and $\{|b_j\rangle\}$, $j = 1, 2, ..., dim(\mathcal{H}_B)$ are two orthonormal bases of $\mathcal{H}_A$ and $\mathcal{H}_B$, respectively. As an example, the Hilbert space of two qubits, q_A and q_B is, $\mathcal{H}_{q_A q_B} = \mathcal{H}_{q_A} \otimes \mathcal{H}_{q_B} = \mathbb{C}^2 \otimes \mathbb{C}^2 = \mathbb{C}^4$ with the computational basis: $\{|00\rangle, |01\rangle, |10\rangle, |11\rangle\} = \{|0\rangle \otimes |0\rangle, |0\rangle \otimes |1\rangle, |1\rangle \otimes |0\rangle, |1\rangle \otimes |1\rangle\} = \{|0\rangle, |1\rangle\} \otimes \{|0\rangle, |1\rangle\}$.

The Hilbert space of a mesoscopic system that consists of N two-level quantum systems[2] is the tensor product of the Hilbert spaces of its constituents,

$$\mathcal{H}_{\text{MS}} = \mathcal{H}_1 \otimes \mathcal{H}_2 \otimes ... \otimes \mathcal{H}_N = \mathbb{C}^2 \otimes \mathbb{C}^2 \otimes ... \otimes \mathbb{C}^2 = (\mathbb{C}^2)^{\otimes N} = \mathbb{C}^{2^N} \tag{2.4}$$

with the computational basis: $\{|0\rangle^{\otimes N}, |0\rangle^{\otimes N-1} \otimes |1\rangle, ..., |1\rangle^{\otimes N}\} = \{|0\rangle, |1\rangle\}^{\otimes N}$.

Pure Entangled States

A pure state of a bipartite composite system $|\psi\rangle_{AB} \in \mathcal{H}_{AB}$ is called a *product state* if it can be expressed as $|\psi\rangle_{AB} = |\psi\rangle_A \otimes |\psi\rangle_B$ for some $|\psi\rangle_A \in \mathcal{H}_A$ and $|\psi\rangle_B \in \mathcal{H}_B$. Any bipartite pure state that is not a product state is an *entangled state*.

For instance, state $|\psi\rangle_{AB} = a|00\rangle + b|11\rangle$ of two qubits is an entangled state unless a or b equals zero; in particular for $|a| = |b| = 1/\sqrt{2}$, state $|\psi\rangle_{AB}$ is a *maximally entangled state*. The following four orthogonal maximally entangled states, called the Bell states, form a basis for the Hilbert space of two qubits,

$$\begin{aligned} |e_\pm\rangle &= \frac{1}{\sqrt{2}}(|00\rangle \pm |11\rangle) \\ |o_\pm\rangle &= \frac{1}{\sqrt{2}}(|01\rangle \pm |10\rangle) \end{aligned} \tag{2.5}$$

[2]We do not call the two-level systems constituting the mesoscopic system qubits; since the term qubit usually implies universal control (to be defined in section 2.2), which we do not assume to be available for the two-level elements of the mesoscopic system.

2.1.2 Mixed States and Density Operators

Not all preparation procedures produce pure states. The quantum states that are not pure are called *mixed*. From an operational point of view, the state of a quantum system describes the knowledge one has about the system. Mixed states are associated with incomplete knowledge about the quantum system. A mixed state is represented by a non-negative Hermitian operator with trace one, called a *density matrix* or a *density operator*.

Suppose that a quantum system is prepared in state $|\psi_1\rangle$ with probability p_1 and in state $|\psi_2\rangle$ with probability $p_2 = 1 - p_1$. The state of the quantum system is a mixed state with the density operator,

$$\rho = p_1 |\psi_1\rangle\langle\psi_1| + p_2 |\psi_2\rangle\langle\psi_2| \tag{2.6}$$

More generally the density matrix of a quantum system that is prepared in one of the states $\{|\psi_i\rangle\}$, $i = 1, 2, ..., n$ each with probability $p_i \geq 0$ ($\sum_i p_i = 1$), is,

$$\rho = \sum_{i=1}^{n} p_i |\psi_i\rangle\langle\psi_i| \tag{2.7}$$

The special case of $n = 1$ corresponds to a pure state preparation,

$$\rho = p_1 |\psi_1\rangle\langle\psi_1| = |\psi_1\rangle\langle\psi_1| \tag{2.8}$$

Thus, density matrices give a general description of quantum systems that can represent any pure or mixed state. Conversely, any density matrix can be expressed as a probabilistic mixture of pure states and represents a pure or mixed quantum state.

In addition to probabilistic preparations, density matrices describe the state of a subsystem of a composite quantum system. Consider a composite system with the density matrix ρ_{AB} that is either a pure state or a probabilistic mixture of pure states. The reduced state of the subsystem A is represented by the density operator,

$$\rho_A = \mathrm{Tr}_B(\rho_{AB}) \tag{2.9}$$

where $\mathrm{Tr}_B(.)$ is the partial trace over the subsystem B. With an orthonormal basis $\{|b_j\rangle\}, j = 1, 2, ...d_B (= \dim(\mathcal{H}_B))$ of the Hilbert space $\mathcal{H}_B$, the partial trace is defined as,

$$\mathrm{Tr}_B(\rho_{AB}) := \sum_{j=1}^{d_B} (\mathbb{1}_A \otimes \langle b_j|)\rho_{AB}(\mathbb{1}_A \otimes |b_j\rangle) \tag{2.10}$$

A pure bipartite state $\rho_{AB} = |\psi\rangle\langle\psi|_{AB}$, is an entangled state if and only if the reduced state ρ_A (or ρ_B) is a mixed state.

General Entangled States

The notion of entanglement is generalized to mixed states and density operators. A bipartite state ρ_{AB} is a product state if it can be expressed as $\rho_{AB} = \rho_A \otimes \rho_B$ and is a *separable state* if it can written as a convex combination of product states, $\rho_{AB} = \sum_i p_i \rho_A^i \otimes \rho_B^i$; otherwise is an entangled state.

2.2 Transformation

The transformation process of a *closed* quantum system, i.e., a system that is isolated from its surroundings, is operationally represented by a *unitary operator*,

$$|\psi'\rangle = U\,|\psi\rangle \tag{2.11}$$

where $|\psi\rangle$ and $|\psi'\rangle$ are the state vectors representing the pure states of the quantum system before and after the transformation, and U is a unitary matrix satisfying the relation $UU^\dagger = U^\dagger U = \mathbb{1}$. Generalization of Eq. (2.11) to density operators indicates transformation of mixed initial states,

$$\rho' = U\rho U^\dagger \tag{2.12}$$

The underlying physics law for the time evolution of a closed quantum system is the *time-dependent Schrödinger equation*,

$$i\hbar \frac{d\,|\psi(t)\rangle}{dt} = H(t)\,|\psi(t)\rangle \tag{2.13}$$

where $H(t)$ is the Hamiltonian of the system; a Hermitian operator ($H(t) = H(t)^\dagger$) whose eigenvalues are the allowed energies of the quantum system, and $\hbar$ is Plank's constant that is usually absorbed in $H(t)$ and set to one, $\hbar = 1$. Among all unitary operators that describe a valid quantum transformation, *in principle*, the Schrödinger equation indicates which ones are accessible for a specific quantum system, *in practice*. The *von Neumann equation* generalizes the Schrödinger equation to density operators and describes the time evolution of mixed states,

$$i\hbar \frac{d\rho(t)}{dt} = [H(t), \rho(t)] \tag{2.14}$$

where the bracket represents the commutator defined as, $[A, B] := AB - BA$. Solving the Schrödinger equation or the von Neumann equation results in a time-dependant unitary operator, $U(t)$, that specifies the evolution of the quantum system in time,

$$|\psi(t)\rangle = U(t)\,|\psi(0)\rangle\,, \qquad \rho(t) = U(t)\rho(0)U^\dagger(t) \tag{2.15}$$

If the Hamiltonian is time-independent $H(t) = H$, the unitary operator is,

$$U(t) = e^{-iHt} \tag{2.16}$$

The unitary evolution corresponding to a time-dependent Hamiltonian that commutes at different times, $[H(t), H(t')] = 0$, is,

$$U(t) = e^{-i\int_0^t H(t')dt'} \tag{2.17}$$

For a time-dependent Hamiltonian that does not commute at different times $[H(t), H(t')] \neq 0$, the unitary operator is,

$$U(t) = \mathcal{T}e^{-i\int_0^t H(t')dt'} \tag{2.18}$$

where $\mathcal{T}$ is the time ordering operator.

Any Hermitian operator acting on the Hilbert space of a qubit $\mathcal{H}_q = \mathbb{C}^2$ can be expanded in terms of the identity operator, and the three Pauli operators with real coefficients. The Pauli operators are defined as,

$$\sigma_x = \begin{pmatrix} 0 & 1 \\ 1 & 0 \end{pmatrix} \qquad \sigma_y = \begin{pmatrix} 0 & -i \\ i & 0 \end{pmatrix} \qquad \sigma_z = \begin{pmatrix} 1 & 0 \\ 0 & -1 \end{pmatrix} \tag{2.19}$$

As a result, any unitary operator on a qubit can be expressed as,

$$U = U_{\hat{n}}(\phi) = e^{-i\frac{\phi}{2}(\hat{n}.\vec{\sigma})} \tag{2.20}$$

up to an unimportant global phase; where $\hat{n} = (n_x, n_y, n_z)$ is a unit vector, ϕ is some phase and $\vec{\sigma} = (\sigma_x, \sigma_y, \sigma_z)$. In the Bloch sphere representation, $U_{\hat{n}}(\phi)$ corresponds to a rotation of the vector representing the state of the quantum system along the axis $\hat{n}$ by the angle ϕ. Unitary operators on a qubit are also called *unitary rotations*, in this sense. Any unitary rotation can be decomposed into Euler rotations,

$$U_{\hat{n}}(\phi) = U_{\hat{z}}(\alpha)U_{\hat{y}}(\beta)U_{\hat{z}}(\gamma). \tag{2.21}$$

In general, rotation about two independant axis in enough for constructing an arbitrary unitary operator on a qubit. In other words, rotation about two independant axis provides *universal control* over a qubit.

In the language of quantum information, quantum transformations and unitary operators are also called *quantum logic gates* or *quantum gates*; usually when the overall result of the transformation only matters, not the underlying time evolution. The Pauli operators, σ_x, σ_y and σ_z, that correspond to π-rotations about $\hat{x}$, $\hat{y}$ and $\hat{z}$ axes, are examples of single

qubit quantum gates, known as *bit flip*, *bit-phase flip*, and *phase flip* gates, respectively. Another widely used single qubit gate is the *Hadamard* gate, defined as,

$$H = \frac{1}{\sqrt{2}} \begin{pmatrix} 1 & 1 \\ 1 & -1 \end{pmatrix} \tag{2.22}$$

Applying Hadamard gate on $|0\rangle$ and $|1\rangle$ states creates equal superposition states with positive and negative phases,

$$H|0\rangle = \frac{1}{\sqrt{2}}(|0\rangle + |1\rangle) := |+\rangle\,, \quad H|1\rangle = \frac{1}{\sqrt{2}}(|0\rangle - |1\rangle) := |-\rangle \tag{2.23}$$

An important two qubit quantum gate is the *Controlled-not (CNOT)* gate that along with single qubit rotations provides universal control over two qubits. The CNOT gate is defined as,

$$\text{CNOT} = |0\rangle\langle 0| \otimes \mathbb{1} + |1\rangle\langle 1| \otimes \sigma_x = \begin{pmatrix} 1 & 0 & 0 & 0 \\ 0 & 1 & 0 & 0 \\ 0 & 0 & 0 & 1 \\ 0 & 0 & 1 & 0 \end{pmatrix} \tag{2.24}$$

It flips the second qubit, called the target qubit, if the first qubit, called the control qubit, is in state $|1\rangle$. The CNOT gate transforms separable initial states to maximally entangled states if the control and the target qubits are prepared in an equal superposition state and a polarized state, respectively. The maximally entangled Bell states can be created this way,

$$\begin{aligned} \text{CNOT}|+\rangle|0\rangle &= \frac{1}{\sqrt{2}}(|00\rangle + |11\rangle) = |e_+\rangle\,, \quad \text{CNOT}|-\rangle|0\rangle = \frac{1}{\sqrt{2}}(|00\rangle - |11\rangle) = |e_-\rangle \\ \text{CNOT}|+\rangle|1\rangle &= \frac{1}{\sqrt{2}}(|01\rangle + |10\rangle) = |o_+\rangle\,, \quad \text{CNOT}|-\rangle|1\rangle = \frac{1}{\sqrt{2}}(|01\rangle - |10\rangle) = |o_-\rangle \end{aligned} \tag{2.25}$$

Implementing a CNOT gate between two qubits, and more generally any gate that transforms a separable state of two qubits to an entangled state, requires the qubits to interact. This thesis concerns with entangling two non-interacting qubits; i.e. entangling two qubits when an entangling gate is not available. The Hamiltonian of two non-interacting qubits can be written as sum of the Hamiltonian on each,

$$H_{q_1 q_2}(t) = H_{q_1}(t) \otimes \mathbb{1}_{q_2} + \mathbb{1}_{q_1} \otimes H_{q_2}(t) \tag{2.26}$$

Solving the Schrödinger equation tells us that the unitary evolution of this system can always be expressed as,

$$U_{q_1 q_2}(t) = U_{q_1}(t) \otimes U_{q_2}(t) \tag{2.27}$$

which always transforms a separable initial state, $|\psi(0)\rangle_{q_1q_2} = |\psi(0)\rangle_{q_1} \otimes |\psi(0)\rangle_{q_2}$, to a separable final state,

$$\begin{aligned} |\psi(t)\rangle_{q_1q_2} &= U_{q_1q_2}(t)\,|\psi(0)\rangle_{q_1q_2} = U_{q_1}(t) \otimes U_{q_2}(t)\left(|\psi(0)\rangle_{q_1} \otimes |\psi(0)\rangle_{q_2}\right) \\ &= \left(U_{q_1}(t)\,|\psi(0)\rangle_{q_1}\right) \otimes \left(U_{q_2}(t)\,|\psi(0)\rangle_{q_2}\right) := |\psi(t)\rangle_{q_1} \otimes |\psi(t)\rangle_{q_2} \end{aligned} \tag{2.28}$$

In section 2.3, we show how a joint measurement can entangle two non-interacting qubits.

Collective Dynamics and Collective Rotation of a Mesoscopic System

Among all unitary transformations of a mesoscopic system, an interesting subset are collective dynamics. Collective dynamics, represented by collective unitary operators, are the transformations that do not discern between the two-level components of the mesoscopic system. They can be, mathematically, defined as the unitary operations that are invariant under any permutations between the states of the particles in the mesoscopic system. An arbitrary permutation can be decomposed into two-body swaps. A swapping operator between ith and jth particle ($i < j$) is,

$$\mathrm{SWAP}^{ij} = |0\rangle\langle 0|_i \otimes |0\rangle\langle 0|_j + |1\rangle\langle 1|_i \otimes |1\rangle\langle 1|_j + |0\rangle\langle 1|_i \otimes |1\rangle\langle 0|_j + |1\rangle\langle 0|_i \otimes |0\rangle\langle 1|_j \tag{2.29}$$

where the identity operators on $N-2$ particles are omitted.

An experimentally relevant subset of collective unitary operators are collective rotations,

$$U^{\mathrm{MS}}_{\hat{n}}(\phi) = U^1_{\hat{n}}(\phi) \otimes U^2_{\hat{n}}(\phi) \otimes ... \otimes U^N_{\hat{n}}(\phi) \tag{2.30}$$

where $U^i_{\hat{n}}(\phi)$ represents a general rotation of the ith particle. The collective rotations correspond to collective external control of the mesoscopic system. The Hamiltonian associated to $U^{\mathrm{MS}}_{\hat{n}}(\phi)$ is,

$$H_{\mathrm{CC}} = \frac{\omega}{2}\sum_{i=1}^{N}(n_x\sigma_x^i + n_y\sigma_y^i + n_z\sigma_z^i) = \frac{\omega}{2}\left(n_x\sum_{i=1}^{N}\sigma_x^i + n_y\sum_{i=1}^{N}\sigma_y^i + n_x\sum_{i=1}^{N}\sigma_z^i\right) \tag{2.31}$$

with $\sigma_a^i = \mathbb{1}^{\otimes i-1} \otimes \sigma_a \otimes \mathbb{1}^{\otimes N-i}$ for $a = x, y, z$. The rotation angle ϕ is the Hamiltonian frequency times the evolution time $\phi = \omega t$.

2.3 Measurement

The measurement procedure is the process of observing a physical property of a quantum system and producing a classical outcome. It is operationally represented by a *projector-valued measure (PVM)* or more generally a *positive-operator valued measure (POVM)*.

2.3.1 Ideal Measurement Process

A projective measurement is described by a Hermitian operator on the Hilbert space of the system, called an *observable*. The observable has a spectral decomposition,

$$O = \sum_m m\Pi_m \tag{2.32}$$

where $\{m\}$ is the set of possible measurement outcomes. Each m is an eigenvalue of the observable and it is a real number. Π_m is the projection operator onto the eigenspace of O with eigenvalue m. The projection operators satisfy the orthogonality condition $\Pi_m\Pi_n = \delta_{mn}\Pi_m$ and they span the Hilbert space, $\sum_m \Pi_m = \mathbb{1}$. The probability of each measurement outcome, m, upon measuring a quantum system in an arbitrary state is given by Born's rule,

$$p_m = Tr(\Pi_m\rho) \tag{2.33}$$

where ρ is the density matrix representing the state of the quantum system prior to the measurement. As an example, measuring a qubit that is prepared in an arbitrary pure state, $|\psi\rangle = a\,|0\rangle + b\,|1\rangle$ ($\rho = |\psi\rangle\langle\psi|$), in the computational basis, with the measurement operators $\{\Pi_0 = |0\rangle\langle 0|\,, \Pi_1 = |1\rangle\langle 1|\}$, results in outcome 0 with the probability $p_0 = |a|^2$ and outcome 1 with the probability $p_1 = |b|^2$.

A counter-intuitive feature of the measurement process is that it not only reveals the measured property of the quantum system, but also updates the state of the quantum system according to the measurement outcome. Thus, it can be regarded as a state preparation process, too. This property is the main idea behind entangling separated qubits using a joint measurement. The state of the system after the measurement and post-selecting on outcome m, according to Luder's state-update-rule, is,

$$\rho_m = \frac{\Pi_m\rho\Pi_m}{Tr(\Pi_m\rho)} = \frac{\Pi_m\rho\Pi_m}{p_m} \tag{2.34}$$

where $\frac{1}{p_m}$ is the normalization factor that guarantees $Tr(\rho_m) = 1$.

In the above example the updated states of the qubit corresponding to the measurement outcomes 0 and 1 are $\rho_0 = |0\rangle\langle 0|$ and $\rho_1 = |1\rangle\langle 1|$.

Joint measurement as an entangling tool

The state update rule provides the key element for preparing qubits in entangled states upon implementing a joint measurement. Parity measurement and Hamming weight measurement are two examples of joint measurements. Parity measurement of two qubits reveals whether the state of the qubits are the same (even parity) or different (odd parity) without uncovering the state of each qubit. The projective operators of parity measurement corresponding to even and odd parities are,

$$\begin{aligned} \Pi_e &= |00\rangle\langle 00| + |11\rangle\langle 11| \\ \Pi_o &= |01\rangle\langle 01| + |10\rangle\langle 10| \end{aligned} \tag{2.35}$$

Two qubits, that are each prepared in an equal superposition state, $|\pm\rangle = \frac{1}{\sqrt{2}}(|0\rangle \pm |1\rangle)$, will be probabilistically projected into the maximally entangled Bell states upon a joint parity measurement,

$$\begin{aligned} |e_\pm\rangle &= \frac{1}{\sqrt{2}}(|00\rangle \pm |11\rangle) \\ |o_\pm\rangle &= \frac{1}{\sqrt{2}}(|01\rangle \pm |10\rangle) \end{aligned} \tag{2.36}$$

where the positive and negative phases correspond to the same and different phases of the qubits' initial superposition states, respectively. The probability of even and odd parity outcomes are each equal to 1/2.

Another joint measurement is Hamming weight measurement that specifies the distance from the all zero state. It is equivalent to collective magnetization measurement for spin qubits. Hamming weight measurement can be defined for any number of qubits. Its projective operators for two qubits are,

$$\begin{aligned} \Pi_0 &= |00\rangle\langle 00| \\ \Pi_1 &= |01\rangle\langle 01| + |10\rangle\langle 10| \\ \Pi_2 &= |11\rangle\langle 11| \end{aligned} \tag{2.37}$$

Projective measurement of two qubits' Hamming weight updates their state to the maximally entangled state with hamming weigh one, $|o_\pm\rangle = \frac{1}{\sqrt{2}}(|01\rangle \pm |10\rangle)$, with a probability of 1/2, provided that the qubits are each prepared in an equal superposition state. The two other outcomes of the measurement are Hamming weights 0 and 2, with the separable updated states $|00\rangle$ and $|11\rangle$, each with a probability of 1/4.

2.3.2 Generalized Measurement Process

The measurement processes are more generally described by POVMs which include PVMs as a subset. A POVM is operationally characterized by a set of measurement operators $\{E_\alpha\}$ that are non-negative $E_\alpha \geq 0$ and complete $\sum_\alpha E_\alpha = \mathbb{1}$. The probability of each measurement outcome α is given by the generalization of the Born's rule,

$$p_\alpha = Tr(E_\alpha \rho) \tag{2.38}$$

and the state of the quantum system updates according to the generalization of Luder's state-update-rule,

$$\rho_\alpha = \frac{M_\alpha \rho M_\alpha^\dagger}{p_\alpha} \tag{2.39}$$

where $E_\alpha = M_\alpha^\dagger M_\alpha$. One set of operators that satisfy these relations is $\{M_\alpha\} = \{\sqrt{E_\alpha}\}$; however, there is no unique choice for $\{M_\alpha\}$ and it depends on the details of implementing the POVM.

As an example, a noisy parity measurement, that mixes between even and odd parities, can be described by the following POVM operators,

$$\begin{aligned} E_e &= (1-\epsilon)\Pi_e + \epsilon\Pi_o \\ E_o &= (1-\epsilon)\Pi_o + \epsilon\Pi_e \end{aligned} \tag{2.40}$$

where ϵ ranges from 0 for no noise to 1/2 for maximum noise and no measurement. Assuming $M_\alpha = \sqrt{E_\alpha}$, the updated states of the qubits, given in Eq. 2.36, are replaced by,

$$\begin{aligned} \rho_e &= (1-\epsilon)\,|e_\pm\rangle\langle e_\pm| + \epsilon\,|o_\pm\rangle\langle o_\pm| + \sqrt{\epsilon(1-\epsilon)}(|e_\pm\rangle\langle o_\pm| + |o_\pm\rangle\langle e_\pm|) \\ \rho_o &= (1-\epsilon)\,|o_\pm\rangle\langle o_\pm| + \epsilon\,|e_\pm\rangle\langle e_\pm| + \sqrt{\epsilon(1-\epsilon)}(|e_\pm\rangle\langle o_\pm| + |o_\pm\rangle\langle e_\pm|) \end{aligned} \tag{2.41}$$

According to Neumarks dilation theorem, any POVM can be realized as a PVM on a bigger Hilbert space of the system and an apparatus [40]. This PVM can always be described as a von Neuman indirect measurement where the measurement is only applied on the apparatus, following a unitary interaction between the apparatus and the system [41]. This process has a unique state-update-rule,

$$\rho_{s,\alpha} = \frac{Tr_a\left((\mathbb{1}_s \otimes \Pi_\alpha^a) U_{sa} (\rho_s \otimes |0\rangle\langle 0|_a) U_{sa}^\dagger (\mathbb{1}_s \otimes \Pi_\alpha^a)\right)}{Tr\left((\mathbb{1}_s \otimes \Pi_\alpha^a) U_{sa} (\rho_s \otimes |0\rangle\langle 0|_a) U_{sa}^\dagger\right)} \tag{2.42}$$

where ρ_s and $\rho_{s,\alpha}$ are the states of the system before the measurement and after the measurement and post-selection on outcome α, and the apparatus is assumed to be prepared in a pure state, $|0\rangle\langle 0|_a$. The operators U_{sa} and Π^a_α represent the unitary operator corresponding to the interaction between the system and the apparatus and the PVM on the apparatus, respectively. Following this process, the measurement operators of the system are uniquely determined, $M_\alpha = \langle\alpha|_a U_{sa} |0\rangle_a$, given that the apparatus PVM operators are rank 1, $\Pi^a_\alpha = |\alpha\rangle\langle\alpha|_a$.

2.3.3 Collective Measurement of a Mesoscopic System

In the following chapters, we deal with collective PVMs and POVMs on a mesoscopic system consisting of N identical two-level systems. The PVM operators of the collective Hamming weight measurement of the mesoscopic system are,

$$\Pi_m = \sum_{i=1}^{\binom{N}{m}} P_i \left(|0\rangle\langle 0|^{\otimes N-m} \otimes |1\rangle\langle 1|^{\otimes m} \right) \tag{2.43}$$

where $m \in \{0, 1, ..., N\}$ and P_i is the permutation operator and the summation is over all permutations. Other collective PVMs over the mesoscopic system are related to the Hamming weight measurement by a collective unitary, $\Pi'_m = U_{\text{Col}} \Pi_m U^\dagger_{\text{Col}}$, for $m = 0, 1, ..., N$. This collective unitary can be regarded as part of the transformation process. Thus, the Hamming weight measurement and the POVMs based on that are enough to describe any collective measurement of the mesoscopic system.

A coarse-grained collective measurement over the mesoscopic system is characterized by a collective POVM. The collective POVM operators, $\{E_\alpha\}$, can be expanded in terms of collective PVM operators as,

$$E_\alpha = \sum_{m=0}^{N} a_{\alpha,m} \Pi_m \tag{2.44}$$

where the coefficients $a_{\alpha,m}$ satisfy the conditions: $a_{\alpha,m} \geq 0$ and $\sum_\alpha a_{\alpha,m} = 1$ following positivity and completeness of the POVM operators.

2.4 Transformation of an open quantum system

A quantum system is generally not isolated from its environment in which case its transformation can not be described by a unitary operator. Evolution of a quantum system is

more generally described by a *quantum dynamical map* defined as a transformation that takes quantum states to quantum states. It can be viewed as the reduced effect of a unitary operator that acts on the quantum system and its environment[3]. Any quantum dynamical map is linear, completely positive and trace preserving. Positivity of a map Λ means that $\Lambda(\rho) \geq 0$ if $\rho \geq 0$. Complete positivity guarantees positivity when the transformed quantum system is part of a composite system,

$$(\Lambda_A \otimes \mathbb{1}_B(\rho_{AB})) \geq 0 \text{ if } \rho_{AB} \geq 0 \tag{2.45}$$

Trace preserving condition ensures that the normalization is preserved, $\mathrm{Tr}(\Lambda(\rho)) = \mathrm{Tr}(\rho) = 1$. Any *completely positive trace preserving (CPTP)* map can be represented by a *Kraus-decomposition*,

$$\Lambda(\rho) = \sum_i K_i \rho K_i^\dagger \tag{2.46}$$

where the *Kraus operators*, K_i's, are linear operators satisfying the constraint $\sum_i K_i^\dagger K_i = \mathbb{1}$.

In the rest of this section, we review CPTP maps of some experimentally relevant noise processes for a qubit, then we discuss their generalization for a mesoscopic system. In the following discussions, a general state of the qubit is considered which is expanded in the eigen-basis defined by the qubit's Hamiltonian as,

$$\rho = \begin{pmatrix} \rho_{00} & \rho_{01} \\ \rho_{10} & \rho_{11} \end{pmatrix} = \rho_{00} |0\rangle\langle 0| + \rho_{01} |0\rangle\langle 1| + \rho_{10} |1\rangle\langle 0| + \rho_{11} |1\rangle\langle 1| \tag{2.47}$$

where $|0\rangle = |g\rangle$ and $|1\rangle = |e\rangle$ represent the ground and the excited state of the Hamiltonian and the normalization condition requires $\rho_{00} + \rho_{11} = 1$.

2.4.1 Amplitude Damping Map

The amplitude damping map models relaxation from excited state to the ground state. It is represented by the Kraus operators,

$$K_0^{\mathrm{A}} = \begin{pmatrix} 1 & 0 \\ 0 & \sqrt{1-\lambda_{\mathrm{A}}} \end{pmatrix} \qquad K_1^{\mathrm{A}} = \begin{pmatrix} 0 & \sqrt{\lambda_{\mathrm{A}}} \\ 0 & 0 \end{pmatrix} \tag{2.48}$$

[3]Note that the reverse is not true; meaning that it is not always possible to assign a quantum dynamical map to the evolution of a quantum system that is interacting with its environment.

where the amplitude damping parameter, λ_{A}, ranges from 0 to 1 and can be interpreted as the probability of relaxation. The qubit's state after applying the amplitude damping map is,

$$\rho^{\mathrm{A}} = \Lambda^{\mathrm{A}}(\rho) = K_0^{\mathrm{A}} \rho K_0^{\mathrm{A}\dagger} + K_1^{\mathrm{A}} \rho K_1^{\mathrm{A}\dagger} = \begin{pmatrix} \rho_{00} + \lambda_{\mathrm{A}} \rho_{11} & \sqrt{1-\lambda_{\mathrm{A}}}\rho_{01} \\ \sqrt{1-\lambda_{\mathrm{A}}}\rho_{10} & (1-\lambda_{\mathrm{A}})\rho_{11} \end{pmatrix} \tag{2.49}$$

The amplitude damping map reduces the population of the excited state and adds to the population of the ground state. It also attenuates the coherence terms between the ground and the excited state. The fixed point of the amplitude map is the ground state: $\rho_{\mathrm{f}}^{\mathrm{A}} = |0\rangle\langle 0|$.

2.4.2 Generalized Amplitude Damping Map

A generalization of the amplitude damping map models relaxation towards an arbitrary diagonal mixed state, $\rho_{\mathrm{f}}^{\mathrm{GA}} = p\,|0\rangle\langle 0| + (1-p)\,|1\rangle\langle 1|$ where $0 \leq p \leq 1$ is the population in the ground state. The generalized amplitude damping map is represented by the following Kraus operators,

$$\begin{aligned} K_0^{\mathrm{GA}} &= \sqrt{p}\begin{pmatrix} 1 & 0 \\ 0 & \sqrt{1-\lambda_{\mathrm{A}}} \end{pmatrix} \qquad K_1^{\mathrm{GA}} = \sqrt{p}\begin{pmatrix} 0 & \sqrt{\lambda_{\mathrm{A}}} \\ 0 & 0 \end{pmatrix} \\ K_2^{\mathrm{GA}} &= \sqrt{1-p}\begin{pmatrix} \sqrt{1-\lambda_{\mathrm{A}}} & 0 \\ 0 & 1 \end{pmatrix} \quad K_3^{\mathrm{GA}} = \sqrt{1-p}\begin{pmatrix} 0 & 0 \\ \sqrt{\lambda_{\mathrm{A}}} & 0 \end{pmatrix} \end{aligned} \tag{2.50}$$

and the evolved density matrix of the qubit is,

$$\rho^{\mathrm{GA}} = \Lambda^{\mathrm{GA}}(\rho) = \begin{pmatrix} (1-\lambda_{\mathrm{A}})\rho_{00} + p\lambda_{\mathrm{A}} & \sqrt{1-\lambda_{\mathrm{A}}}\rho_{01} \\ \sqrt{1-\lambda_{\mathrm{A}}}\rho_{10} & (1-\lambda_{\mathrm{A}})\rho_{11} + \lambda_{\mathrm{A}} - p\lambda_{\mathrm{A}} \end{pmatrix} \tag{2.51}$$

The state of a two-level system in thermal equilibrium with a bath at temperature T is,

$$\rho_{\mathrm{th}} = \frac{e^{-\frac{H}{k_B T}}}{\mathrm{Tr}(e^{-\frac{H}{k_B T}})} = \frac{1}{1+e^{-\frac{\Delta E}{k_B T}}}\,|0\rangle\langle 0| + \frac{e^{-\frac{\Delta E}{k_B T}}}{1+e^{-\frac{\Delta E}{k_B T}}}\,|1\rangle\langle 1| \tag{2.52}$$

where H is the Hamiltonian of the system, $\Delta E = E_e - E_g$ is the energy different between its ground and excited states and k_B is the Boltzmann constant. The T_1 relaxation process, that drives the system towards this thermal equilibrium state, is modelled by a generalized amplitude damping map with the fixed point $\rho_{\mathrm{f}}^{\mathrm{GA}} = \rho_{\mathrm{th}}$ and the damping probability $\lambda_{\mathrm{A}} = 1 - e^{-\Gamma_1 t}$, where $\Gamma_1 = 1/T_1$ is the relaxation rate.

2.4.3 Phase damping Map

The Phase damping map reduces the off-diagonal terms of the density matrix while leaving the diagonal terms intact. The associated Kraus operators are,

$$K_0^{\mathrm{P}} = \begin{pmatrix} 1 & 0 \\ 0 & \sqrt{1-\lambda_{\mathrm{P}}} \end{pmatrix} \qquad K_1^{\mathrm{P}} = \begin{pmatrix} 0 & 0 \\ 0 & \sqrt{\lambda_{\mathrm{P}}} \end{pmatrix} \tag{2.53}$$

and the evolved state of the qubit is,

$$\rho^{\mathrm{P}} = \Lambda^{\mathrm{P}}(\rho) = \begin{pmatrix} \rho_{00} & \sqrt{1-\lambda_{\mathrm{P}}}\rho_{01} \\ \sqrt{1-\lambda_{\mathrm{P}}}\rho_{10} & \rho_{11} \end{pmatrix} \tag{2.54}$$

Decoherence or the T_2 relaxation process that is derived by noise along the quantization axis is modelled by a phase damping map with the damping probability $\lambda_{\mathrm{P}} = 1 - e^{-\Gamma_2 t}$, where $\Gamma_2 = 1/T_2$ is the damping rate.

2.4.4 Depolarizing Map

The depolarizing map models symmetric noise in all directions. The Kraus operators of this map are,

$$\begin{aligned} K_0^{\mathrm{Dep}} &= \sqrt{1-p}\mathbb{1} = \sqrt{1-p}\begin{pmatrix} 1 & 0 \\ 0 & 1 \end{pmatrix} \quad K_1^{\mathrm{Dep}} = \sqrt{\frac{p}{3}}\sigma_x = \sqrt{\frac{p}{3}}\begin{pmatrix} 0 & 1 \\ 1 & 0 \end{pmatrix} \\ K_2^{\mathrm{Dep}} &= \sqrt{\frac{p}{3}}\sigma_y = \sqrt{\frac{p}{3}}\begin{pmatrix} 0 & -i \\ i & 0 \end{pmatrix} \quad K_3^{\mathrm{Dep}} = \sqrt{\frac{p}{3}}\sigma_z = \sqrt{\frac{p}{3}}\begin{pmatrix} 1 & 0 \\ 0 & -1 \end{pmatrix} \end{aligned} \tag{2.55}$$

With the probability of $1-p$ the qubit is intact and each of the three *bit flip*, *phase flip* and *bit-phase flip* errors occurs with the probability of $p/3$. The transformed state of the qubit is,

$$\rho^{\mathrm{Dep}} = \Lambda^{\mathrm{Dep}}(\rho) = \begin{pmatrix} (1-\frac{2p}{3})\rho_{00} + \frac{2p}{3}\rho_{11} & (1-\frac{4p}{3})\rho_{01} \\ (1-\frac{4p}{3})\rho_{10} & (1-\frac{2p}{3})\rho_{11} + \frac{2p}{3}\rho_{00} \end{pmatrix} \tag{2.56}$$

State ρ^{Dep} can be simplified using the normalization condition: $\rho_{00} + \rho_{11} = 1$,

$$\begin{aligned} \rho^{\mathrm{Dep}} = \Lambda^{\mathrm{Dep}}(\rho) &= \begin{pmatrix} (1-\frac{4p}{3})\rho_{00} + \frac{2p}{3} & (1-\frac{4p}{3})\rho_{01} \\ (1-\frac{4p}{3})\rho_{10} & (1-\frac{4p}{3})\rho_{11} + (\frac{2p}{3}) \end{pmatrix} \\ &= (1-\frac{4p}{3})\rho + \frac{4p}{3}\frac{\mathbb{1}}{2} := (1-\lambda_{\mathrm{Dep}})\rho + \lambda_{\mathrm{Dep}}\frac{\mathbb{1}}{2} \end{aligned} \tag{2.57}$$

where the depolarizing parameter, λ_{Dep}, is proportional to the error probability, $\lambda_{\text{Dep}} = \frac{4p}{3}$. The error probability, p, ranges from 0 to 1, thus λ_{Dep} is between 0 and $\frac{4}{3}$. Based on equation 2.57, if $\lambda_{\text{Dep}} \leq 1$, it can be interpreted as the probability that the depolarizing map replaces the qubit's state with the fully mixed state, $\frac{\mathbb{1}}{2}$; i.e. erases all the information of the qubit and $1 - \lambda_{\text{Dep}}$ is the probability that the qubit's state is left unchanged.

2.4.5 Noise of a mesoscopic system

The mathematical model of the noise effect on a mesoscopic system depends on the many-body interaction among the two-level components of the mesoscopic system and the interaction between the mesoscopic system and its environment. Nevertheless, assuming that each of the two-level particles in the mesoscopic system is subject to an independant external noise, a simple generalization of the CPTP maps on a qubit models the transformation of an open mesoscopic system.

Consider that a quantum dynamical map, Λ_s, with a set of Kraus operators, $\{K_1, K_2, ..., K_m\}$, represents external noise on one of the two-level systems in the mesoscopic system. A natural generalization of Λ_s for the mesoscopic system in the special case where the mesoscopic system's state is a product state of its constituents, $\rho_{\text{MS}}^{\text{Pro}} = \rho_1 \otimes \rho_1 \otimes ... \otimes \rho_N$, is,

$$\Lambda_{\text{MS}}(\rho_{\text{MS}}^{\text{Pro}}) = \Lambda_s(\rho_1) \otimes \Lambda_s(\rho_2) \otimes ... \otimes \Lambda_s(\rho_N). \tag{2.58}$$

Replacing each $\Lambda_s(\rho_j)$ with $\sum_{i=1}^{m} K_i \rho_j K_i^\dagger$ in the above relation creates a set of Kraus operators for Λ_{MS} that can be used to apply Λ_{MS} to an arbitrary input state,

$$\begin{aligned}
\Lambda_{\text{MS}}(\rho_{\text{MS}}^{\text{Pro}}) &= \sum_{i_1=1}^{m} K_{i_1}\rho_1 K_{i_1}^\dagger \otimes \sum_{i_1=1}^{m} K_{i_2}\rho_2 K_{i_2}^\dagger \otimes ... \otimes \sum_{i_N=1}^{m} K_{i_N}\rho_N K_{i_N}^\dagger \\
&= \sum_{i_1,i_2,...,i_N=1}^{m} (K_{i_1} \otimes K_{i_2} \otimes ... \otimes K_{i_N})(\rho_1 \otimes \rho_2 \otimes ... \otimes \rho_N)(K_{i_1}^\dagger \otimes K_{i_2}^\dagger \otimes ... \otimes K_{i_N}^\dagger) \\
&= \sum_{i_1,i_2,...,i_N=1}^{m} (K_{i_1} \otimes K_{i_2} \otimes ... \otimes K_{i_N})(\rho_{\text{MS}}^{\text{Pro}})(K_{i_1}^\dagger \otimes K_{i_2}^\dagger \otimes ... \otimes K_{i_N}^\dagger)
\end{aligned} \tag{2.59}$$

Thus, the quantum dynamical map Λ_{MS} can be characterized by m^N Kraus operators constructed by tensor product of the single particle Kraus operators, $\{K_1^{\text{MS}}, K_2^{\text{MS}}, ..., K_{m^N}^{\text{MS}}\} = \{K_1, K_2, ..., K_m\}^{\otimes N}$.

This approach to modelling noise of the mesoscopic system is applied in Chapter 3 where the effect of the depolarizing map on the mesoscopic system is evaluated *analytically*. Note that the number of Kraus operators grows exponentially with the size of the mesoscopic system, which significantly reduces the size of the mesoscopic systems that can be simulated.

Another practically helpful technique for estimating the noise effect on the mesoscopic system is to average over the independent transformations of each two-level component. Considering a product input state, the evolved state will be,

$$\begin{aligned}\Lambda'_{\mathrm{MS}}(\rho^{\mathrm{Pro}}_{\mathrm{MS}}) &= \frac{1}{N}\sum_{j=1}^{N}\rho_1\otimes...\otimes\Lambda_s(\rho_j)\otimes...\otimes\rho_N \\ &= \frac{1}{N}\sum_{j=1}^{N}\rho_1\otimes...\otimes\sum_{i=1}^{m}K_i\rho_jK_i^{\dagger}\otimes...\otimes\rho_N \end{aligned} \tag{2.60}$$

Thus, the map Λ'_{MS} is characterized by a set of $m\times N$ Kraus operators that is the union of Kraus operators on each particle scaled by $\frac{1}{\sqrt{N}}$ to satisfy the normalization condition, $\{K_1'^{\mathrm{MS}},K_2'^{\mathrm{MS}},...,K_{mN}'^{\mathrm{MS}}\}=\mathrm{U}_{j=1}^{N}\{K_1^j,K_2^j,...,K_m^j\}$ with $K_i^j=\frac{1}{\sqrt{N}}\mathbb{1}_2^{\otimes j-1}\otimes K_i^j\otimes\mathbb{1}_2^{\otimes N-j}$,

$$\Lambda'_{\mathrm{MS}}(\rho_{\mathrm{MS}})=\sum_{l=1}^{mN}K_l'^{\mathrm{MS}}\rho_{\mathrm{MS}}K_l'^{\mathrm{MS}\dagger} \tag{2.61}$$

This approach does not limit the size of the mesoscopic systems that can be simulated and is used is chapter 5 where a generalized amplitude damping noise is simulated for a mesoscopic spin system.

2.5 Quantification of entanglement

A pure bipartite state of a composite quantum system, $|\psi\rangle_{AB}$, is entangled, if and only if, the reduced state of each subsystem, $\rho_A=\mathrm{Tr}_B(|\psi\rangle\langle\psi|_{AB})$ or $\rho_B=\mathrm{Tr}_A(|\psi\rangle\langle\psi|_{AB})$, is a mixed state. The more entangled the pure bipartite state is, the more information is lost when one of the parties is ignored; thus, the more mixed the reduced density matrices are. The *entropy of entanglement* quantifies entanglement of pure bipartite states based on this property [42]. It is defined as the von Neumann entropy of any of the two reduced states,

$$\begin{aligned}E(|\psi\rangle_{AB}) &:= S(\rho_A)=S(\rho_B) \\ S(\rho) &:= -\mathrm{Tr}(\rho\log_2(\rho))\end{aligned} \tag{2.62}$$

where the equality $S(\rho_A) = S(\rho_B)$ follows the purity of the bipartite state $\rho_{AB} = |\psi\rangle\langle\psi|_{AB}$. The von Neumann entropy of a quantum state, $S(\rho)$, is a measure of its purity and ranges from 0 for pure states, to $D = \log_2(\mathrm{Dim}(\mathcal{H}))$ for a maximally mixed state. Consequently, the entropy of entanglement of a pure bipartite state $E(|\psi\rangle_{AB})$ ranges from 0 for separable states, to $\log_2(\min(\mathrm{Dim}(\mathcal{H}_A), \mathrm{Dim}(\mathcal{H}_B)))$. If $\mathrm{Dim}(\mathcal{H}_A) = \mathrm{Dim}(\mathcal{H}_B) := D$, the maximum, $\log_2(D)$, corresponds to a maximally entangled state,

$$|\psi\rangle_{AB} = \frac{1}{\sqrt{D}} \sum_{i=1}^{D} |i\rangle_A \otimes |i\rangle_B \tag{2.63}$$

where $\{|i\rangle_A\}$ and $\{|i\rangle_B\}$ are two arbitrary orthonormal bases of $\mathcal{H}_A$ and $\mathcal{H}_B$.

As an example, consider the pure bipartite entangled state of two qubits discussed in section 2.1, $|\psi\rangle_{AB} = a\,|00\rangle + b\,|11\rangle$. The reduced density matrices of the subsystems A and B are: $\rho_A = \rho_B = |a|^2\,|0\rangle\langle 0| + |b|^2\,|1\rangle\langle 1|$ and the entropy of entanglement is: $E(|\psi\rangle_{AB}) = S(\rho_A) = S(\rho_B) = -|a|^2 \log_2 |a|^2 - |b|^2 \log_2 |b|^2$.

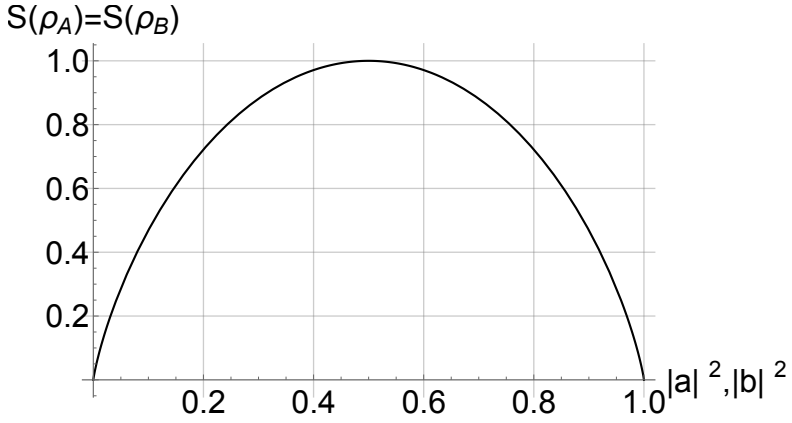

Figure 2.2: The entropy of entanglement of the state $|\psi\rangle_{AB} = a\,|00\rangle + b\,|11\rangle$. State $|\psi\rangle_{AB} = \frac{1}{\sqrt{2}}(|00\rangle + e^{i\phi}\,|11\rangle)$ is maximally entangled for any choice of ϕ.

Characterizing and quantifying entanglement of a mixed quantum state is challenging. Various measures have been proposed. Many of them, such as distillable entanglement [43, 44] and entanglement of projection [45], are generalizations of the entropy of entanglement and reduce to the entropy when applied to pure states. There are also measures that are defined independently, e.g. negativity and logarithmic negativity [46]. For reviews on entanglement and its measures see [47, 39]. In the rest of this section, we discuss

computable measures that are used in this thesis for quantifying bipartite entanglement between the target qubits or between one target qubit and the mesoscopic system.

2.5.1 Fidelity

When the goal is to produce a specific known maximally entangled state between two qubits, $|\phi\rangle_{AB}$, the fidelity, defined as the overlap between the produced state, ρ_{AB}, and the ideal state $|\phi\rangle_{AB}$, can be used as a measure for success of the preparation process,

$$F_{\phi}\left(\rho_{AB}\right) := Tr\left(|\phi\rangle\langle\phi|\,\rho_{AB}\right) = \langle\phi|\,\rho_{AB}\,|\phi\rangle\,. \tag{2.64}$$

The fidelity specifies whether or not the state ρ_{AB} can be distilled towards the maximally entangled state $|\phi\rangle_{AB}$ [44, 43]. It ranges from 0 to 1 and $F_{\phi}\left(\rho\right) > \frac{1}{2}$ guarantees that the state ρ_{AB} is entangled and distillable towards the state $|\phi\rangle_{AB}$.

Note that the fidelity is not a standard generally applicable measure for entanglement, e.g., the fidelity of the state $\rho_{AB} = |e_{+}\rangle\langle e_{+}|$ with the state $|e_{-}\rangle$ is zero but both states are maximally entangled; nevertheless it is easy to compute and is appropriate to use when it is known, *a priori*, that ρ_{AB} is a distorted version of $|\phi\rangle_{AB}$.

2.5.2 Negativity

Negativity is a measure of entanglement for a general bipartite system; regardless of the size of each party and purity of the overall state. For a bipartite system in an arbitrary state, ρ_{AB}, negativity is defined as [46, 39],

$$\mathcal{N}\left(\rho_{AB}\right) := \frac{||\rho_{AB}^{T_A}||_1 - 1}{2} \tag{2.65}$$

where $\rho_{AB}^{T_A}$ is the partial transpose of the state ρ_{AB} and $||X||_1 := \mathrm{Tr}(\sqrt{X^{\dagger}X})$ is the trace norm. Negativity is also equal to the sum of the absolute values of the negative eigenvalues of $\rho_{AB}^{T_A}$, $\mathcal{N}\left(\rho_{AB}\right) = \sum_{\lambda<0}|\lambda|$. It ranges from 0 for separable states to 0.5 for maximally entangled states.

The essence of this measure is based on the well-known positive partial transpose (PPT) criteria for bipartite separable states [48]. The PPT criteria states that for any separable state represented by a density matrix, the partial transpose with respect to one of the parities is also a valid density matrix thus it is a positive semi-definite operator and has only

non-negative eigenvalues. PPT is a necessary condition for separability for any dimension and any bi-partition. It is also a sufficient condition for $2 \otimes 2$ and $2 \otimes 3$ (partial transpose with respect to the second party) systems [49]. Thus, in general, if $\mathcal{N}(\rho_{AB}) > 0$ the state ρ_{AB} is entangled but $\mathcal{N}(\rho_{AB}) = 0$ does not prove separability.

A related measure of bipartite entanglement is logarithmic negativity defined as [46, 39],

$$E_{\mathcal{N}}(\rho_{AB}) := \log_2\left(||\rho_{AB}^{T_A}||_1\right) = \log_2(2\mathcal{N}(\rho_{AB}) + 1) \tag{2.66}$$

Logarithmic negativity ranges between 0 for separable states to 1 for maximally entangled states. These measures will be used to quantify entanglement between one qubit and a mesoscopic system.

2.5.3 Entanglement of projection

Entanglement of projection, introduced in [45], provides a simple computable measure of bipartite entanglement for mixed states regardless of the size of each party. Consider a bipartite mixed state, ρ_{AB}, with an arbitrary decomposition,

$$\rho_{AB} = \sum_{i=1}^{m} p_i \left|\psi_i\right\rangle\!\left\langle\psi_i\right|_{AB} \tag{2.67}$$

In the above decomposition, the states $\left|\psi_i\right\rangle_{AB}$ are not necessarily orthogonal and the number of the states, m, is equal to or bigger than the number of nonzero eigenvalues of ρ_{AB}. The state ρ_{AB} can be purified by adding a tagging particle,

$$\left|\Psi_{ABT}\right\rangle = \sum_{i=1}^{m} \sqrt{p_i}\left|\psi_i\right\rangle_{AB}\left|i\right\rangle_T \tag{2.68}$$

where the states $\left|i\right\rangle_T$ are orthogonal states of the taggant and $\rho_{AB} = \mathrm{Tr}_T(\left|\Psi_{ABT}\right\rangle\!\left\langle\Psi_{ABT}\right|)$. The entanglement of projection of ρ_{AB}, with respect to the purification in Eq. 2.68, is defined as,

$$E_{p\{|i\rangle\}_T}(\Psi_{ABT}) := \sum_{i=1}^{m} p_i E(\left|\psi_i\right\rangle_{AB}) \tag{2.69}$$

where $E(\left|\psi_i\right\rangle_{AB})$ is the entropy of entanglement defined in Eq. 2.62. Equation 2.69 can be interpreted as the average entanglement between systems A and B upon measuring the tagging particle projectively in the basis $\{\left|i\right\rangle_T\}$; this explains the idea behind the name *Entanglement of projection*.

Entanglement of projection depends on the basis in which the taggant is measured. Measuring the tagging particle in the basis $\{|i'\rangle_T = U|i\rangle_T\}$ results in Entanglement of projection $E_{p\{|i'\rangle\}_T}(\Psi_{ABT}) = \sum_{i=1}^m p'_i E(|\psi'_i\rangle_{AB})$ where $|\Psi_{ABT}\rangle = \sum_{i=1}^m \sqrt{p_i}\,|\psi_i\rangle_{AB}\,|i\rangle_T = \sum_{i=1}^m \sqrt{p'_i}\,|\psi'_i\rangle_{AB}\,|i'\rangle_T$. This change of basis of measuring the taggant corresponds to a different decomposition of the state of the system $\rho_{AB} = \sum_{i=1}^m p'_i\,|\psi'_i\rangle\langle\psi'_i|_{AB}$.

Entanglement of formation, which is a well-known measure for entanglement of mixed bipartite states, is defined as,

$$E_f(\rho_{AB}) := \min\left(\sum_{i=1}^m p_i E(|\psi_i\rangle_{AB})\right) \tag{2.70}$$

where the minimum is taken over all decompositions of ρ_{AB} [50]. The entanglement of formation can be written as the minimum of entanglement of projection over the choice of taggant's basis [45],

$$E_f(\rho_{AB}) = \min_U E_{p,\{U\}}(\Psi_{ABT}) \tag{2.71}$$

Thus, entanglement of projection with an arbitrary choice of taggant's basis provides an upper bound for entanglement of formation $E_f(\rho_{AB}) \leq E_{p,\{|i\rangle_T\}}(\Psi_{ABT})$.

Entanglement of projection will also be used to quantify entanglement between one target qubit and the mesoscopic system.

Chapter 3

Two successive projective measurements

Projective measurements are powerful tools that not only reveal the state of a quantum system but also prepare it in an eigenstate of the observable. Here, we present a general and simple procedure for entangling two non-interacting qubits through an intermediate mesoscopic spin system (MSS), that solely relies on projective measurements over the MSS. The MSS consists of an ensemble of identical spin half particles over which we have collective control and collective measurement[1]. Each target qubits is locally coupled to one nearby spin within the MSS [51], and universal control over the pair is available.

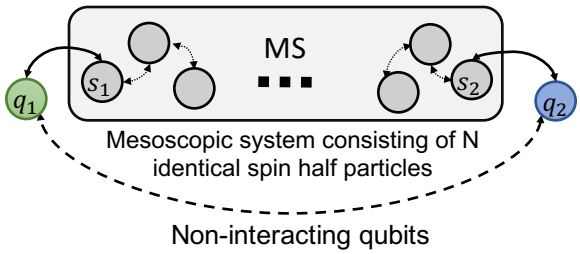

Figure 3.1: A schematic figure showing target qubits locally coupled to the mesoscopic system.

[1]Although, in this chapter, we refer to the mesoscopic system as the mesoscopic spin system, the arguments are not limited to spin systems only; they are valid for any mesoscopic system consisting of identical two-level quantum systems that can be measured collectively.

In this method, the target qubits are entangled by first entangling their nearby spins in the MSS, s_1 and s_2, then locally swapping the states between s_i and q_i $(i = 1, 2)$. Entanglement between s_1 and s_2 is achieved by successively applying two projective collective magnetization measurements on the MSS along the same axis e.g. z-axis and post-selecting on outcomes being the same. The first measurement reveals the total magnetization of all spins in the MSS, including s_1 and s_2, and the second measurement excludes s_1 and s_2. Excluding s_1 and s_2 in the measurement is feasible since the interaction of these two spins with the external qubits distinguishes them from the rest of the spins in the MSS. Post-selection on having identical outcomes implies opposite spins of s_1 and s_2, but it does not uncover whose state is up, $|\uparrow\rangle$, and whose is down, $|\downarrow\rangle$. With an appropriate initial state, this lack of information can be utilized to prepare s_1 and s_2 in the maximally entangled singlet, $|S\rangle = \frac{1}{\sqrt{2}}(|\uparrow\downarrow\rangle - |\downarrow\uparrow\rangle)$, or triplet zero, $\left|T^{(0)}\right\rangle = \frac{1}{\sqrt{2}}(|\uparrow\downarrow\rangle + |\downarrow\uparrow\rangle)$, state. This strategy entirely relies on the power of post-selected projective measurements and it has little additional requirements on the MSS in terms of purity of the initial state, control and size.

We will prove that a general and easy to generate class of states are suited as the initial state of the MSS. It suffices to prepare s_1 and s_2 in an equal superposition state, $|+\rangle = \frac{1}{\sqrt{2}}(|\uparrow\rangle + |\downarrow\rangle)$, separable from the rest of the spins in the MSS,

$$\rho_N = |+\rangle\langle+|_{s_1} \otimes |+\rangle\langle+|_{s_2} \otimes \rho_{N-2} \tag{3.1}$$

There are no requirements on the state of the MSS-$\{s_1, s_2\}$, ρ_{N-2} i.e., it can be any pure or mixed state. The ability to initialize the target qubits, q_1 and q_2, and universal control over the pairs of $\{q_1, s_1\}$ and $\{q_2, s_2\}$ is enough for preparing an initial state of the form 3.1. Two successive measurements on this initial state create the triplet zero state on s_1 and s_2 for any measurement outcomes as long as the two measurements have the same outcomes. The probability of success i.e., the probability of having the same outcomes for the two measurements is $\frac{1}{2}$. The singlet state can be produced simply by preparing an equal superposition state with positive phase, $|+\rangle$, on one of the spins and with negative phase, $|-\rangle = \frac{1}{\sqrt{2}}(|\uparrow\rangle - |\downarrow\rangle)$, on the other one.

The steps of the method can be summarized as:

1. Prepare the MSS in the initial state: $\rho_N = |+\rangle\langle+|_{s_1} \otimes |+\rangle\langle+|_{s_2} \otimes \rho_{N-2}$. The qubits are each prepared in any arbitrary state, separable from the state of the MSS, $\rho_{q_1} \otimes \rho_{q_2} \otimes \rho_N$.

2. Apply a projective collective magnetization measurement along z-axis on the MSS. The outcome of this measurement is called m_0.

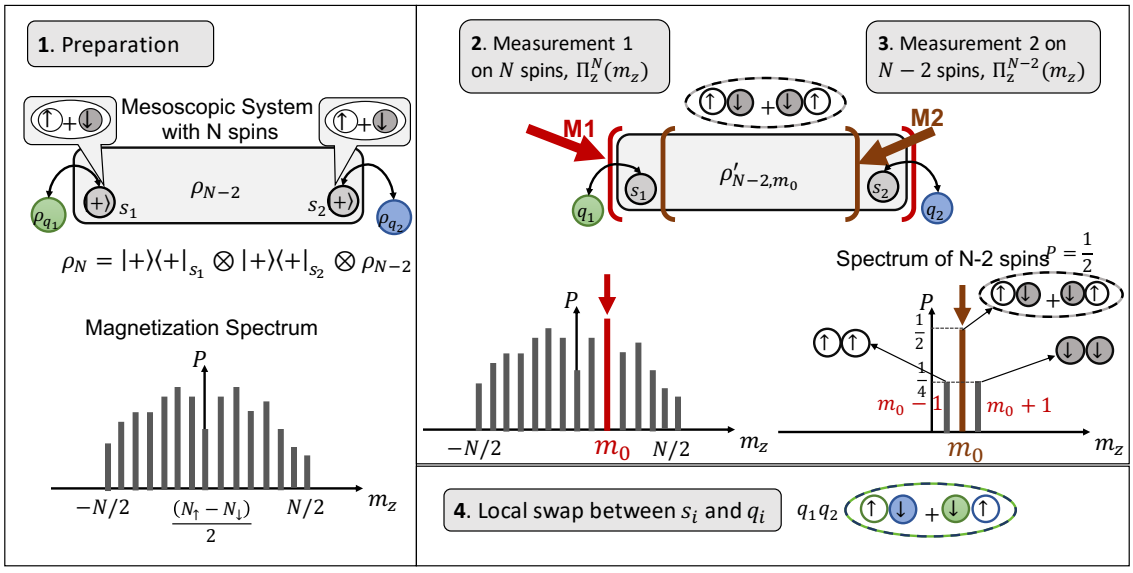

Figure 3.2: A schematic summary of the method

3. Apply a projective collective magnetization measurement along z-axis on the MSS excluding s_1 and s_2 and post-select on the same outcome as the previous measurement, m_0. The probability of having the same outcomes is $\frac{1}{2}$ and the updated state of s_1 and s_2 is the maximally entangled triplet zero state. The other two possible outcomes of this measurement are m_0-1 and m_0+1, each can happen with a probability of $\frac{1}{4}$.

4. Prepare q_1 and q_2 in the triplet zero entangled state by applying a swap gate between s_1 and q_1 and also between s_2 and q_2.

Figures 3.2 and 3.3 show a schematic and the quantum circuit of the two successive measurement procedure, respectively.

Implementing collective projective measurement on a mesoscopic spin system using one two-level probe spin is discussed in [52]. It is shown that to determine the collective magnetization of a mesoscopic system of size N, it is enough to prepare the probe spin and interact it with the mesoscopic system $\sim \log_2(N)$ times.

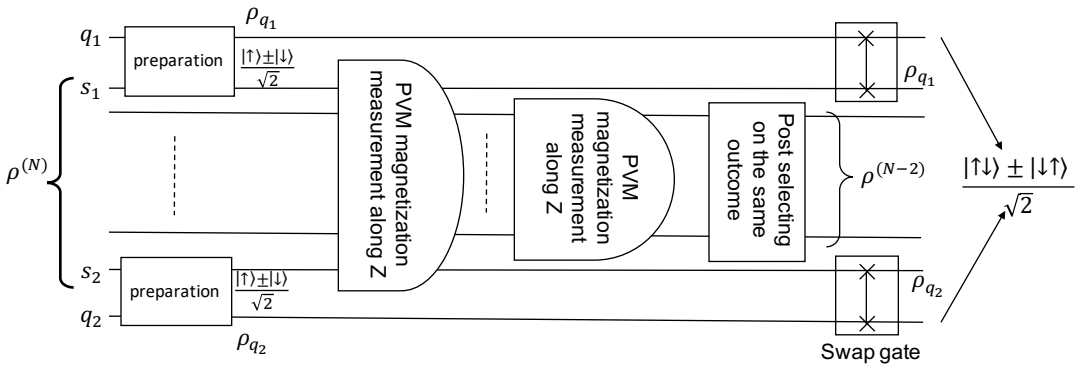

Figure 3.3: The quantum circuit summarizing the method

3.1 Proof

In this section we will analytically prove that the introduced procedure produces the maximally entangled triplet zero state over s_1 and s_2. We will also show that the probability of success is $\frac{1}{2}$.

The observable operator for the collective magnetization measurement along the quantization axis, z, for N spin half particles is,

$$J_z^{(N)} = \hbar \sum_{m=-\frac{N}{2}}^{\frac{N}{2}} m\Pi_m^{(N)}, \tag{3.2}$$

where $m \in \{-\frac{N}{2}, -\frac{N}{2}+1, ..., \frac{N}{2}\}$ is the outcome of the measurement up to the constant $\hbar$ which we set to 1 now on. The operator $\Pi_m^{(N)}$ projects onto a subspace where the difference in the number of spins in state $|\uparrow\rangle$ and in state $|\downarrow\rangle$ is $2m$. It can be expanded as,

$$\Pi_m^{(N)} = \sum_i P_i \left(|\uparrow\rangle\langle\uparrow|^{\otimes N/2+m} |\downarrow\rangle\langle\downarrow|^{\otimes N/2-m} \right) \tag{3.3}$$

where P_i is the permutation operator and the summation is over all possible permutations[2]. The outcome of the first projective measurement, m_0, is randomly chosen from

[2]The PVM collective magnetization measurement along the quantization axis is a physical implementation of Hamming weight measurement, introduced in section 2.3, for spin systems.

all possible outcomes according to the probability distribution, $\{P_{m_0}^{(N)}\} = \{\mathrm{Tr}\left(\Pi_{m_0}^{(N)}\rho_N\right)\}$. The updated state of the system after the measurement is,

$$\rho'_{N,m_0} = \frac{1}{P_{m_0}^{(N)}}\Pi_{m_0}^{(N)}\rho_N\Pi_{m_0}^{(N)} \tag{3.4}$$

To simplify the above equation, we rewrite $\Pi_{m_0}^{(N)}$ as a summation of projective operators on s_1 and s_2 tensor product with the projective operators on the rest of the spins in the MSS,

$$\begin{aligned}
\Pi_{m_0}^{(N)} &= \sum_i P_i \left(|\uparrow\rangle\langle\uparrow|^{\otimes N/2+m_0}\,|\downarrow\rangle\langle\downarrow|^{\otimes N/2-m_0}\right) \\
&= |\uparrow\uparrow\rangle\langle\uparrow\uparrow| \otimes \sum_i P'_i \left(|\uparrow\rangle\langle\uparrow|^{\otimes (N-2)/2+(m_0-1)}\,|\downarrow\rangle\langle\downarrow|^{\otimes (N-2)/2-(m_0-1)}\right) \\
&\quad + (|\uparrow\downarrow\rangle\langle\uparrow\downarrow| + |\downarrow\uparrow\rangle\langle\downarrow\uparrow|) \otimes \sum_i P''_i \left(|\uparrow\rangle\langle\uparrow|^{\otimes (N-2)/2+m_0}\,|\downarrow\rangle\langle\downarrow|^{\otimes (N-2)/2-m_0}\right) \\
&\quad + |\downarrow\downarrow\rangle\langle\downarrow\downarrow| \otimes \sum_i P'''_i \left(|\uparrow\rangle\langle\uparrow|^{\otimes (N-2)/2+(m_0+1)}\,|\downarrow\rangle\langle\downarrow|^{\otimes (N-2)/2-(m_0+1)}\right) \\
&= \Pi_1^{(2)} \otimes \Pi_{m_0-1}^{(N-2)} + \Pi_0^{(2)} \otimes \Pi_{m_0}^{(N-2)} + \Pi_{-1}^{(2)} \otimes \Pi_{m_0+1}^{(N-2)}
\end{aligned} \tag{3.5}$$

By substituting equation 3.5 in equation 3.4 and replacing ρ_N from equation 3.1 one finds,

$$\begin{aligned}
\rho'_{N,m_0} &= \frac{1}{4P_{m_0}^{(N)}} \Big(|\uparrow\uparrow\rangle\langle\uparrow\uparrow| \otimes \Pi_{m_0-1}^{(N-2)}\rho_{N-2}\Pi_{m_0-1}^{(N-2)} \\
&\quad + (|\uparrow\downarrow\rangle + |\downarrow\uparrow\rangle)\,(\langle\uparrow\downarrow| + \langle\downarrow\uparrow|) \otimes \Pi_{m_0}^{(N-2)}\rho_{N-2}\Pi_{m_0}^{(N-2)} \\
&\quad + |\downarrow\downarrow\rangle\langle\downarrow\downarrow| \otimes \Pi_{m_0+1}^{(N-2)}\rho_{N-2}\Pi_{m_0+1}^{(N-2)}\Big)
\end{aligned} \tag{3.6}$$

After applying the second projective measurement on $N-2$ spins and post-selecting on

the outcome m_0, the density matrix of the MSS will be updated to,

$$\begin{aligned}
\rho''_{N,m_0} &= \frac{\left(\mathbf{1}_2 \otimes \Pi_{m_0}^{(N-2)}\right) \rho'_{N,m_0} \left(\mathbf{1}_2 \otimes \Pi_{m_0}^{(N-2)}\right)}{\mathrm{Tr}\left(\left(\mathbf{1}_2 \otimes \Pi_{m_0}^{(N-2)}\right) \rho'_{N,m_0} \left(\mathbf{1}_2 \otimes \Pi_{m_0}^{(N-2)}\right)\right)} \\
&= \frac{\frac{1}{4P_{m_0}^{(N)}} \left(|\uparrow\downarrow\rangle + |\downarrow\uparrow\rangle\right) \left(\langle\uparrow\downarrow| + \langle\downarrow\uparrow|\right) \otimes \left(\Pi_{m_0}^{(N-2)} \rho_{N-2} \Pi_{m_0}^{(N-2)}\right)}{\frac{2P_{m_0}^{(N-2)}}{4P_{m_0}^{(N)}}} \\
&= \frac{1}{P_{m_0}^{(N-2)}} \left|T^{(0)}\right\rangle\!\left\langle T^{(0)}\right| \otimes \left(\Pi_{m_0}^{(N-2)} \rho_{N-2} \Pi_{m_0}^{(N-2)}\right)
\end{aligned} \tag{3.7}$$

where $P_{m_0}^{(N-2)} = \mathrm{Tr}\left(\Pi_{m_0}^{(N-2)} \rho_{N-2}\right)$ and $\frac{1}{P_{m_0}^{(N-2)}}$ is the normalization factor. Tracing over $N-2$ spins gives the state of s_1 and s_2,

$$\rho_{s_1 s_2} = \mathrm{Tr}_{(N-2)}\left(\rho''_{N,m_0}\right) = \frac{1}{P_{m_0}^{(N-2)}} \left|T^{(0)}\right\rangle\!\left\langle T^{(0)}\right| \mathrm{Tr}\left(\Pi_{m_0}^{(N-2)} \rho_{N-2} \Pi_{m_0}^{(N-2)}\right) = \left|T^{(0)}\right\rangle\!\left\langle T^{(0)}\right| \tag{3.8}$$

The above relation completes the proof for creating entangled state over s_1 and s_2. Next, we will show that the probability of success i.e., the probability of the same outcomes on both measurements, is $\frac{1}{2}$. Let's call the first measurement's outcome m_1 and the second measurement's outcome, m_2. Then the probability of success is,

$$\begin{aligned}
P_s &:= P(m_1 = m_2) = \sum_{m_0=-\frac{N-2}{2}}^{+\frac{N-2}{2}} P(m_1 = m_2 = m_0) \\
&= \sum_{m_0=-\frac{N-2}{2}}^{+\frac{N-2}{2}} P(m_1 = m_0) \times P(m_2 = m_0 | m_1 = m_0) \\
&= \sum_{m_0=-\frac{N-2}{2}}^{+\frac{N-2}{2}} P_{m_0}^{(N)} \times \mathrm{Tr}\left((\mathbb{1}_2 \otimes \Pi_{m_0}^{(N-2)}) \rho'_{N,m_0}\right)
\end{aligned} \tag{3.9}$$

Replacing ρ'_{N,m_0} with relation 3.4 results in,

$$P_s = \sum_{m_0=-\frac{N-2}{2}}^{+\frac{N-2}{2}} \mathrm{Tr}\left((\mathbb{1}_2 \otimes \Pi_{m_0}^{(N-2)}) \left(\Pi_{m_0}^{(N)} \rho_N \Pi_{m_0}^{(N)}\right)\right) \tag{3.10}$$

which can be simplified using relation 3.5 and the orthogonality of projection operators, $\Pi_m \Pi_n = \delta_{mn} \Pi_m$,

$$\begin{aligned} P_s &= \sum_{m_0=-\frac{N-2}{2}}^{+\frac{N-2}{2}} \mathrm{Tr}\left(\left(\Pi_0^{(2)} \otimes \Pi_{m_0}^{(N-2)}\right) \rho_N \Pi_{m_0}^{(N)}\right) \\ &= \mathrm{Tr}\left(\left(\Pi_0^{(2)} \otimes \left(\sum_{m_0=-\frac{N-2}{2}}^{+\frac{N-2}{2}} \Pi_{m_0}^{(N-2)}\right)\right) \rho_N\right) \\ &= \mathrm{Tr}\left(\left(\Pi_0^{(2)} \otimes \mathbb{1}_{N-2}\right) \rho_N\right) \end{aligned} \tag{3.11}$$

The second equality follows two properties of the trace function: cyclic invariance, $\mathrm{Tr}(ABC) = \mathrm{Tr}(CAB)$, and linearity, $\mathrm{Tr}(A+B) = \mathrm{Tr}(A) + \mathrm{Tr}(B)$. The third equality holds since the projection operators span the whole Hilbert space. The above relation proves that the probability of success, which is defined as the probability of equal outcome on both measurements, is equal to the probability of having zero total magnetization over s_1 and s_2. Replacing ρ_N by 3.1 completes the proof for $P_s = \frac{1}{2}$,

$$\begin{aligned} P_s &= \mathrm{Tr}\left(\left(\Pi_0^{(2)} \otimes \mathbb{1}_{N-2}\right) \left(|+\rangle\langle+|_{s_1} \otimes |+\rangle\langle+|_{s_2} \otimes \rho_{N-2}\right)\right) \\ &= \mathrm{Tr}\left(\Pi_0^{(2)} |+\rangle\langle+|_{s_1} \otimes |+\rangle\langle+|_{s_2}\right) \times \mathrm{Tr}\left(\rho_{N-2}\right) = \frac{1}{2} \times 1 = \frac{1}{2} \end{aligned} \tag{3.12}$$

3.2 Sensitivity to noise

A requirement for the success of the introduced procedure is that the collective magnetization of the MSS$-\{s_1, s_2\}$ is preserved between the two successive measurements. A single spin flip among the $N-2$ spins results in the outcome $|\uparrow\uparrow\rangle\langle\uparrow\uparrow|$ or $|\downarrow\downarrow\rangle\langle\downarrow\downarrow|$ instead of the maximally entangled state $\left|T^{(0)}\right\rangle\left\langle T^{(0)}\right|$. Thus, assuming instantaneous measurements, the time constant of the spin flip error, T_{bf}, divided by the number of spins needs be large compared to the time between the measurements, Δt, $T_{\mathrm{bf}}/N \gg \Delta t$. We can account for the measurements' time by adding the duration of the second measurement, t_2, $T_{\mathrm{bf}}/N \gg \Delta t + t_2$. Moreover, no bit flip or phase flip on s_1 and s_2 is acceptable during the experiment.

In this section, we analyze how the entangled state of the qubits is degraded due to the mentioned errors, assuming that the time constant of the errors is long compared to

the experiment time. To include both spin flip on $N-2$ spins in the MSS, and phase flip and spin flip on s_1 and s_2, we model noise on the MSS as a depolarizing map, acting independently on each of the spins. Depolarizing map on a qubit corresponds symmetric noise in all directions i.e. equal probability of the three possible errors: bit flip (σ_x), phase flip (σ_z) and bit-phase flip (σ_y). It operates on a qubit's state as, $\Lambda(\rho) = (1-\lambda)\rho + \lambda\frac{\mathbb{1}}{2}$. With the probability of $1-\lambda$ the state is intact and with the probability of λ it is replaced by the maximally mixed state. We will show that the entangled state of the spins after the second measurement up to the first order in λ is,

$$\begin{aligned}\rho_{s_1 s_2}(\lambda) &= \left(1 - \frac{N\lambda}{4} - 2\lambda\right)\left|T^{(0)}\right\rangle\!\left\langle T^{(0)}\right| + \frac{\lambda}{2}\left(|\uparrow\downarrow\rangle\langle\uparrow\downarrow| + |\downarrow\uparrow\rangle\langle\downarrow\uparrow|\right) \\ &+ \frac{N\lambda}{8}\left(1 + \frac{2m_0+4}{N}\right)|\uparrow\uparrow\rangle\langle\uparrow\uparrow| + \frac{N\lambda}{8}\left(1 - \frac{2m_0-4}{N}\right)|\downarrow\downarrow\rangle\langle\downarrow\downarrow| \end{aligned} \tag{3.13}$$

where m_0 is the outcome of the measurements and we have used the simplifying assumption, $\mathrm{Tr}(\Pi^{(N-2)}_{m_0-1}\rho_{N-2}) \approx \mathrm{Tr}(\Pi^{(N-2)}_{m_0}\rho_{N-2}) \approx \mathrm{Tr}(\Pi^{(N-2)}_{m_0+1}\rho_{N-2})$. The main source of error is leakage into $\{|\uparrow\uparrow\rangle\langle\uparrow\uparrow|, |\downarrow\downarrow\rangle\langle\downarrow\downarrow|\}$ subspace which is associated to bit flip on $N-2$ spins in the MSS and scales as $N\lambda$. A small portion of error, proportional to λ, comes from reduction in the off-diagonal terms of $\left|T^{(0)}\right\rangle\!\left\langle T^{(0)}\right|$ with respect to the diagonal terms, which is resulting from phase flip error of s_1 and s_2. The fidelity of $\rho_{s_1 s_2}(\lambda)$ with the maximally entangled state, $\left|T^{(0)}\right\rangle$, up to the first order in λ is,

$$F_{T^{(0)}}\left(\rho_{s_1 s_2}(\lambda)\right) = \mathrm{Tr}\left(\left|T^{(0)}\right\rangle\!\left\langle T^{(0)}\right|\rho_{s_1 s_2}(\lambda)\right) = 1 - \frac{N\lambda}{4} - \frac{3\lambda}{4} \tag{3.14}$$

As derived in section 2.4, the probability of error in each of the three directions is proportional to λ, $p_{\mathrm{bf}} = p_{\mathrm{pf}} = p_{\mathrm{bpf}} = p/3 = \lambda/4$. Moreover, the probability of each error is related to the time between the two measurements and the second measurement duration as, $p/3 = \frac{\Delta t + t_2}{T_{\mathrm{error}}}$, where $T_{\mathrm{error}} = T_{\mathrm{bf}} = T_{\mathrm{pf}} = T_{\mathrm{bpf}}$ is the time constant of the errors. Thus, the fidelity being close to one requires,

$$\frac{N\lambda}{4} \ll 1 \Rightarrow \frac{Np}{3} \ll 1 \Rightarrow N\frac{\Delta t + t_2}{T_{\mathrm{error}}} \ll 1 \Rightarrow \Delta t + t_2 \ll \frac{T_{\mathrm{error}}}{N}. \tag{3.15}$$

3.2.1 Proof

Here, we prove that the ideal maximally entangled state of the qubits, $\left|T^{(0)}\right\rangle\!\left\langle T^{(0)}\right|$, degrades to the state in Eq. 3.13, when spins in the MSS are subject to the depolarizing noise.

The state of the MSS after the first measurement and post-selection on outcome m_0, given in equation 3.6, can be rewritten as,

$$\rho'_{N,m_0} = \frac{1}{4}\left(|\uparrow\uparrow\rangle\langle\uparrow\uparrow| \otimes \rho_{N-2}^{m_0-1} + |\downarrow\downarrow\rangle\langle\downarrow\downarrow| \otimes \rho_{N-2}^{m_0+1} + 2\left|T^{(0)}\right\rangle\left\langle T^{(0)}\right| \otimes \rho_{N-2}^{m_0}\right) \tag{3.16}$$

where $\rho_{N-2}^{m_0-1} = \Pi_{m_0-1}^{(N-2)}\rho_{N-2}\Pi_{m_0-1}^{(N-2)}/P_{m_0}^{(N)}$, $\rho_{N-2}^{m_0+1} = \Pi_{m_0+1}^{(N-2)}\rho_{N-2}\Pi_{m_0+1}^{(N-2)}/P_{m_0}^{(N)}$ and $2\rho_{N-2}^{m_0} = 2\Pi_{m_0}^{(N-2)}\rho_{N-2}\Pi_{m_0}^{(N-2)}/P_{m_0}^{(N)}$ are the states of the MSS$-\{s_1, s_2\}$ after the first measurement (not necessarily normalized) correlated to the states $|\uparrow\uparrow\rangle\langle\uparrow\uparrow|$, $|\downarrow\downarrow\rangle\langle\downarrow\downarrow|$ and $\left|T^{(0)}\right\rangle\left\langle T^{(0)}\right|$ of s_1 and s_2 respectively. If no error happens, the second measurement with post selection on m_0 projects the state of the MSS into the state $\left|T^{(0)}\right\rangle\left\langle T^{(0)}\right| \otimes \rho_{N-2}^{m_0}$.

We consider depolarization of the MSS as independent maps on all of the spins in the MSS each with probability λ. The depolarizing channel acts as following on each of the terms of one spin's density matrix,

$$\begin{aligned}
\Lambda\left(|\uparrow\rangle\langle\uparrow|\right) &= \left(1-\frac{\lambda}{2}\right)|\uparrow\rangle\langle\uparrow| + \frac{\lambda}{2}|\downarrow\rangle\langle\downarrow| \\
\Lambda\left(|\downarrow\rangle\langle\downarrow|\right) &= \left(1-\frac{\lambda}{2}\right)|\downarrow\rangle\langle\downarrow| + \frac{\lambda}{2}|\uparrow\rangle\langle\uparrow| \\
\Lambda\left(|\uparrow\rangle\langle\downarrow|\right) &= (1-\lambda)|\uparrow\rangle\langle\downarrow| \\
\Lambda\left(|\downarrow\rangle\langle\uparrow|\right) &= (1-\lambda)|\downarrow\rangle\langle\uparrow|
\end{aligned} \tag{3.17}$$

The state of the MSS after the first measurement is depolarized as,

$$\begin{aligned}
\Lambda(\rho'_{N,m_0}) = \frac{1}{4}\Big(&\Lambda(|\uparrow\rangle\langle\uparrow|) \otimes \Lambda(|\uparrow\rangle\langle\uparrow|) \otimes \Lambda(\rho_{N-2}^{m_0-1}) + \Lambda(|\downarrow\rangle\langle\downarrow|) \otimes \Lambda(|\downarrow\rangle\langle\downarrow|) \otimes \Lambda(\rho_{N-2}^{m_0+1}) \\
&+2\Lambda(\left|T^{(0)}\right\rangle\left\langle T^{(0)}\right|) \otimes \Lambda(\rho_{N-2}^{m_0})\Big)
\end{aligned} \tag{3.18}$$

After the second measurement on $N-2$ spins in the MSS and post selection on outcome m_0 the state of the MSS is,

$$\begin{aligned}
\rho''_{N,m_0}(\lambda) = \frac{1}{\mathrm{Tr}(...)}\Big(&\Lambda(|\uparrow\rangle\langle\uparrow|) \otimes \Lambda(|\uparrow\rangle\langle\uparrow|) \otimes (\Pi_{m_0}^{(N-2)}\Lambda(\rho_{N-2}^{m_0-1})\Pi_{m_0}^{(N-2)}) \\
&+ \Lambda(|\downarrow\rangle\langle\downarrow|) \otimes \Lambda(|\downarrow\rangle\langle\downarrow|) \otimes (\Pi_{m_0}^{(N-2)}\Lambda(\rho_{N-2}^{m_0+1})\Pi_{m_0}^{(N-2)}) \\
&+ 2\Lambda(\left|T^{(0)}\right\rangle\left\langle T^{(0)}\right|) \otimes (\Pi_{m_0}^{(N-2)}\Lambda(\rho_{N-2}^{m_0})\Pi_{m_0}^{(N-2)})\Big)
\end{aligned} \tag{3.19}$$

The overlap between $\Lambda(\rho_{N-2}^{m_0+1})$ and $\Lambda(\rho_{N-2}^{m_0-1})$ and $\Pi_{m_0}^{(N-2)}$ is of the first order in λ; thus, to compute the above relation up to first order in λ it is enough to keep $\Lambda(|\uparrow\rangle\langle\uparrow|)$ and

$\Lambda(|\downarrow\rangle\langle\downarrow|)$ to the zeroth order. Tracing over MSS-$\{s_1, s_2\}$ the state of s_1 and s_2 up to the first order is λ is,

$$\begin{aligned}\rho_{s_1 s_2}(\lambda) &= \frac{1}{\mathrm{Tr}(...)}\left(\mathrm{Tr}((\Pi_{m_0}^{(N-2)}\Lambda(\rho_{N-2}^{m_0-1}))\,|\uparrow\uparrow\rangle\langle\uparrow\uparrow| + \mathrm{Tr}(\Pi_{m_0}^{(N-2)}\Lambda(\rho_{N-2}^{m_0+1}))\,|\downarrow\downarrow\rangle\langle\downarrow\downarrow|\right.\\ &\left. + 2\mathrm{Tr}((\Pi_{m_0}^{(N-2)}\Lambda(\rho_{N-2}^{m_0}))\Lambda(\left|T^{(0)}\right\rangle\left\langle T^{(0)}\right|)\right) \qquad (3.20)\end{aligned}$$

The state $\rho_{s_1 s_2}(\lambda)$ deviates from the maximally entangled $\left|T^{(0)}\right\rangle\left\langle T^{(0)}\right|$ state mainly because of leakage into $\{|\uparrow\uparrow\rangle\langle\uparrow\uparrow|, |\downarrow\downarrow\rangle\langle\downarrow\downarrow|\}$ subspace and also because of loss in the coherence. depolarization of the state $\left|T^{(0)}\right\rangle\left\langle T^{(0)}\right|$ up to the first order in λ is,

$$\begin{aligned}\Lambda(\left|T^{(0)}\right\rangle\left\langle T^{(0)}\right|) &= \frac{1-\lambda}{2}\left(|\uparrow\downarrow\rangle\langle\uparrow\downarrow| + |\downarrow\uparrow\rangle\langle\downarrow\uparrow|\right) + \frac{1-2\lambda}{2}\left(|\uparrow\downarrow\rangle\langle\downarrow\uparrow| + |\downarrow\uparrow\rangle\langle\uparrow\downarrow|\right)\\ &+ \frac{\lambda}{2}\left(|\uparrow\uparrow\rangle\langle\uparrow\uparrow| + |\downarrow\downarrow\rangle\langle\downarrow\downarrow|\right)\\ &= (1-2\lambda)\left|T^{(0)}\right\rangle\left\langle T^{(0)}\right| + \frac{\lambda}{2}\mathbb{1}_2 \qquad (3.21)\end{aligned}$$

In order to compute $\Lambda\left(\rho_{N-2}^k\right)$, we expand the state ρ_{N-2}^k with $k = m_0 - 1, m_0, m_0 + 1$ in $\{|\uparrow\rangle, |\downarrow\rangle\}$ basis,

$$\begin{aligned}\rho_{N-2}^k &= \sum_{i,j=1}^{\binom{N-2}{\frac{N-2}{2}+k}} a_{ij}^k P_i(|\uparrow\rangle^{\otimes\frac{N-2}{2}+k}|\downarrow\rangle^{\otimes\frac{N-2}{2}-k})P_j(\langle\uparrow|^{\otimes\frac{N-2}{2}+k}\langle\downarrow|^{\otimes\frac{N-2}{2}-k})\\ &= \sum_{i=1}^{\binom{N-2}{\frac{N-2}{2}+k}} a_{ii}^k P_i(|\uparrow\rangle\langle\uparrow|^{\otimes\frac{N-2}{2}+k}\otimes|\downarrow\rangle\langle\downarrow|^{\frac{N-2}{2}-k}) + \text{off diagonal terms} \qquad (3.22)\end{aligned}$$

where P_i is the permutation operator and the summations are over all possible permutations. In order to compute $\mathrm{Tr}((\Pi_{m_0}^{(N-2)}\Lambda(\rho_{N-2}^k))$, we only need to keep track of the diagonal terms of ρ_{N-2}^k since the off-diagonal terms would remain off-diagonal after applying the depolarizing map and they would vanish either when projecting into m_0 magnetization subspace or when computing the trace.

$$\begin{aligned}\Lambda(\rho_{N-2}^k) = \sum_{i=1}^{\binom{N-2}{\frac{N-2}{2}+k}} a_{ii}^k \quad P_i \quad &\left(\left((1-\frac{\lambda}{2})\,|\uparrow\rangle\langle\uparrow| + \frac{\lambda}{2}\,|\downarrow\rangle\langle\downarrow|\right)^{\otimes\frac{N-2}{2}+k}\right. \qquad (3.23)\\ &\left.\otimes\left((1-\frac{\lambda}{2})\,|\downarrow\rangle\langle\downarrow| + \frac{\lambda}{2}\,|\uparrow\rangle\langle\uparrow|\right)^{\otimes\frac{N-2}{2}-k}\right) + \text{off diagonal terms}\end{aligned}$$

To the first order in λ, $\Lambda(\rho_{N-2}^k)$ is,

$$\begin{aligned}
\Lambda(\rho_{N-2}^k) &= \sum_{i=1}^{\binom{N-2}{\frac{N-2}{2}+k}} a_{ii}^k \left(1-(N-2)\frac{\lambda}{2}\right) P_i(|\uparrow\rangle\langle\uparrow|^{\otimes\frac{N-2}{2}+k}\,|\downarrow\rangle\langle\downarrow|^{\frac{N-2}{2}-k}) \\
&+ \sum_{i=1}^{\binom{N-2}{\frac{N-2}{2}+k}} a_{ii}^k \frac{\lambda}{2} P_i\left(\left(\sum_{j=1}^{\binom{\frac{N-2}{2}+k}{1}} P_j(|\downarrow\rangle\langle\downarrow|\otimes|\uparrow\rangle\langle\uparrow|^{\otimes\frac{N-2}{2}+k-1})\right)\otimes|\downarrow\rangle\langle\downarrow|^{\frac{N-2}{2}-k}\right) \\
&+ \sum_{i=1}^{\binom{N-2}{\frac{N-2}{2}+k}} a_{ii}^k \frac{\lambda}{2} P_i\left(|\uparrow\rangle\langle\uparrow|^{\frac{N-2}{2}+k}\otimes\left(\sum_{j=1}^{\binom{\frac{N-2}{2}-k}{1}} P_j(|\uparrow\rangle\langle\uparrow|\otimes|\downarrow\rangle\langle\downarrow|^{\otimes\frac{N-2}{2}-k-1})\right)\right) \\
&+ \text{off diagonal terms}
\end{aligned} \tag{3.24}$$

For $k = m_0-1, m_0, m_0+1$, $\mathrm{Tr}((\Pi_{m_0}^{(N-2)}\Lambda(\rho_{N-2}^k))$ is,

$$\mathrm{Tr}\left((\Pi_{m_0}^{(N-2)}\Lambda(\rho_{N-2}^{m_0})\right) = \left(1-(N-2)\frac{\lambda}{2}\right)\sum_{i=1}^{\binom{N-2}{\frac{N-2}{2}+m_0}} a_{ii}^{m_0} = \left(1-(N-2)\frac{\lambda}{2}\right)\mathrm{Tr}(\rho_{N-2}^{m_0}) \tag{3.25}$$

$$\mathrm{Tr}\left((\Pi_{m_0}^{(N-2)}\Lambda(\rho_{N-2}^{m_0-1})\right) = \frac{\lambda}{2}\left(\frac{N-2}{2}-(m_0-1)\right)\sum_{i=1}^{\binom{N-2}{\frac{N}{2}+m_0-2}} a_{ii}^{m_0-1} = \frac{\lambda}{2}\left(\frac{N}{2}-m_0\right)\mathrm{Tr}(\rho_{N-2}^{m_0-1})$$

$$\mathrm{Tr}\left((\Pi_{m_0}^{(N-2)}\Lambda(\rho_{N-2}^{m_0+1})\right) = \frac{\lambda}{2}\left(\frac{N-2}{2}+(m_0+1)\right)\sum_{i=1}^{\binom{N}{\frac{N}{2}+m_0}} a_{ii}^{m_0+1} = \frac{\lambda}{2}\left(\frac{N}{2}+m_0\right)\mathrm{Tr}(\rho_{N-2}^{m_0+1})$$

where $\mathrm{Tr}(\rho_{N-2}^{m_0}) = \mathrm{Tr}(\Pi_{m_0}^{(N-2)}\rho_{N-2})/\mathrm{Tr}(\Pi_{m_0}^{(N)}\rho_N)$ is the probability of having magnetization m_0 on $N-2$ spins in the MSS conditioned on magnetization m_0 of the whole MSS. Similarly $\mathrm{Tr}(\rho_{N-2}^{m_0-1}) = \mathrm{Tr}(\Pi_{m_0-1}^{(N-2)}\rho_{N-2})/\mathrm{Tr}(\Pi_{m_0}^{(N)}\rho_N)$ and $\mathrm{Tr}(\rho_{N-2}^{m_0+1}) = \mathrm{Tr}(\Pi_{m_0+1}^{(N-2)}\rho_{N-2})/\mathrm{Tr}(\Pi_{m_0}^{(N)}\rho_N)$ are the probabilities of having magnetization m_0-1 and m_0+1 on $N-2$ spins in the MSS conditioned on outcome m_0 of the first measurement. Replacing the equations 3.21 and 3.25 in the equation 3.20, the state of s_1 and s_2 after the second measurement and post selection on m_0, the same outcome as the first measurement, is,

$$\begin{aligned}
\rho_{s_1s_2}(\lambda) &= \frac{1}{\mathrm{Tr}(...)}\left(2\left((1-N\frac{\lambda}{2}-\lambda)\left|T^{(0)}\right\rangle\!\left\langle T^{(0)}\right| + \frac{\lambda}{2}\mathbb{1}_2\right)\mathrm{Tr}(\rho_{N-2}^{m_0})\right. \\
&+ \left.\frac{\lambda}{2}\left(\frac{N}{2}+m_0\right)\mathrm{Tr}(\rho_{N-2}^{m_0-1})\,|\uparrow\uparrow\rangle\langle\uparrow\uparrow| + \frac{\lambda}{2}\left(\frac{N}{2}-m_0\right)\mathrm{Tr}(\rho_{N-2}^{m_0+1})\,|\downarrow\downarrow\rangle\langle\downarrow\downarrow|\right)
\end{aligned} \tag{3.26}$$

With the simplifying assumption $\mathrm{Tr}(\rho_{N-2}^{m_0}) \approx \mathrm{Tr}(\rho_{N-2}^{m_0-1}) \approx \mathrm{Tr}(\rho_{N-2}^{m_0+1})$ and including the normalization factor the above relation reduces to,

$$\begin{aligned}
\rho_{s_1 s_2}(\lambda) &\approx \left(1 - \frac{N\lambda}{4} - 2\lambda\right) \left|T^{(0)}\right\rangle\!\left\langle T^{(0)}\right| + \frac{\lambda}{2}\mathbb{1}_2 + \frac{N\lambda}{8}\left(1 + \frac{2m_0}{N}\right)|\uparrow\uparrow\rangle\langle\uparrow\uparrow| \\
&+ \frac{N\lambda}{8}\left(1 - \frac{2m_0}{N}\right)|\downarrow\downarrow\rangle\langle\downarrow\downarrow| \\
&= \left(1 - \frac{N\lambda}{4} - 2\lambda\right) \left|T^{(0)}\right\rangle\!\left\langle T^{(0)}\right| + \frac{\lambda}{2}\left(|\uparrow\downarrow\rangle\langle\uparrow\downarrow| + |\downarrow\uparrow\rangle\langle\downarrow\uparrow|\right) \\
&+ \frac{N\lambda}{8}\left(1 + \frac{2m_0+4}{N}\right)|\uparrow\uparrow\rangle\langle\uparrow\uparrow| + \frac{N\lambda}{8}\left(1 - \frac{2m_0-4}{N}\right)|\downarrow\downarrow\rangle\langle\downarrow\downarrow| \qquad (3.27)
\end{aligned}$$

This relation completes the proof for equation 3.13.

3.3 Mesoscopic system requirements

The introduced method requires a very high-resolution measurement on the MSS, capable of detecting a single spin flip. The magnetization of the $N-2$ spins in the mesoscopic system must be preserved between the two measurements. This criterion requires the time constant of the error, T_{error}, to be long compared to the experiment time and the internal interaction among the spins in the mesoscopic system to be either compatible with the measurement operators or weak enough to not influence the total magnetization. There should also be no magnetization exchange between s_1 and s_2 and the rest of the spins in the mesoscopic system to preserve their separable initial state. On the other hand, this method needs only preparation of two of the spins in the MSS, s_1 and s_2, which can be accomplished through their interaction with the target qubits. The rest of the spins can be in any mixed or pure state. Any number of spins in the mesoscopic system is admissible as long as the MSS's magnetization can be measured with resolution $\Delta m = 1$, and no spin flip happens after the first measurement, $N(t + t_2) \ll T_{\mathrm{bf}}$.

3.4 Conclusion

In this chapter, we introduced a procedure based on projective collective magnetization measurements for entangling two non-interacting qubits, that are locally coupled to a MSS. The presented approach has little requirements on the initial state of the MSS but it needs very high resolution measurements. The success of this method solely relies on the power

of projective measurements and it does not take advantage from the large number of spins in the MSS. In the next chapter, we build on this strategy by introducing a scheme that benefits from the large size of the MSS to amplify the state of the target qubits, and needs only coarse-grained collective measurements on the MSS.

Chapter 4

Indirect Joint measurement

In this chapter, we presents a new method for entangling two non-interacting qubits by measuring their parity or hamming weight indirectly through an intermediate mesoscopic system.

4.1 Introduction

We show how a mesoscopic system (MS) can entangle two qubits by measuring the parity of the two qubits' wave-function. The role of the MS is to magnify the qubits' parity such that the distinguishability of the two parity outcomes grows linearly with the MS's size. The initial state is separable over each qubit, and the qubits interact only with the MS. Relying only on collective control of the MS, a low-resolution collective measurement is still sufficient to prepare a post-selected entangled state with high confidence.

A parity measurement is a two-outcome measurement that determines whether an even or odd number of qubits is in a particular logical state. For two qubits, each prepared in an equal superposition state, a projective measurement that reveals the qubits' parity but provides no information on individual qubits creates a post-selected entangled Bell state. Procedures for entangling two qubits through parity measurement have been proposed for different quantum systems [53, 54, 55, 56, 57, 58] and performed experimentally with superconducting qubits [59, 60, 61, 62] and nuclear spins next to a nitrogen-vacancy center in diamond [63].

Here we propose implementing a projective parity measurement on two qubits indirectly through a MS. The MS in this model consists of hundreds to thousands of identical two-level

systems over which we have collective control [1]. This method leverages local interactions between each qubit and the MS and global control over the MS to correlate the two parity states of the qubits with the distinguishable collective states of the MS. Global measurement of the MS and post-selection then creates an entangled state on the qubits due to the qubits' correlation with the MS. This indirect measurement must detect on the order of N excitations, where N is the MS's size, unlike single qubit flip detection required in direct parity measurement of qubits.

Previous proposals on entangling two qubits via an intermediate MS have used the MS to generate an effective interaction Hamiltonian between the target qubits [14, 19]. In contrast, our novel approach relies solely on indirect joint measurement of the qubits facilitated by the MS. By relying only upon the measurement, the distinguishability of the states of the MS corresponding to different parities of the qubits is a natural parameter for the success of our protocol. This distinguishability can be characterized over the classical probability distributions of the measurement outcomes. This characterization helps us derive a rigid upper bound for entanglement of the target qubits as a function of the MS's size and initial polarization. Our analysis complements ongoing efforts to control the quantum aspects of MSs for quantum processing and metrology [64, 65, 19, 66, 67, 68, 14].

In this chapter, we introduce the general scheme for indirect parity measurement of two qubits through a MS. In section 4.2, we present the general circuit consisting of the evolution, measurement and post-processing steps and determine the success criteria of the protocol. We explain the method with some idealized examples emphasizing on the role of the evolution step which magnifies the qubits' parity in the collective state of the MS. We show that collective control of the MS and local interaction between the qubits and the MS is enough to implement this magnification. In section 4.3 we discuss the measurement step, demonstrating that a course-grained two outcome collective measurement on the MS with post-selection is sufficient for producing maximally entangled states on the qubits. In section 4.4, we consider the effect of beginning with a non-ideal mixed initial state of the MS and find a rigid upper bound on the qubits' entanglement caused by MS's limited polarization. Finally in the conclusion section 4.5 we summarize the results and discuss the future works.

[1] An example of this ensemble of identical two-level systems is an ensemble of spin half particles as will be discussed in the next chapter 5. But the general indirect joint measurement procedure is not only limited to spin systems. To emphasize on this generality we do not refer to the elements of the mesoscopic system as spins in this chapter.

4.2 General circuit

FIG. 4.1 shows a schematic of the proposed indirect parity measurement circuit. Each qubit is prepared in the coherent $|+\rangle = \frac{1}{\sqrt{2}}(|0\rangle+|1\rangle)$ state, and the MS is provisionally prepared in the polarized state, $|0\rangle^{\otimes N}$. The MS evolves conditional on the qubits' state with the general unitary, $U_{q,MS} = |00\rangle\langle 00|_q \otimes U_{00}^{MS} + |01\rangle\langle 01|_q \otimes U_{01}^{MS} + |10\rangle\langle 10|_q \otimes U_{10}^{MS} + |11\rangle\langle 11|_q \otimes U_{11}^{MS}$, creating the following entangled state of the qubits and MS,

$$\begin{aligned} |\psi\rangle_{q,MS} &= \frac{1}{2}(|00\rangle \otimes |\psi_{00}\rangle + |01\rangle \otimes |\psi_{01}\rangle \\ &+ |10\rangle \otimes |\psi_{10}\rangle + |11\rangle \otimes |\psi_{11}\rangle) \end{aligned} \tag{4.1}$$

with $|\psi_\gamma\rangle = U_\gamma^{MS} |0\rangle^{\otimes N}$ for $\gamma = 00, 01, 10, 11$.

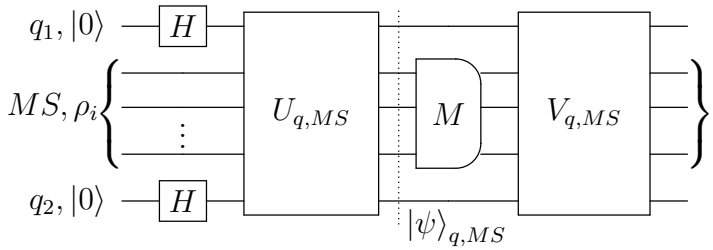

Figure 4.1: The general circuit of the parity measurement through an intermediate MS.

The evolution is followed by a Positive-Operator Valued Measure (POVM) of the collective excitation on the MS and post-selection with the measurement operators $\{E_\alpha\}$ and the state-update-rule, $\rho_{MS;\alpha} = \frac{\sqrt{E_\alpha}.\rho_{MS}.\sqrt{E_\alpha}}{Tr(E_\alpha.\rho_{MS})}$. ρ_{MS} and $\rho_{MS;\alpha}$ are the MS's states before and after the measurement with post-selecting the outcome α, respectively [2]. For a mesoscopic *spin* system, this measurement corresponds to a total angular momentum measurement. Adding the qubits, the state-update-rule becomes,

$$\begin{aligned} \rho_{q,MS;\alpha} &= \frac{(\mathbb{1}_2 \otimes \sqrt{E_\alpha}).\rho_{q,MS}.(\mathbb{1}_2 \otimes \sqrt{E_\alpha})}{Tr((\mathbb{1}_2 \otimes E_\alpha).\rho_{q,MS})} \\ E_\alpha &= \sum_{m=0}^{N} a_{\alpha,m}\Pi(m), \;\; m = 0, 1, ..., N \end{aligned} \tag{4.2}$$

[2] There is no general state-update-rule for the POVMs, and the post-measurement state depends on the details of the measurement procedure. Nevertheless any POVM is operationally equivalent to a von Neumann indirect measurement, which follows the mentioned state-update-rule. [38].

where $\Pi(m)$ is the operator that projects into the subspace with m excitations and the coefficients $a_{\alpha,m}$ satisfy the conditions $0 \leq a_{\alpha,m} \leq 1$ and $\sum_\alpha a_{\alpha,m} = 1$, so that the POVM operators satisfy both the positivity, $E_\alpha \geq 0$, and trace-preserving, $\sum_\alpha E_\alpha = \mathbb{1}$, conditions.

To measure the target qubits' parity, the combination of the evolution and measurement must be such that the two pairs of states $\{|\psi_{01}\rangle, |\psi_{10}\rangle\}$ *and* $\{|\psi_{00}\rangle, |\psi_{11}\rangle\}$*, called the odd and even pair, respectively, are discerned by the measurement but the states in each pair are not.*

With this criterion, the measurement and post-selection project the target qubits' state into even or odd parity subspaces due to its correlation with the MS's state. If the MS's states within the odd and even pair are identical, post-selection on the measurement outcome ideally updates the state of the qubits to one of the two maximally entangled Bell states, $|e_+\rangle := \frac{1}{\sqrt{2}}(|00\rangle + |11\rangle)$ or $|o_+\rangle := \frac{1}{\sqrt{2}}(|01\rangle + |10\rangle)$, each with a probability of $\frac{1}{2}$. However, if the odd or even pair states are not identical, a post-processing gate is required to disentangle the qubits from the MS (gate $V_{q,MS}$ in FIG. 4.1). Thus, different and even orthogonal states in each pair are acceptable at the price of an extra gate after the measurement.

Even if measuring the MS distinguishes between the even pair states, which corresponds to hamming weight measurement of the target qubits, there is a $\frac{1}{2}$ probability that the qubits will end up in the entangled state $|o_+\rangle$ with a hamming weight of one. The remaining outcomes are hamming weights of zero and two, each with a probability of $\frac{1}{4}$ and with the updated states $|00\rangle$ and $|11\rangle$, respectively.

We evaluate the success of our method by the amount of entanglement in the qubits' state, quantified by the fidelity, defined as the overlap of the qubits' state, $\rho_{q_1 q_2}$, and the ideal maximally entangled state, $|\phi\rangle$,

$$F_\phi(\rho_{q_1 q_2}) := Tr(\rho_{q_1 q_2} |\phi\rangle\langle\phi|) = \langle\phi| \rho_{q_1 q_2} |\phi\rangle . \tag{4.3}$$

The fidelity ranges between 0 and 1. If $F_\phi(\rho_{q_1 q_2}) > \frac{1}{2}$, the state $\rho_{q_1 q_2}$ is entangled and can be distilled towards the maximally entangled state $|\phi\rangle$ [43, 44].

4.2.1 Collective conditional gates

FIG. 4.2 shows an idealized parity measurement circuit. Two global π-rotations on the MS, conditioned on the state of each target qubit, correlate the target qubits' parity with the MS's collective excitation. The evolved state of the target qubits and MS is,

$$|\psi_1\rangle_{q,MS} = \frac{|00\rangle + |11\rangle}{2} \otimes |0\rangle^{\otimes N} + \frac{|01\rangle + |10\rangle}{2} \otimes |1\rangle^{\otimes N} . \tag{4.4}$$

The odd pair states are equal to each other and are therefore indistinguishable by any measurement, as are those of the even pair. Furthermore, the two pairs are maximally separated in the collective excitation spectrum, and thus can be distinguished with the lowest resolution global measurement.

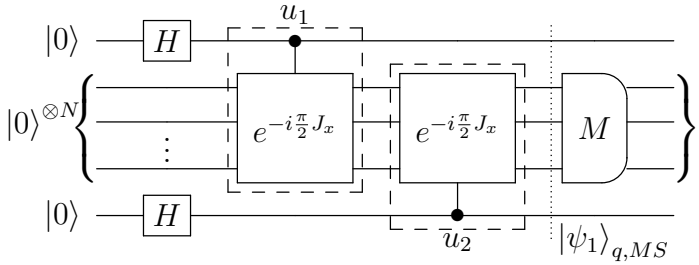

Figure 4.2: An idealized example of indirect parity measurement. During the evolution the MS's qubits are rotated conditioned on each external qubit's state, sequentially. The operator $J_x = \sum_j \sigma_x^j$ where σ_x^j is the Pauli operator along x on the j'th qubit.

In order to flawlessly distinguish between the states $|0\rangle^{\otimes N}$ with $m = 0$ and $|1\rangle^{\otimes N}$ with $m = N$ number of excitations, it is sufficient that $Tr(E_\alpha.\Pi(0)) \times Tr(E_\alpha.\Pi(N)) = 0$ for any measurement operator, E_α. If this condition is not satisfied, the qubits' state will be perturbed from the maximally entangled states $|e_+\rangle$ or $|o_+\rangle$. For example, if the measurement outcome is β, and the probabilities corresponding to even and odd pairs are $p_{e,\beta} = Tr(E_\beta.|0\rangle\langle 0|^{\otimes N})$ and $p_{o,\beta} = Tr(E_\beta.|1\rangle\langle 1|^{\otimes N})$ where $p_{e,\beta} > p_{o,\beta} > 0$, the qubits' entangled state is $\rho_{q_1q_2} = \frac{p_{e,\beta}}{p_{e,\beta}+p_{o,\beta}}|e_+\rangle\langle e_+| + \frac{p_{o,\beta}}{p_{e,\beta}+p_{o,\beta}}|o_+\rangle\langle o_+|$ with fidelity $F_{e_+}(\rho_{q_1q_2}) = \frac{p_{e,\beta}}{p_{e,\beta}+p_{o,\beta}}$.

A variation of the circuit outlined in FIG. 4.2 measures the hamming weight of the target qubits and illustrates the role of the post-processing gate. If during the evolution step, half of the MS's qubits are flipped conditioned on the first qubit's state and the other half on the second qubit's state, the whole system evolves into the state,

$$\begin{aligned} |\psi_2\rangle_{q,MS} &= \frac{1}{2}(|00\rangle \otimes |0\rangle^{\otimes N} + |01\rangle \otimes |0\rangle^{\otimes \frac{N}{2}} |1\rangle^{\otimes \frac{N}{2}} \\ &+ |10\rangle \otimes |1\rangle^{\otimes \frac{N}{2}} |0\rangle^{\otimes \frac{N}{2}} + |11\rangle \otimes |1\rangle^{\otimes N}). \end{aligned} \tag{4.5}$$

Neither the odd nor even pair states are equal. However, the odd pair states share the same collective excitation, $m = \frac{N}{2}$, and thus are indistinguishable by any collective measurement. In contrast, the even pair states have the maximum separation in the collective excitation spectrum. Nevertheless, depending on the details of the POVM on the MS, they may or may not be distinguished by the measurement, which correspond to indirect hamming

weight and parity measurements of the qubits, respectively. We illustrate the hamming weight measurement here and later discuss the parity measurement.

Suppose that the POVM on the MS distinguishes between $m = 0$, $m = \frac{N}{2}$ and $m = N$ number of excitations. Then, post-selection on the outcome $m = \frac{N}{2}$ projects the qubits' state into the odd parity subspace, $\frac{1}{\sqrt{2}}(|01\rangle \otimes |0\rangle^{\otimes \frac{N}{2}} |1\rangle^{\otimes \frac{N}{2}} + |10\rangle \otimes |1\rangle^{\otimes \frac{N}{2}} |0\rangle^{\otimes \frac{N}{2}})$, but the state of the qubits is entangled with the MS's state. Thus, a disentangling gate is required to restore the coherence of the qubits' state. A general choice for this gate is to reverse the evolution step, leading to the state $\frac{1}{\sqrt{2}}(|01\rangle + |10\rangle) \otimes |0\rangle^{\otimes N}$, which includes the maximally entangled $|o_+\rangle$ state on the qubits, separable from the MS's state.

To perfectly distinguish the odd pair from both states of the even pair, any measurement operator, E_β, that can select the odd pair, i.e., $Tr(E_\beta \Pi(N/2)) \neq 0$, must not overlap with the even pair, i.e., $Tr(E_\beta \Pi(0)) = Tr(E_\beta \Pi(N)) = 0$. If this condition is not satisfied, the fidelity of the updated state is $F_{o_+}(\rho_{q_1 q_2}) = \frac{2p_{01,\beta}}{2p_{01,\beta}+p_{00,\beta}+p_{11,\beta}}$ where $p_{\gamma,\beta} = Tr(E_\beta |\psi_\gamma\rangle\langle\psi_\gamma|)$, with $\gamma = 00, 01, 10, 11$, is the probability of the measurement outcome β corresponding to the MS's state $|\psi_\gamma\rangle$.

4.2.2 Local interaction

The two examples discussed require a collective rotation of the MS controlled by the target qubits' state. The target qubits' parity or hamming weight can also be encoded in the MS's collective state by the local interaction between each target qubit and its nearby qubit in the MS, by preparing the MS in an entangled state prior to their interaction. FIG. 4.3 shows this effect in its extreme limit. First the MS is prepared in the maximally entangled GHZ state, $\frac{1}{\sqrt{2}}(|0\rangle^{\otimes N} + i\,|1\rangle^{\otimes N})$, by evolving under the collective unitary operation $e^{-i\frac{\pi}{4}\Pi_j \sigma_x^j}$ where σ_x^j represents the Pauli operator along x on the jth particle. Second, the target qubits' parity is encoded in the phase of the GHZ state by applying two controlled-Z gates controlled by each target qubit on its nearby qubit in the MS. This global phase information is then transformed into population by reversing the first gate, leading to the state $|\psi_1\rangle_{q,MS}$ in equation 4.4, the same as the evolved state of the first circuit.

Similar to the first example, the qubits' parity is correlated with the states of the MS that are maximally separated in the collective excitation spectrum. This infers that these two circuits use the maximum capacity of the MS.

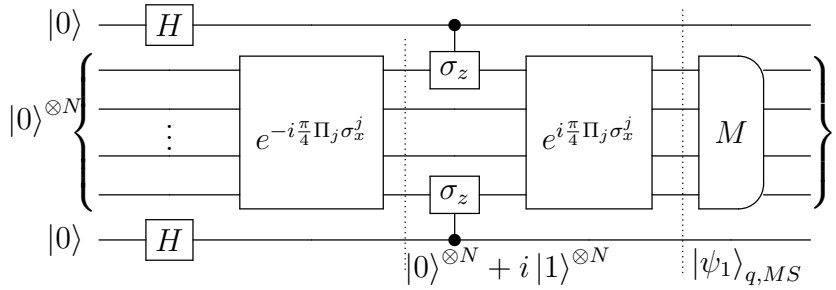

Figure 4.3: Entanglement among the qubits in the MS and local interaction with target qubits.

4.3 Measurement

Entangling two qubits by direct parity measurement requires detection of single qubit flip, while our approach of indirect parity measurement only needs distinguishing between the odd and even pair states of the MS that differ by many qubits' flip. A wide range of measurements could achieve the desired goal. In this section we show that a coarse-grained two-outcome POVM on the MS is sufficient to distinguish between the odd and even pair states. We also demonstrate that this POVM can be implemented through a PVM on a two-level apparatus system.

Consider the general form of a two-outcome POVM of the collective excitation, parameterized with an angle $\theta(m)$,

$$E_0 = \sum_m \cos\left(\theta(m)\right)^2 \Pi(m),\ E_1 = \sum_m \sin\left(\theta(m)\right)^2 \Pi(m) \tag{4.6}$$

Any two-outcome collective excitation measurement can be written in this form by properly choosing the corresponding function $\theta(m)$. According to Neumark's dilation theorem, any POVM on the system's Hilbert space, H_S, can be realized operationally as a projector valued measure (PVM) on an extended Hilbert space of the system and an apparatus $H_S \otimes H_A$ [40]. This PVM can always be realized, operationally, as a von Neumann's indirect measurement [41]. A von Neumann's indirect measurement consists of a unitary interaction between the system and the apparatus, followed by a PVM on the apparatus [38]. FIG. 4.4 shows such an indirect measurement for the POVM in equation 4.6. The gate $U_M = \sum_{m=0}^{N} \Pi(m) \otimes e^{-i\theta(m)\sigma_y^a}$ with $\Pi(m)$ and σ_y^a acting on the MS and the apparatus qubit respectively, rotates the apparatus qubit by an angle that depends on the MS's collective excitation. Next a PVM is performed on the apparatus qubit with the measurement operators, $\Pi_a(0) = |0\rangle\langle 0|$ and $\Pi_a(1) = |1\rangle\langle 1|$. The combination of the above unitary

evolution and PVM effectively performs the POVM in equation 4.6 on the MS with the state-update-rule in equation 4.2.

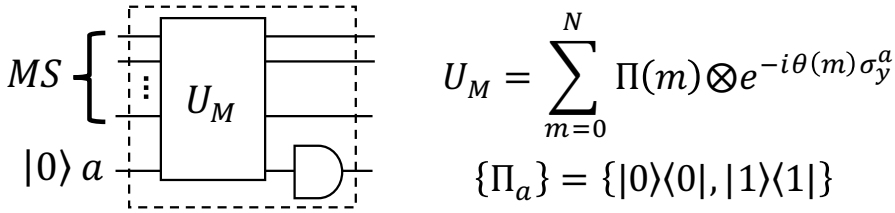

Figure 4.4: A simple two-outcome POVM for the MS implemented through collective interaction with an apparatus qubit.

The gate U_M can be conveniently realized through collective linear interaction between the MS and the apparatus qubit with the Hamiltonian $H_M = gJ_z \otimes \sigma_y^a$, where the operator J_z is defined as $J_z = \sum_{j=1}^{N}(\sigma_z^j + \mathbb{1}^j)/2 = \sum_{m=0}^{N} m\Pi(m)$. With this interaction, $\theta(m) = gmt_M$ is proportional to the collective excitation of the MS, m; where g and t_M are the interaction strength and time, respectively.

Based on the expected spectrum of the odd and even pair states prior to the measurement, t_M is chosen to achieve the maximum contrast between the two pairs. FIG. 4.5 shows the proper choices of $\theta(m)$ (t_M) for the examples discussed. For $|\psi_1\rangle_{q,MS}$, the two-outcome POVM with $\theta(m) = \frac{\pi}{2N}m$ ($t_M = \pi/2Ng$) flawlessly distinguishes between the two pairs, resulting in the updated states $|e_+\rangle \otimes |0\rangle^{\otimes N}$ or $|o_+\rangle \otimes |1\rangle^{\otimes N}$, with equal probability. For $|\psi_2\rangle_{q,MS}$, the POVM with $\theta(m) = \frac{\pi}{N}m$ ($t_M = \pi/Ng$) updates the qubits-MS state to $\frac{1}{\sqrt{2}}(|00\rangle \otimes |0\rangle^{\otimes N} + |11\rangle \otimes |1\rangle^{\otimes N})$ or $\frac{1}{\sqrt{2}}(|01\rangle \otimes |0\rangle^{\otimes N/2}|1\rangle^{\otimes N/2} + |10\rangle \otimes |1\rangle^{\otimes N/2}|0\rangle^{\otimes N/2})$, with equal probability. These states will be evolved into the separable states between the qubits and the MS $|e_+\rangle \otimes |0\rangle^{\otimes N}$ and $|o_+\rangle \otimes |0\rangle^{\otimes N}$ by the following disentangling gate. With this POVM, the second example desirably measures the target qubits' parity, not their hamming weight, since the two states $|0\rangle^{\otimes N}$ and $|1\rangle^{\otimes N}$ are not distinguishable by the measurement due to the cyclic form of the measurement operators expansion.

4.4 Mixed initial state

So far we have considered the ideal pure fully polarized state, $|0\rangle^{\otimes N}$, as the initial state of the MS. Here we discuss the mixed initial state of the MS as one of the experimental

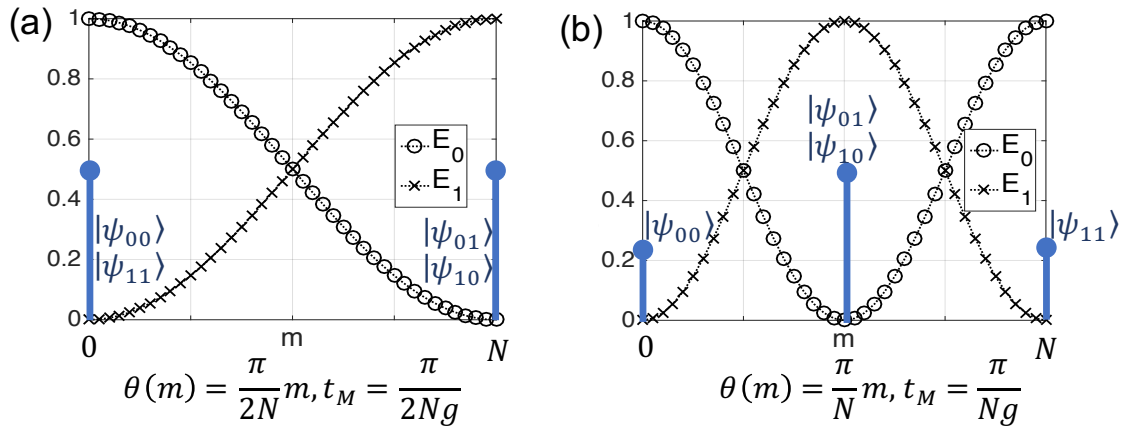

Figure 4.5: (a) The collective excitation spectrum of the MS with $|\psi_1\rangle_{q,MS}$ and the expansion of the appropriate two-outcome POVM. The measurement operator E_0 (E_1) selects the odd (even) pair over the even (odd) pair perfectly. (b) Similar to (a) but for the state $|\psi_2\rangle_{q,MS}$.

imperfections; in particular, we find an upper bound on the qubits' entanglement when the MS is initially in the experimentally relevant mixed state,

$$\rho_i = \rho_\epsilon := \left(\frac{\mathbb{1} + (1-\epsilon)\sigma_z}{2}\right)^{\otimes N} \tag{4.7}$$

where N is the number of particles in the MS and $(1-\epsilon)$ is the polarization of each. Without loss of generality we assume positive polarization; thus $0 < (1-\epsilon) \leq 1$. Consider the general indirect parity measurement circuit depicted in FIG. 4.1. In deriving the upper bound imposed by the initial state of the MS, we allow any collective excitation measurement on the MS and any conditional unitary evolution of the form,

$$U_{q,MS} = (|00\rangle\langle 00| + |11\rangle\langle 11|) \otimes V_e + (|01\rangle\langle 01| + |10\rangle\langle 10|) \otimes V_o. \tag{4.8}$$

The above unitary evolution guarantees that the odd pair states equal each other as do the even ones; therefore, a post-processing gate is not required.

In this section, we first find a general relation between the entanglement of the target qubits and the probability distributions of the measurement outcomes for any initial state of the MS, any collective excitation measurement and unitary evolution of the form 4.8. We also relate the upper bound on the entanglement to the distinguishability of the even and odd pair states of the MS. Next, we find an analytic relation for the upper bound on

entanglement of the target qubits assuming that the MS is prepared in the state 4.7. Last, we discuss the relation between the amplitude damping noise on the MS and limited initial polarization of the MS.

4.4.1 Fidelity and probability of the measurement outcomes

With a fixed evolution and measurement, the average fidelity over all measurement outcomes is,

$$F_{avg} := \sum_{\alpha} p_{\alpha} \mathcal{F}_{\alpha}(\rho_{q_1 q_2, \alpha}) \tag{4.9}$$

where p_α is the probability of the measurement outcome α. $\rho_{q_1 q_2, \alpha}$ is the updated state of the qubits after the measurement on the MS with post-selecting the outcome α, and $\mathcal{F}_{\alpha}(\rho_{q_1 q_2, \alpha})$ is defined as, $\mathcal{F}_{\alpha}(\rho_{q_1 q_2, \alpha}) := \max\left(F_{o_+}(\rho_{q_1 q_2, \alpha}), F_{e_+}(\rho_{q_1 q_2, \alpha})\right)$. This maximizing occurs as one of the two entangled states $|o_+\rangle$ or $|e_+\rangle$ is more probable depending on the measurement outcome. The corresponding fidelity is the appropriate measure of the entanglement.

Assuming that the evolution has the form 4.8, the average fidelity is related to the two classical probability distributions of the measurement outcomes corresponding to the even, $\rho_e = V_e \rho_i V_e^\dagger$, and odd, $\rho_o = V_o \rho_i V_o^\dagger$, states of the MS measured by the collective POVM $\{E_\alpha\}$, as,

$$F_{avg}(V_o, V_e, \{E_\alpha\}) = \sum_{\alpha} \frac{1}{2} \max\left(p_{o,\alpha}, p_{e,\alpha}\right) \tag{4.10}$$

where $p_{o,\alpha} = Tr(\rho_o E_\alpha)$ and $p_{e,\alpha} = Tr(\rho_e E_\alpha)$. See subsection below for the derivation. Maximizing the average fidelity over all pairs of unitary operators, $\{V_e, V_o\}$, and all collective POVMs, $\{E_\alpha\}$, gives the entanglement's upper bound,

$$F_{avg,max} := \max_{V_o, V_e \{E_\alpha\}} F_{avg}(V_o, V_e, \{E_\alpha\}). \tag{4.11}$$

This upper bound on the qubits' entanglement has an interesting physical interpretation as following. The classical trace distance of two probability distributions is defined as $D_c(\vec{p}_1, \vec{p}_2) := \frac{1}{2}\sum_\alpha |p_{1,\alpha} - p_{2,\alpha}| = \sum_\alpha \max\left(p_{1,\alpha}, p_{2,\alpha}\right) - 1$, [38, 37]. Thus the average fidelity can be written in terms of the classical trace distance between the probability distributions $\vec{p}_o$ and $\vec{p}_e$ as,

$$F_{avg}(V_o, V_e, \{E_\alpha\}) = \frac{1}{2}\left(1 + D_c(\vec{p}_o, \vec{p}_e)\right). \tag{4.12}$$

The quantum trace distance between two states ρ_1 and ρ_2 is defined as the maximum of the classical trace distance between their associated probability distributions over all possible

POVM measurements, $D_q(\rho_1, \rho_2) := \max_{\{E_\alpha\}} D_c(\vec{p}_1, \vec{p}_2)$. The quantum trace distance has an important operational meaning. It quantifies how distinguishable the two states are by a single shot measurement via the relation Pr(correctly inferring ρ_1 over ρ_2) $= \frac{1}{2}(1 + D_q(\rho_1, \rho_2))$ [38, 37]. According to equations 4.12 and 4.11 the entanglement's upper bound is a function of the quantum trace distance of the states ρ_o and ρ_e as,

$$F_{avg,max} = \frac{1}{2}\left(1 + \max_{V_o,V_e} D_q(\rho_o, \rho_e)\right). \tag{4.13}$$

Hence the desirable states, $\rho_o^\star = V_o^\star.\rho_\epsilon.V_o^{\star\dagger}$ and $\rho_e^\star = V_e^\star.\rho_\epsilon.V_e^{\star\dagger}$, that maximize the average fidelity are the ones that have the maximum quantum trace distance i.e. are the most distinguishable with a single shot measurement. Besides, the upper bound on the qubits' entanglement is the probability of successfully distinguishing between the states $\rho_o^\star$ and $\rho_e^\star$ of the MS with a single shot measurement, $F_{avg,max} = \frac{1}{2}(1 + D_q(\rho_o^\star, \rho_e^\star))$.

Average fidelity as a function of classical probability distributions

Following the circuit 4.1 with the unitary evolution 4.8 the state of the target qubits and the MS after the evolution is:

$$\begin{aligned} \rho_{q,MS} &= \frac{1}{2}\left(|o_+\rangle\langle o_+| \otimes \rho_o + |e_+\rangle\langle e_+| \otimes \rho_e\right. \\ &+ \left.|o_+\rangle\langle e_+| \otimes \chi_{oe} + |e_+\rangle\langle o_+| \otimes \chi_{eo}\right) \end{aligned} \tag{4.14}$$

where $\rho_o = V_o.\rho_i.V_o^\dagger$, $\rho_e = V_e.\rho_i.V_e^\dagger$, $\chi_{oe} = V_o.\rho_i.V_e^\dagger$, $\chi_{eo} = \chi_{oe}^\dagger = V_e.\rho_i.V_o^\dagger$. According to the state update rule 4.2, the state of the qubits after the measurement, post-selection on the outcome α, and tracing over the MS is:

$$\begin{aligned} \rho_{q_1q_2,\alpha} &= \frac{|o_+\rangle\langle o_+|\, Tr(E_\alpha\rho_o) + |e_+\rangle\langle e_+|\, Tr(E_\alpha\rho_e)}{Tr(E_\alpha\rho_o) + Tr(E_\alpha\rho_e)} \\ &+ \frac{|o_+\rangle\langle e_+|\, Tr(E_\alpha\chi_{oe}) + |e_+\rangle\langle o_+|\, Tr(E_\alpha\chi_{eo}}{Tr(E_\alpha\rho_o) + Tr(E_\alpha\rho_e)} \\ &:= \frac{p_{o,\alpha}\,|o_+\rangle\langle o_+| + p_{e,\alpha}\,|e_+\rangle\langle e_+| + ...}{p_{o,\alpha} + p_{e,\alpha}} \end{aligned} \tag{4.15}$$

where $p_{o,\alpha} := Tr(E_\alpha\rho_o)$ and $p_{e,\alpha} := Tr(E_\alpha\rho_e)$ are the probabilities of the measurement outcome α corresponding to the states ρ_o and ρ_e of the MS respectively. The fidelity of

the state $\rho_{q_1q_2,\alpha}$ with the odd and even parity states is,

$$\begin{aligned} F_{o_+}(\rho_{q_1q_2,\alpha}) &= Tr(\rho_{q_1q_2,\alpha}\,|o_+\rangle\langle o_+|) = \frac{p_{o,\alpha}}{p_{o,\alpha}+p_{e,\alpha}} \\ F_{e_+}(\rho_{q_1q_2,\alpha}) &= Tr(\rho_{q_1q_2,\alpha}\,|e_+\rangle\langle e_+|) = \frac{p_{e,\alpha}}{p_{o,\alpha}+p_{e,\alpha}}. \end{aligned} \tag{4.16}$$

Substituting in equation 4.9 we find the average fidelity for a particular choice of the evolution gates, $\{V_o, V_e\}$, and the measurement, $\{E_\alpha\}$,

$$\begin{aligned} F_{avg}(V_o, V_e, \{E_\alpha\}) &= \sum_\alpha p_\alpha \max\left(\frac{p_{o,\alpha}}{p_{o,\alpha}+p_{e,\alpha}}, \frac{p_{e,\alpha}}{p_{o,\alpha}+p_{e,\alpha}}\right) \\ &= \sum_\alpha \frac{1}{2}\max\left(p_{o,\alpha}, p_{e,\alpha}\right). \end{aligned} \tag{4.17}$$

The second equality follows the fact that the probability of the outcome α is $p_\alpha = Tr((\mathbb{1}_2 \otimes E_\alpha)\rho_{q,MS}) = \frac{1}{2}(p_{o,\alpha}+p_{e,\alpha})$.

4.4.2 Analytic relation for entanglement's upper bound

With the initial state $\rho_i = \rho_\epsilon$, one choice for the states $\rho_e^\star$ and $\rho_o^\star$ are $\rho_e^\star = \rho_\epsilon = \left(\frac{\mathbb{1}+(1-\epsilon)\sigma_z}{2}\right)^{\otimes N}$ and $\rho_o^\star = \left(\frac{\mathbb{1}-(1-\epsilon)\sigma_z}{2}\right)^{\otimes N}$ corresponding to the gates $V_e^\star = \mathbb{1}^{\otimes N}$ and $V_o^\star = e^{-i\pi/2J_x} = \sigma_x^{\otimes N}$; meaning that the best one can do is flipping all the two-level systems in the MS conditioned on the parity of the two target qubits similar to the circuit depicted in the FIG. 4.1. In this case, the optimal measurement on the MS is the PVM of the collective excitation, $\{E_\alpha^\star\} = \{\Pi(m)\}$ [3]. See the following subsection for the proof.

Replacing the above choices for $\rho_e^\star$, $\rho_o^\star$ and $\{E_\alpha^\star\}$ in the average fidelity relation in equation 4.10 gives the upper bound on entanglement as a function of the number of particles in the MS, N, and their polarization, $(1-\epsilon)$,

$$\begin{aligned} F_{avg,max} &= \sum_\alpha \frac{1}{2}\max(b(\alpha; N, 1-\frac{\epsilon}{2}), b(\alpha; N, \frac{\epsilon}{2})) \\ &= \begin{cases} B(\frac{N-1}{2}; N, \frac{\epsilon}{2}) & \text{odd } N \\ B(\frac{N}{2}-1; N, \frac{\epsilon}{2}) + \frac{1}{2}b(\frac{N}{2}; N, \frac{\epsilon}{2}) & \text{even } N \end{cases} \end{aligned} \tag{4.18}$$

[3] The coarse-grained PVM as long as $m \leq N/2$ and $m > N/2$ excitations do not mix are acceptable too, e.g., a two-outcome PVM with the operators, $E_0 = \sum_{m=0}^{\lfloor N/2 \rfloor} \Pi(m)$ and $E_1 = \sum_{m=\lfloor N/2 \rfloor+1}^{N} \Pi(m)$.

where the function b represents the probability density function (PDF) and the function B represents the cumulative distribution function (CDF) of the Binomial distribution. The second line follows the assumption that $\epsilon < 1$. A concrete general proof for equation 4.18 is given below.

FIG. 4.6 displays the plots of the entanglement's upper bound as a function of the number of qubits in the MS and their polarization. Increasing the number of qubits or average polarization raises $F_{avg,max}$, as expected. Moreover, this bound is not limiting for

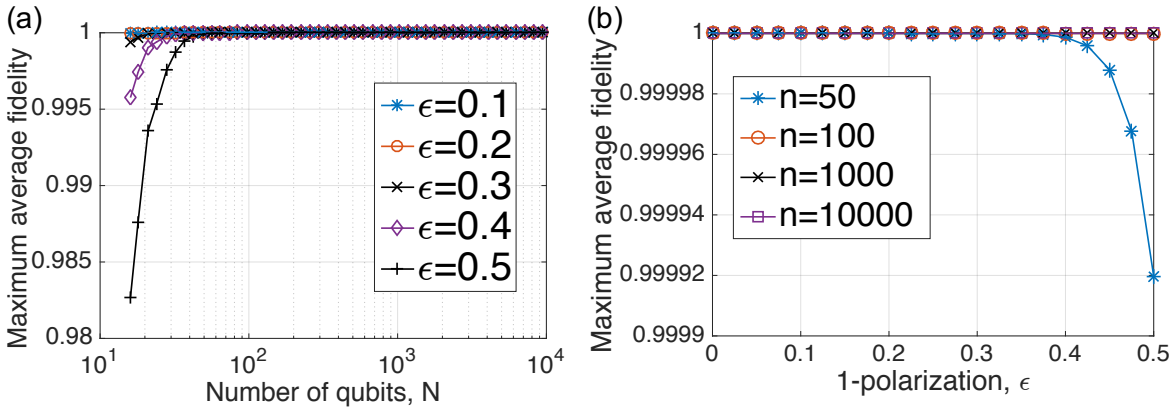

Figure 4.6: Upper bound on target qubits' entanglement (a) as a function of the number of qubits in the MS for different polarizations, (b) as a function of the polarization for different numbers of qubits in the MS .

physically realistic amounts of polarization e.g. with the polarization $1 - \epsilon = 0.5$ and only 50 qubits the upper bound is remarkably $F_{avg,max} = 0.9999$. In order to violate Clauser-Horne-Shimony-Holt (CHSH) inequality the fidelity of $F > (2 + 3\sqrt{2})/8 \approx 0.78$ is sufficient [44, 69]. As an example, the thermal polarization of an ensemble of electron spins in temperature $T = 1°\text{K}$ and the magnetic field $B = 4\text{T}$ is 0.99.

Proof for the Entanglement Upper Bound

Here we prove that $F_{avg,max}$ given in equation 4.18 is the upper bound on the entanglement of the target qubits when the initial state of the MS is mixed state of the form 4.7. We also show that the unitary gates $V_o^\star = e^{-i\pi/2J_x}$ and $V_e^\star = \mathbb{1}^{\otimes N}$ and the set of the measurement operators $\{E_\alpha^\star\} = \{\Pi(m)\}$ saturate this upper bound.

The state ρ_ϵ can be expanded as,

$$\begin{aligned}\rho_\epsilon &= \left(\frac{\mathbb{1}+(1-\epsilon)\sigma_z}{2}\right)^{\otimes N} = \left((1-\frac{\epsilon}{2})\left|0\right\rangle\!\left\langle 0\right| + (\frac{\epsilon}{2})\left|1\right\rangle\!\left\langle 1\right|\right)^{\otimes N} \\ &= \sum_{j=0}^{N} q^{N-j}(1-q)^j \sum_{i=1}^{\binom{N}{j}} P_i \left(\left|0\right\rangle\!\left\langle 0\right|^{\otimes N-j} \otimes \left|1\right\rangle\!\left\langle 1\right|^{\otimes j}\right) \end{aligned} \tag{4.19}$$

where q is defined as $q := 1 - \frac{\epsilon}{2}$ and P_i represents the permutation operator and the summation over i is over all permutations. In a compact form, ρ_ϵ can be written as:

$$\rho_\epsilon = \sum_{k=1}^{2^N} c_k \left|\psi_k\right\rangle\!\left\langle\psi_k\right| \tag{4.20}$$

where $\{\left|\psi_k\right\rangle\} = \{\left|0\right\rangle^{\otimes N}, \left|0\right\rangle^{\otimes N-1} \otimes \left|1\right\rangle, \left|0\right\rangle^{\otimes N-2} \otimes \left|1\right\rangle \otimes \left|0\right\rangle, ..., \left|1\right\rangle^{\otimes N}\}$ is the orthonormal basis along the quantization axis (Z axis) and the set of the corresponding coefficients is,

$$\begin{aligned}\{c_k\} &= \{q^N, \binom{N}{1} \text{ times } q^{N-1}(1-q) \\ &\quad , \binom{N}{2} \text{ times } q^{N-2}(1-q)^2, ..., (1-q)^N\}. \end{aligned} \tag{4.21}$$

With the assumption that $\epsilon < 1$, q is bigger than $\frac{1}{2}$ and the above set of $\{c_k\}$ has a decreasing order.

Any unitary evolution rotates the orthonormal basis $\{\left|\psi_k\right\rangle\}$ to another orthonormal basis, but it does not change the coefficients c_k; therefore the evolved states, ρ_o and ρ_e, have similar expansions,

$$\begin{aligned}\rho_o &= V_o \rho_\epsilon V_o^\dagger = \sum_{k=1}^{2^N} c_k \left|\phi_{o,k}\right\rangle\!\left\langle\phi_{o,k}\right| \\ \rho_e &= V_e \rho_\epsilon V_e^\dagger = \sum_{k=1}^{2^N} c_k \left|\phi_{e,k}\right\rangle\!\left\langle\phi_{e,k}\right| \end{aligned} \tag{4.22}$$

where $\left|\phi_{o,k}\right\rangle = V_o \left|\psi_k\right\rangle$ and $\left|\phi_{e,k}\right\rangle = V_e \left|\psi_k\right\rangle$. With a fixed POVM measurement, $\{E_\alpha\}$, the probability distribution of the measurement outcomes corresponding to the state ρ_o is,

$$\begin{aligned}p_{o,\alpha} &= Tr\left(E_\alpha \rho_o\right) = \sum_{k=1}^{2^N} c_k Tr\left(E_\alpha \left|\phi_{o,k}\right\rangle\!\left\langle\phi_{o,k}\right|\right) \\ &= \sum_{k=1}^{2^N} a_{o,\alpha k} c_k \end{aligned} \tag{4.23}$$

The variable $a_{o,\alpha k} := Tr\left(E_\alpha \left|\phi_{o,k}\right\rangle\!\left\langle\phi_{o,k}\right|\right)$ has the following properties:

$$\begin{aligned}
&0 \le E_\alpha \le \mathbb{1} \longrightarrow 0 \le a_{o,\alpha k} \le 1 \\
&\sum_k a_{o,\alpha k} = Tr(E_\alpha \sum_k \left|\phi_{o,k}\right\rangle\!\left\langle\phi_{o,k}\right|) = Tr(E_\alpha) \\
&\sum_\alpha a_{o,\alpha k} = Tr((\sum_\alpha E_\alpha) \left|\phi_{o,k}\right\rangle\!\left\langle\phi_{o,k}\right|) = 1 \\
&\sum_{k,\alpha} a_{o,\alpha k} = \sum_k Tr(\mathbb{1} \left|\phi_{o,k}\right\rangle\!\left\langle\phi_{o,k}\right|) = \sum_k 1 = 2^N
\end{aligned} \tag{4.24}$$

Similarly $p_{e,\alpha} = \sum_{k=1}^{2^N} a_{e,\alpha k} c_k$ with $a_{e,\alpha k} := Tr\left(E_\alpha \left|\phi_{e,k}\right\rangle\!\left\langle\phi_{e,k}\right|\right)$ which has all the above properties. Substituting the relations for $p_{o,\alpha}$ and $p_{e,\alpha}$ in equation 4.17 the average fidelity is,

$$\begin{aligned}
F_{avg} &= \frac{1}{2}\sum_\alpha \max\left(\sum_{k=1}^{2^N} a_{o,\alpha k} c_k, \sum_{k=1}^{2^N} a_{e,\alpha k} c_k\right) \\
&= \frac{1}{2}\sum_\alpha \left(s_\alpha \sum_{k=1}^{2^N} a_{o,\alpha k} c_k + (1-s_\alpha)\sum_{k=1}^{2^N} a_{e,\alpha k} c_k\right) \\
&= \frac{1}{2}\sum_{k=1}^{2^N} \left(\left(\sum_\alpha s_\alpha a_{o,\alpha k}\right) + \left(\sum_\alpha (1-s_\alpha) a_{e,\alpha k}\right)\right) c_k \\
&= \frac{1}{2}\sum_{k=1}^{2^N} \left(\beta_{o,k} + \beta_{e,k}\right) c_k = \frac{1}{2}\sum_{k=1}^{2^N} \beta_k c_k.
\end{aligned} \tag{4.25}$$

We introduce the coefficient s_α, which acts as a switch; it is equal to 1 if $p_{o,\alpha} \ge p_{e,\alpha}$ and equal to 0 otherwise. We also define $\beta_{o,k} := \sum_\alpha s_\alpha a_{o,\alpha k}$, $\beta_{e,k} := \sum_\alpha (1-s_\alpha) a_{e,\alpha k}$ and $\beta_k := \beta_{o,k} + \beta_{e,k}$. Note that

$$\left.\begin{array}{l} \beta_{o,k} = \sum_\alpha s_\alpha a_{o,\alpha k} \\ \sum_\alpha a_{o,\alpha k} = 1,\ 0 \le a_{o,\alpha k} \le 1 \\ s_\alpha = 0, 1 \end{array}\right\} \longrightarrow 0 \le \beta_{o,k} \le 1 \tag{4.26}$$

Similarly one can show that $0 \le \beta_{e,k} \le 1$; and thus $0 \le \beta_k \le 2$. Also note that the

coefficients β_k add up to 2^N,

$$\begin{aligned}\sum_k \beta_k &= \sum_k \beta_{o,k} + \beta_{e,k} \\ &= \sum_k \left(\sum_\alpha s_\alpha a_{o,\alpha k} + \sum_\alpha (1-s_\alpha) a_{e,\alpha k} \right) \\ &= \sum_\alpha \left(s_\alpha \left(\sum_k a_{o,\alpha k} \right) + (1-s_\alpha) \left(\sum_k a_{e,\alpha k} \right) \right) \\ &= \sum_\alpha Tr(E_\alpha)(s_\alpha + 1 - s_\alpha) = Tr(\sum_\alpha E_\alpha) = 2^N.\end{aligned} \tag{4.27}$$

As a summary,

$$F_{avg} = \frac{1}{2} \sum_k \beta_k c_k \text{ with } 0 \leq \beta_k \leq 2 \ , \ \sum_k^{2^N} \beta_k = 2^N. \tag{4.28}$$

As mentioned before, the set of the coefficients $\{c_k\}$ is fixed by the initial state and with $q > \frac{1}{2}$ has the decreasing order displayed in equation 4.21. Thus in order to maximize F_{avg} one should choose $\beta_k = 2$ for half of c_k with higher values and $\beta_k = 0$ for the other half with lower values, if possible, i.e.

$$\begin{cases} \beta_k = 2 & 1 \leq k \leq 2^{N-1} \\ \beta_k = 0 & 2^{N-1} + 1 \leq k \leq 2^N \end{cases} . \tag{4.29}$$

This choice of β_k results in the following maximum average fidelity and proves equation 4.18.

$$\begin{aligned} & F_{avg,max} \\ &= \begin{cases} \sum_{l=0}^{\frac{N-1}{2}} (1-q)^l q^{N-l} \binom{N}{l} & \text{odd } N \\ \sum_{l=0}^{\frac{N}{2}-1} (1-q)^l q^{N-l} \binom{N}{l} + q^{\frac{N}{2}} (1-q)^{\frac{N}{2}} \binom{N}{\frac{N}{2}} & \text{even } N \end{cases} \\ &= \begin{cases} B(\frac{N-1}{2}; N, 1-q) & \text{odd } N \\ B(\frac{N}{2}-1; N, 1-q) + \frac{1}{2} b(\frac{N}{2}; N, 1-q) & \text{even } N \end{cases} \\ &= \begin{cases} B(\frac{N-1}{2}; N, \frac{\epsilon}{2}) & \text{odd } N \\ B(\frac{N}{2}-1; N, \frac{\epsilon}{2}) + \frac{1}{2} b(\frac{N}{2}; N, \frac{\epsilon}{2}) & \text{even } N \end{cases} . \end{aligned} \tag{4.30}$$

It is straight forward to show that the choices of $V_e^\star = \mathbb{1}^{\otimes N}$ and $V_o^\star = \sigma_x^{\otimes N}$ and $\{E_\alpha^\star\} = \{\Pi_\alpha\}$ saturates the above upper bound for the average fidelity. The probability distributions associated with the state $\rho_e^\star = V_e^\star.\rho_\epsilon.V_e^{\star\dagger} = \rho_\epsilon = (\frac{\mathbb{1}+(1-\epsilon)\sigma_z}{2})^{\otimes N}$ and $\rho_o^\star = V_o^\star.\rho_\epsilon.V_o^{\star\dagger} = (\frac{\mathbb{1}-(1-\epsilon)\sigma_z}{2})^{\otimes N}$ are,

$$\begin{aligned} p_{o,\alpha}^\star &= Tr(\Pi_\alpha \rho_o^\star) = (1-q)^\alpha q^{N-\alpha}\binom{N}{\alpha} \\ p_{e,\alpha}^\star &= Tr(\Pi_\alpha^\star \rho_e^\star) = q^\alpha (1-q)^{N-\alpha}\binom{N}{\alpha}. \end{aligned} \tag{4.31}$$

Since $q > \frac{1}{2}$, the $\max(p_{e,\alpha}^\star, p_{o,\alpha}^\star)$ is,

$$\max(p_{e,\alpha}^\star, p_{o,\alpha}^\star) = \begin{cases} p_{o,\alpha}^\star = (1-q)^\alpha q^{N-\alpha}\binom{N}{\alpha} & \alpha \leq \frac{N}{2} \\ p_{e,\alpha}^\star = q^\alpha (1-q)^{N-\alpha}\binom{N}{\alpha} & \alpha > \frac{N}{2} \end{cases}. \tag{4.32}$$

Combining the above equality with the relation 4.17 for the average fidelity, results in the maximum average fidelity as given in equation 4.30.

4.5 Conclusion

In summary, we proposed a new procedure for entangling two non-interacting qubits in interaction with an intermediate mesoscopic system of identical two-level systems. The method is based on measuring the parity or hamming weight of the qubits' state indirectly by first coherently amplifying it in the collective state of the MS and then measuring the MS. This generic method is not limited to a specific MS or target qubit and is enabling in systems where measurement-device sensitivity is inadequate to detect a single qubit flip.

We demonstrated that, by preparing the MS in an entangled state, the local interaction between target qubits and nearby qubit from the MS is enough to magnify the target qubits's parity in the collective state of the MS. We discussed the measurement requirements and showed that with an ideal initial state and evolution, a course-grained two-outcome collective measurement of the MS can result in maximally entangled states of the target qubits. Our analysis shows that in general the measurement needs to detect only on the order of the number of qubits in the MS's flips compared to the direct parity measurement that needs to detect single qubit's flip. We derived a rigid upper bound on entanglement of the target qubits imposed by the initial polarization of the MS's state and verified that our scheme performs well even under limited polarization. Thus perfect

preparation of the MS is not required. Analysis of further experimental imperfections such as limited control depends on the specific choice of the target qubits and the MS. We will present those analysis for spin target qubits and mesoscopic system system in the next chapter.

Chapter 5

Resources Needed for Implementing Indirect Joint Measurement with a Mesoscopic Spin System

In this chapter, we evaluate the resources required for implementing the indirect joint measurement method using a mesoscopic *spin* system (MSS) consisting of dipolarly coupled spin-1/2 particles. A MSS with two non-interacting halves, each coupled to one of the target qubits is identified as a helpful geometry that allows implementing the magnification process with the experimentally available control tools. We show that the requirements on the amplified state of the target qubits and the MSS perfectly maps to the specifications of micro-macro entanglement between each target qubit and its nearby half of the MSS. This equivalence is used to quantify the sensitivity of the indirect joint measurement technique to the experimental imperfections.

5.1 Introduction

Coherent control via a mesoscopic system is an emerging tool in quantum information processing [14, 19, 18, 70, 17, 71, 15, 72]. In the previous chapter, using a mesoscopic system to indirectly measure a joint property of two noninteracting qubits through a coarse-grained collective measurement was introduced as a new approach for entangling uncoupled qubits. Here, we analyze creating micro-macro entanglement between target spin qubits and a mesoscopic spin system as a robust strategy for implementing indirect joint measurement

on spin qubits. Micro-macro entangled states have two main characteristics, bipartite entanglement between a microscopic system e.g., a qubit and a many-body system e.g., a mesoscopic system and macroscopic distinctness between the states of the many-body system that are correlated with different states of the microscopic system [73, 74, 75].

Interest in micro-macro entangled states dates back to Schrödinger's well-known thought cat experiment [76] which was designed to formulate fundamental questions such as to what extent the quantum mechanics laws apply? Or what causes quantum to classical transition? [75, 77]. It took several decades for quantum technology to reach the capability to allow realizing purely quantum correlations at macroscopic scales (of course not as macroscopic as a cat). Micro-macro entangled states have been produced with Rydberg atoms as the microscopic system coupled to photons confined in a cavity [78, 79], transmon qubit coupled to photons in a waveguide cavity resonator [80], path degree of freedom of a single photon and optical coherent states with different phases [74, 81] and internal state of trapped ions entangled to their motional degrees of freedom [82, 83]. These experiments pave the way for the application of micro-macro entangled states in quantum processing. Here, we study the requirements for generating micro-macro entangled states between individual spin qubits and mesoscopic spin systems and using such states to entangle two uncoupled spin qubits by indirect joint measurement. In particular, we show that with the experimentally available control on the mesoscopic spin system including collective rotations and internal magnetic dipole-dipole interactions, local coupling between a target spin qubit and one nearby spin within the mesoscopic spin system suffices for generating an extended micro-macro entangled state.

Bipartite entanglement between separated qubits is equivalent to quantum state transfer (QST) up to local operations and classical communications [32, 20]. An entangled pair of qubits can be used to transfer a quantum state using quantum teleportation protocols [30]. On the other hand, two separated qubits can be entangled by first entangling one of them with a nearby ancilla qubit with local operations then transferring the state of the ancilla to the second qubit through QST. There are extensive studies on QST through a (hypothetical) 1D spin chain [20, 21, 22, 23, 24, 25, 26, 27, 28, 84, 29]. These studies usually consider spin preserving interaction Hamiltonians and fully polarized initial state, which allows restricting the dynamics to the first excitation manifold [20, 21, 22, 23, 24]. Nearest-neighbor coupling is also widely assumed, which enables finding analytical solutions through Jordan-Wigner transformation [85]. Although these simplified models are very insightful, when it comes to physical systems, such as dipolarly coupled spin systems, they do not provide a complete enough description of the dynamics. Here, we focus on analyzing a fair model of the intermediate MSS. We consider the experimentally available grade-raising Hamiltonian not the spin preserving flip-flop (XY) or Heisenberg Hamilto-

nian and all-to-all dipolar coupling and not only nearest-neighbor interaction. Thus the many-body dynamics of the spin system neither is limited to the first excitation manifold nor can be solved analytically. We simulate the dynamics for up to 20 spins and extrapolate the results for larger sizes of the MSS. We also do not limit the geometry to a 1D spin chain. In fact, we observe significantly faster responses in higher dimensions. Comparing to QST proposals, high fidelity bipartite entanglement between separated qubits is anticipated without assuming single spin addressability, engineering the interaction between the spins in the chain [21, 26] or adaptive two-qubit gates at the end of the spin chain [24] given that a coarse-grained collective non-destructive magnetization measurement on the MSS is available. The difference in the requirements is because our approach is based on magnification of the state of the target qubits and global measurement of the MSS, compared to directional information transfer from one qubit to the other needed in the QST procedures.

5.2 Statement of the problem

Consider two uncoupled spin qubits and an intermediate mesoscopic spin system (MSS). The target spin qubits are spin-half particles that can be initialized, controlled, and measured individually. The MSS is an ensemble of identical electron spins or spin half nuclei that can be controlled and measured collectively. The spins in the MSS interact with each other according to the two-body magnetic dipole coupling,

$$H_{dip} = \sum_{i,j;i<j} d_{ij}(2\sigma_z^i\sigma_z^j - \sigma_x^i\sigma_x^j - \sigma_y^i\sigma_y^j) \tag{5.1}$$

where σ_x, σ_y and σ_z are the Pauli operators and the interaction strength is proportional to the inverse cube of the distance between the spins, $d_{ij} \propto 1/|\vec{r}_{ij}|^3$. Each target qubit is locally coupled to the MSS. To be specific, we consider that each qubit, q_i, is interacting with one nearby spin within the MSS, s_i, and universal control over the pair is available [51]. An example of such a set-up consists of two nitrogen-vacancy (NV) centers in a diamond as the target qubits and electronic P_1 defects in the diamond or electron spins of phosphorous defects in a silicon lattice attached to the surface of the diamond as the MSS.

The goal is to evaluate the resources required for entangling the target qubits by indirect joint measurement through the MSS. The analyzed resources of the MSS are the purity of the initial state, the size, control and internal dynamics, measurement, and robustness to noise. The approach is to limit the coherent control tools to experimentally available ones, (including collective rotations, internal dipolar interaction among the spins in the MSS

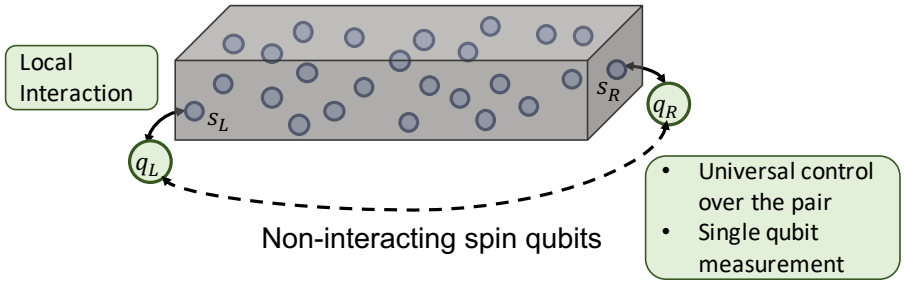

Figure 5.1: A schematic of a MSS in local contact with two non-interacting individual qubits

and local coupling between each target qubit and the MSS), and find the requirement on the other resources.

This chapter is organized as follows. In section 5.3, the general scheme for entangling two non-interacting spin qubits through indirect joint measurement is reviewed, the role of micro-macro entangled states is highlighted, and the measurement requirements are identified. In section 5.4, we present a scheme that can generate a mesoscopic superposition state with micro-macro entanglement between a spin qubit and a mesoscopic spin system using experimentally available control including collective rotations and internal dipole-dipole interaction in the MSS and local coupling between the qubit and the MSS. The scaling of the magnification time with the size of the MSS and its dependency on the geometry and dimension are discussed. In section 5.5, the entanglement of the target qubits is quantified based on the magnification procedure of section 5.4 and a general collective measurement through a two-level apparatus. In sections 5.6 and 5.7, the sensitivity of the scheme to limited initial polarization of the MSS and particle loss is analyzed. In particular, it is shown that limited initial polarization can be compensated for by enlarging the MSS. We summarize the required resources for entangling two uncoupled spin qubits through a MSS and conclude the chapter in section 5.8.

5.3 Indirect joint measurement

Two non-interacting qubits can be entangled either by creating an indirect interaction between them or by projectively measuring a joint property of them. Measuring the parity of two qubits each prepared in a superposition state, $|\pm\rangle = \frac{1}{\sqrt{2}}(|0\rangle \pm |1\rangle)$ projects their state into a maximally entangled state with odd, $|o_\pm\rangle = \frac{1}{\sqrt{2}}(|01\rangle \pm |10\rangle)$, or even, $|e_\pm\rangle =$

$\frac{1}{\sqrt{2}}(|00\rangle \pm |11\rangle)$, parity. Similarly, total magnetization measurement of the qubits projects their state into the maximally entangled state $|m_0\rangle = \frac{1}{\sqrt{2}}(|01\rangle \pm |10\rangle)$ or separable states $|m_{-1}\rangle = |11\rangle$ and $|m_{+1}\rangle = |00\rangle$ with the probabilities of $\frac{1}{2}$, $\frac{1}{4}$ and $\frac{1}{4}$, respectively. Here, the qubit states $|0\rangle$ and $|1\rangle$ represent the spin states $|\uparrow\rangle$ and $|\downarrow\rangle$. Entangling two spin qubits by projective measurement needs a very high-resolution joint measurement able to detect a single spin flip. Indirect joint measurement through a MSS relaxes this criterion by first coherently amplifying the state of the target qubits in the collective magnetization of the MSS along a known direction (called z) (gate $U_{q,MSS}$ in Fig. 5.2), then measuring the MSS by a coarse-grained collective magnetization measurement that is capable to detect only many spin flips (operation M in Fig. 5.2).

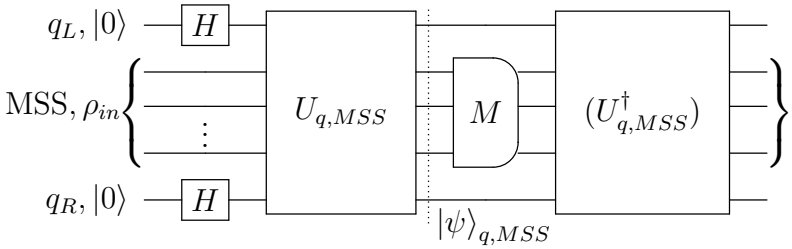

Figure 5.2: The general circuit of indirect joint measurement on two separated qubits through an intermediate MSS introduced in chapter 4.

The coherent magnification process, represented by gate $U_{q,MSS}$ in Fig. 5.2, changes the state of the MSS conditioned on the state of the target qubits, $U_{q,MSS} = |00\rangle\langle 00|_q \otimes U_{00} + |01\rangle\langle 01|_q \otimes U_{01} + |10\rangle\langle 10|_q \otimes U_{10} + |11\rangle\langle 11|_q \otimes U_{11}$. With a pure initial state over the MSS, $|\psi_{in}\rangle$, the state of the qubits and the MSS after applying this gate is,

$$|\psi\rangle_{q,MSS} = \frac{1}{2}\left(|00\rangle_q |\psi_{00}\rangle + |01\rangle_q |\psi_{01}\rangle + |10\rangle_q |\psi_{10}\rangle + |11\rangle_q |\psi_{11}\rangle\right) \tag{5.2}$$

where $|\psi_{ij}\rangle = U_{ij}|\psi_{in}\rangle$, for $i, j = 0, 1$. To indirectly measure the joint magnetization of the target qubits, the combination of the maginifaction and the measurement needs to be such that the collective coarse-grained magnetization measurement over the MSS distinguishes the pair of states $\{|\psi_{01}\rangle, |\psi_{10}\rangle\}$ from the pair $\{|\psi_{00}\rangle, |\psi_{11}\rangle\}$ but does not discern between the states $|\psi_{01}\rangle$ and $|\psi_{10}\rangle$. With these criteria, the state of the qubits and the MSS after the measurement and post-selection ideally is,

$$|\psi^{m_0}\rangle_{q,MSS} = \frac{1}{\sqrt{2}}\left(|01\rangle_q |\psi_{01}\rangle + |10\rangle_q |\psi_{10}\rangle\right) \tag{5.3}$$

In general the states $|\psi_{01}\rangle$ and $|\psi_{10}\rangle$ are not equal, thus $|\psi^{m_0}\rangle_{q,MSS}$ is an entangled state between the target qubits and the MSS. To prepare the target qubits in the maximally

entangled triplet zero state, $|m_0\rangle = \frac{1}{\sqrt{2}}(|01\rangle + |10\rangle)$, they need to be disentangled from the MSS by undoing the magnification step (gate $U^{\dagger}_{q,MSS}$ in Fig. 5.2). In the quantum eraser language the MSS is like a tagging particle and the target qubits' entanglement needs to be restored similar to the reversible eraser scheme [45].

5.3.1 Micro-macro Entanglement

With the experimentally available control tools, an interesting and potentially implementable geometry consists of a MSS with a barrier in the middle; such that there is no internal interaction, and thus no flow of information, between the two sides of the barrier. The state of each target qubit is magnified in the collective state of its nearby side. However, the collective measurement is implemented on the whole MSS, as schematically depicted in Fig. 5.3.

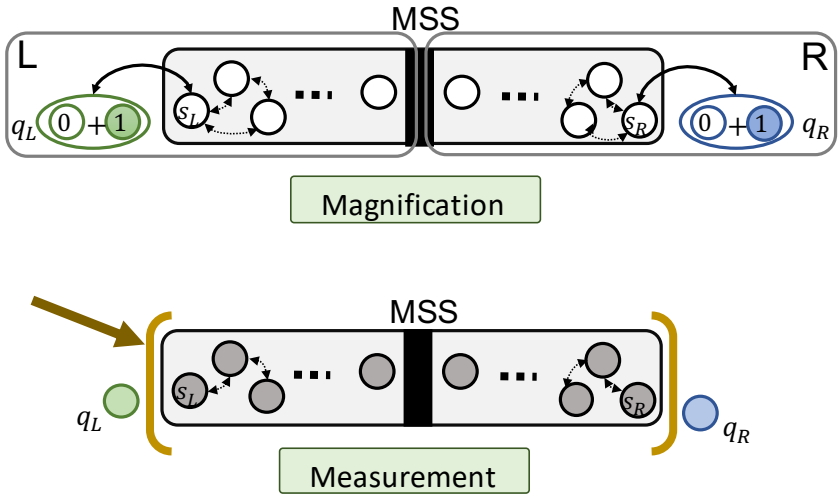

Figure 5.3: A schematic of a MSS with two non-interacting halves, each in contact with one target qubit. The state of each target qubit is magnified in the collective magnetization of its nearby side of the MSS, but the measurement is applied on the whole MSS.

The main benefit of this configuration is that it enables satisfying the mentioned distinguishability criteria on the magnified state of the target qubits and the MSS, while using only the experimentally available control tools. Here, we show that, within this geometry, the conditions on the magnified state of the qubits and the MSS entirely maps to the specifications of micro-macro entangled states between each target qubit and its nearby half

of the MSS. In section 5.4, we will show that creating micro-macro entanglement between each target qubit and half the MSS needs only experimentally available control tools including local interaction between the qubit and the MSS, collective rotations on the MSS and internal magnetic dipole interaction between the spins in the MSS.

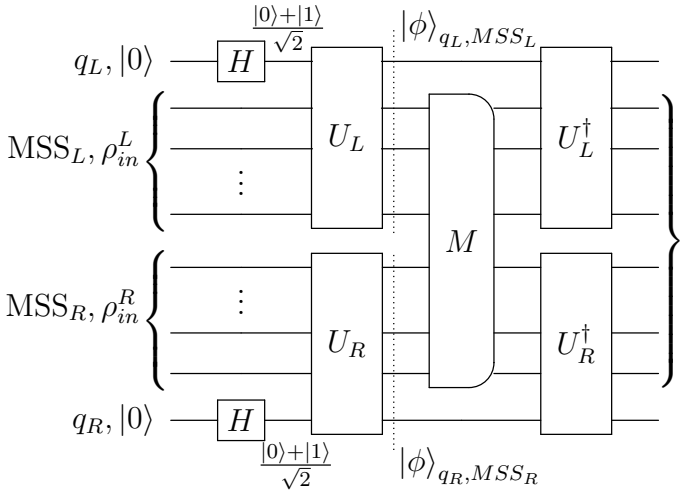

Figure 5.4: Indirect joint measurement with a MSS consisting of two non-interacting halves

The general circuit for this geometry, depicted in Fig. 5.4, is a subset of the generic indirect joint measurement circuit in Fig. 5.2, in which the magnification gate is decomposed into two parts $U_{q,MSS} = U_L \otimes U_R$, each being a conditional gate on half of the MSS controlled by its nearby target qubit,

$$U_i = |0\rangle\langle 0|_{q_i} \otimes U_0^{MSS_i} + |1\rangle\langle 1|_{q_i} \otimes U_1^{MSS_i}, i = L, R \tag{5.4}$$

With an ideal pure separable initial state of the MSS, $|\psi_{in}\rangle = \left|\psi_{in}^L\right\rangle \otimes \left|\psi_{in}^R\right\rangle$, the general state of each target qubit and its nearby half of the MSS after applying this gate and before the measurement is,

$$|\phi\rangle_{q_i,MSS_i} = \frac{1}{\sqrt{2}}\left(|0\rangle_{q_i}\left|\psi_0^i\right\rangle + |1\rangle_{q_i}\left|\psi_1^i\right\rangle\right), i = L, R \tag{5.5}$$

This state is a micro-macro entangled state if $|\psi_0^i\rangle$ and $|\psi_1^i\rangle$ are orthogonal and macroscopically distinct i.e., distinguishable by a coarse-grained collective measurement [73, 74, 75]. Macroscopic distinctness between the states $|\psi_0^i\rangle$ and $|\psi_1^i\rangle$ mathematically means that the difference in the expectation value of a particular collective observable e.g. the collective magnetization along z, $J_z = \sum_j \sigma_z^j$, for these two states is large compared both to the

quanta of the collective observable (e.g. $\hbar$ for collective magnetization) and to the sum of their standard deviation [73, 74, 75].,

$$\frac{|\langle J_z^i\rangle_0 - \langle J_z^i\rangle_1|}{\max((\Delta J_z^i)_0 + (\Delta J_z^i)_1, \hbar)} \gg 1 \tag{5.6}$$

Taking the maximum between $(\Delta J_z^i)_0 + (\Delta J_z^i)_1$ and $\hbar$ ensures meaningful answer when both $(\Delta J_z^i)_0$ and $(\Delta J_z^i)_1$ are zero. In addition, to effectively use all the spins in the MSS, the difference in the expectation value of the collective magnetization observable preferably should be proportional to the size of the MSS,

$$\langle J_z^i\rangle_0 - \langle J_z^i\rangle_1 \propto N \tag{5.7}$$

The collective magnetization observable, J_z, for N spins follows the spectral decomposition,

$$J_z = \sum_{m_z=-\frac{N}{2}}^{\frac{N}{2}} m_z \Pi^N(m_z) \tag{5.8}$$

where the operator $\Pi^N(m_z)$ projects onto the subspace with total magnetization of m_z and $\hbar$ is set to one. The magnetization spectrum of an arbitrary state, $|\phi\rangle$, is,

$$P_\phi(m_z) = \mathrm{Tr}(\Pi^N(m_z)\,|\phi\rangle\langle\phi|) \tag{5.9}$$

Macroscopic distinctness between the states $|\psi_0^i\rangle$ and $|\psi_1^i\rangle$ requires them to have well separated magnetization spectra, as depicted in Fig. 5.5a.

The states of the whole MSS associated with different states of the target qubits are, $|\psi_{00}\rangle = |\psi_0^L\rangle|\psi_0^R\rangle$, $|\psi_{01}\rangle = |\psi_0^L\rangle|\psi_1^R\rangle$, $|\psi_{10}\rangle = |\psi_1^L\rangle|\psi_0^R\rangle$ and $|\psi_{11}\rangle = |\psi_1^L\rangle|\psi_1^R\rangle$. To implement indirect magnetization measurement on the qubits, the states $\{|\psi_{10}\rangle, |\psi_{10}\rangle\}$ not only need to be orthogonal to the states $\{|\psi_{00}\rangle, |\psi_{11}\rangle\}$ but also must be distinguishable from them by a coarse-grained collective magnetization measurement. In addition, the states $|\psi_{10}\rangle$ and $|\psi_{10}\rangle$ must not be distinguishable from each other.These three conditions are satisfied if and only if each qubit and its nearby half of the MSS are prepared in (similar) micro-macro entangled states.

The pair of the states $\{|\psi_{10}\rangle, |\psi_{10}\rangle\}$ and $\{|\psi_{00}\rangle, |\psi_{11}\rangle\}$ are orthogonal if and only if the states $|\psi_0^i\rangle$ and $|\psi_1^i\rangle$ are orthogonal to each other for $i = L, R$. The second criterion requires macroscopic distinctness between the states $|\psi_0^i\rangle$ and $|\psi_1^i\rangle$. The magnetization spectra of the states $|\psi_{00}\rangle$, $|\psi_{01}\rangle$, $|\psi_{10}\rangle$ and $|\psi_{11}\rangle$ of the whole MSS are the convolution of the spectra

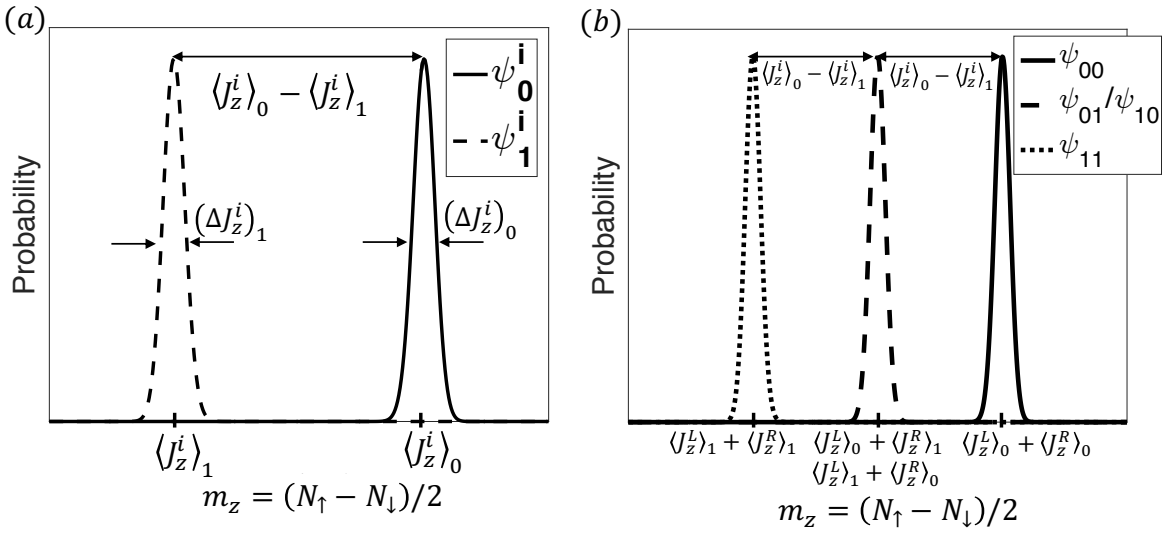

Figure 5.5: Magnetization spectrum of (a) An example of two macroscopically distinct states of half of the MSS and (b) the corresponding states of the whole MSS.

of the corresponding states of the halves. Consequently, their means and variances are sum of the means and variances of the spectra of the corresponding states of the halves,

$$\begin{aligned} \langle J_z \rangle_{kj} &= \langle J_z^L \rangle_k + \langle J_z^R \rangle_j \\ (\Delta J_z)_{kj} &= \sqrt{((\Delta J_z^L)_k)^2 + ((\Delta J_z^R)_j)^2} \end{aligned} \tag{5.10}$$

for $k, j = 0, 1$. The equivalence between macroscopic distinctness between the states $|\psi_0^i\rangle$ and $|\psi_1^i\rangle$ and the distinguishablity between the pairs $\{|\psi_{01}\rangle, |\psi_{10}\rangle\}$ and $\{|\psi_{00}\rangle, |\psi_{11}\rangle\}$ follows from these relations. The distinguishablity between $\{|\psi_{01}\rangle, |\psi_{10}\rangle\}$ and $\{|\psi_{00}\rangle, |\psi_{11}\rangle\}$, by a course-grained collective magnetization measurement along a particular axis e.g., z-axis, requires that,

$$\begin{aligned} |\langle J_z \rangle_{01} - \langle J_z \rangle_{00}| &\gg (\Delta J_z)_{01} + (\Delta J_z)_{00} \\ |\langle J_z \rangle_{01} - \langle J_z \rangle_{11}| &\gg (\Delta J_z)_{01} + (\Delta J_z)_{11} \\ |\langle J_z \rangle_{10} - \langle J_z \rangle_{00}| &\gg (\Delta J_z)_{10} + (\Delta J_z)_{00} \\ |\langle J_z \rangle_{10} - \langle J_z \rangle_{11}| &\gg (\Delta J_z)_{10} + (\Delta J_z)_{11} \end{aligned} \tag{5.11}$$

Replacing the means and the standard deviations according to Eq. (5.10) and assuming that the two target qubits and their nearby sides of the MSS are prepared in similar states

i.e., $\langle J_z^R \rangle_k \approx \langle J_z^L \rangle_k$ and $(\Delta J_z^L)_k \approx (\Delta J_z^R)_k$, the above conditions are met if [1],

$$\begin{aligned} |\langle J_z^i \rangle_1 - \langle J_z^i \rangle_0| &\gg (\Delta J_z^i)_1 + (1+\sqrt{2})(\Delta J_z^i)_0 \\ |\langle J_z^i \rangle_1 - \langle J_z^i \rangle_0| &\gg (\Delta J_z^i)_0 + (1+\sqrt{2})(\Delta J_z^i)_1 \end{aligned} \tag{5.12}$$

for $i = L, R.$ or more simply if,

$$|\langle J_z^i \rangle_1 - \langle J_z^i \rangle_0| \gg (1+\sqrt{2})((\Delta J_z^i)_1 + (\Delta J_z^i)_0) \tag{5.13}$$

which is the same as the macroscopic distinctness condition in Eq. (5.6) up to a small coefficient $(1+\sqrt{2}) \approx 2.41$. Satisfaction of relation (5.13) clearly requires the macroscopic distinctness condition given in Eq. (5.6) to be fulfilled. Thus, each target qubit and its nearby half of the MSS need to be in a micro-macro entangled state prior to the measurement step. On the other hand, preparing each qubit and its nearby half of the MSS in similar micro-macro entangled states guarantees that the states $\{|\psi_{01}\rangle, |\psi_{10}\rangle\}$ have similar magnetization spectra separated from the spectra of the states $\{|\psi_{00}\rangle, |\psi_{11}\rangle\}$. Thus, the two pairs can be distinguished by a coarse-grained collective measurement while the states $|\psi_{01}\rangle$ and $|\psi_{10}\rangle$ will not be discerned due to their similar spectra.

5.3.2 Coarse-grained Collective Measurement

The measurement and post-selection must project the state of the qubits into zero magnetization subspace along with the states of the MSS. In other words, the collective magnetization measurement on the MSS and post-selection not only need to discern the MSS's states correlated with zero magnetization of the qubits from states associated with ± 1 magnetizations; but also must update the MSS's state according to the measurement outcome, with minimum disturbance on the selected states. The state of the qubits and the MSS after the measurement ideally is,

$$|\psi\rangle_{q,MSS} = \frac{1}{\sqrt{2}} \left(|01\rangle_q |\psi_0^L\rangle |\psi_1^R\rangle + |10\rangle_q |\psi_1^L\rangle |\psi_0^R\rangle \right) \tag{5.14}$$

Bipartite entangled state between the qubits separable from the MSS can be created from this state simply by reversing the magnification gate, similar to reversible quantum eraser protocol [45, 36],

$$|\psi\rangle_{q,MSS} = \frac{1}{\sqrt{2}} \left(|01\rangle_q + |10\rangle_q \right) \otimes |\psi_{in}\rangle \tag{5.15}$$

[1] For any $a \geq 0$ and $b \geq 0$, $\sqrt{a^2+b^2} \leq a+b$

The desired coarse-grained collective magnetization measurement is mathematically represented by a Positive-Operator Valued Measure (POVM) with measurement operators, $\{E_\alpha\}$, satisfying two conditions: positivity, $E_\alpha \geq 0$, and trace-preserving, $\sum_\alpha E_\alpha = \mathbb{1}$. Since the measurement is collective, the POVM operators can be expanded in terms of the collective magnetization projection operators, $\Pi^N(m_z)$,

$$E_\alpha = \sum_{m_z} a_{\alpha,m_z} \Pi^N(m_z) \tag{5.16}$$

The expansion coefficients, a_{α,m_z}, satisfy two conditions $0 \leq a_{\alpha,m_z} \leq 1$ and $\sum_\alpha a_{\alpha,m_z} = 1$ following the positivity and trace-preserving of the E_α operators. The probability of each measurement outcome, α, upon measuring the MSS in a general state ρ_{MSS} is,

$$P_\alpha = \mathrm{Tr}(E_\alpha \rho_{MSS}) \tag{5.17}$$

and the state of the MSS after the measurement is,

$$\rho_{MSS,\alpha} = \frac{M_\alpha \rho_{MSS} M_\alpha^\dagger}{P_\alpha} \tag{5.18}$$

where the operator M_α satisfies the relation $M_\alpha M_\alpha^\dagger = E_\alpha$. Following the expansion of E_α in Eq. (5.16), the operators M_α are expanded in terms of collective projectors as,

$$M_\alpha = \sum_{m_z} e^{i\phi_{\alpha,m_z}} \sqrt{a_{\alpha,m_z}} \Pi^N(m_z) \tag{5.19}$$

The phase factor, $e^{i\phi_{\alpha,m_z}}$, depends on the details of the measurement implementation. The operator M_α simplifies to $\sqrt{E_\alpha}$ if ϕ_{α,m_z} does not depend on m_z, $\phi_{\alpha,m_z} := \phi_\alpha$.

The measurement requirements can be specified by the necessity that the measurement and post-selection updates the qubits and the MSS's state from the state in Eq. (5.2) into the state in Eq. (5.3). There should exist as least one measurement operator, M_β, that overlaps with the states $\left|\psi_0^L\right\rangle \left|\psi_1^R\right\rangle$ and $\left|\psi_1^L\right\rangle \left|\psi_0^R\right\rangle$ but does not overlap with the states $\left|\psi_0^L\right\rangle \left|\psi_0^R\right\rangle$ and $\left|\psi_1^L\right\rangle \left|\psi_1^R\right\rangle$. Moreover, this measurement operator ideally must preserve the amplitude and the phase of the spectral expansion of the states $\left|\psi_0^L\right\rangle \left|\psi_1^R\right\rangle$ and $\left|\psi_1^L\right\rangle \left|\psi_0^R\right\rangle$ i.e. in the expansion of the measurement operators in Eq. (5.19) the amplitudes, a_{β,m_z}, and the phases, $e^{i\phi_{\beta,m_z}}$, should be equal for all the collective magnetizations that the spectra of the states $\left|\psi_0^L\right\rangle \left|\psi_1^R\right\rangle$ and $\left|\psi_1^L\right\rangle \left|\psi_0^R\right\rangle$ contain. The former condition guarantees that ± 1 magnetizations of the target qubits i.e. the states $|00\rangle_q$ and $|11\rangle_q$ are not selected by the measurement and the latter ensures that the coherence between $|01\rangle_q$ and $|10\rangle_q$ states of

the qubits can be restored by disentangling the MSS through reversing the magnification gate.

If these two measurement requirements are not perfectly satisfied, the final entangled state of the target qubits, ρ_q, deviates from the maximally entangled state $|m_0\rangle = \frac{1}{\sqrt{2}}(|01\rangle_q + |10\rangle_q)$. However, ρ_q is an entangled state and can be distilled towards the state $|m_0\rangle$, if the fidelity defined as the overlap of these two states is greater than 0.5 [44, 43],

$$F_{m_0}(\rho_q) := \mathrm{Tr}(\rho_q \, |m_0\rangle\langle m_0|) \tag{5.20}$$

Fidelity ranges between 0 and 1 and if $F_{m_0}(\rho_q) > (2 + 3\sqrt{2})/8 \approx 0.78$, ρ_q is entangled enough to violate Clauser-Horne-Shimony-Holt (CHSH) inequality [44, 69] [2].

Entangling the target spin qubits by first entangling each with the nearby half of MSS and then measuring the whole MSS might remind one of entanglement swapping [86]. One main difference is the measurement process. In the entanglement swapping procedure, measurement of two qubits, each from an entangled pair, in the Bell basis entangles the two other qubits. The analogy in our case is measuring an observable that $\frac{1}{\sqrt{2}}(|\psi_0^L\rangle\,|\psi_1^R\rangle \pm |\psi_1^L\rangle\,|\psi_0^R\rangle)$ and $\frac{1}{\sqrt{2}}(|\psi_0^L\rangle\,|\psi_0^R\rangle \pm |\psi_1^L\rangle\,|\psi_1^R\rangle)$ are four of its eigenstates with different eigenvalues. Such an observable, in general, is not a collective observable in contrast to the observable in the indirect joint measurement procedure.

5.4 Creation of micro-macro entanglement

In this section, we discuss producing a mesoscopic superposition state with micro-macro entanglement between one target spin qubit and a MSS, half the size of the whole MSS, as the first step towards implementing indirect joint measurement on two non-interacting target qubits. The focus is on using experimentally available control elements namely local control of the qubit, interaction between the target qubit, q, and one nearby spin within the MSS, s [3], collective rotations on the MSS and magnetic dipole-dipole interaction among

[2] Note that we use the fidelity, defined in Eq. (5.20), as a measure for entanglement since we know a priori what the expected maximally entangled state is. However fidelity is not a measure for entanglement in general e.g. the maximally entangled states $\frac{1}{\sqrt{2}}(|00\rangle \pm |11\rangle)$ have zero overlap with $|m_0\rangle$ state.

[3] It is sufficient for the target qubit to interact with only one spin within the MSS but it is not required, i.e., the qubit may interact with more than one spin. The main requirement on the local interaction between the target qubit and the MSS is that it needs to enable creating a local conditional gate on the MSS, controlled by the state of the qubit. We consider the most local form of interaction between the target qubit and the MSS to show that it is possible to create micro-macro entangled state with the entanglement extended to the whole MSS even in this case.

the spin in the MSS. The qubit is prepared in the superposition state, $|+\rangle = \frac{1}{\sqrt{2}}(|0\rangle + |1\rangle)$, and the MSS is ideally prepared in the polarized state, $|\uparrow\rangle^{\otimes N_h}$, where $N_h \approx N/2$ is the number of spins in the MSS.

We start with an intuitive approach based on repetitive application of a conditional local gate on the MSS controlled by the qubit and a duration of internal interaction between the spins of the MSS. The internal evolution of the MSS redistributes the magnetization between the spins in the MSS but preserves the total magnetization. The collective magnetization is only changed conditioned on the state of the target qubit. After enough repetitions, on the order of N_h, the states of the MSS correlated with different states of the target qubit become macroscopically distinct and a micro-macro entangled state is produced.

Next we present a different scheme in which the target qubit interacts with the MSS only once. The key feature of this approach is that the MSS is prepared in a globally correlated state prior to its interaction with the target qubit such that a local change in the MSS conditioned on the state of the target qubit has a global conditional effect. The maximally entangled GHZ state, $\frac{1}{\sqrt{2}}\left(|\uparrow\rangle^{\otimes N_h} + |\downarrow\rangle^{\otimes N_h}\right)$, is an ideal state for this purpose [36]. However preparing the GHZ state is challenging for a mesoscopic size system [4]; we show that micro-macro entanglement between the target qubit and the MSS can be produced by preparing less demanding correlated states, created through the experimentally available two-body dipolar coupling and collective rotations.

After presenting these two approaches, the magnification time and its relation to the size of the MSS and its dimensionality are discussed.

5.4.1 Repeated interactions

The circuit in Fig. 5.6 shows an intuitive approach for making a macroscopic global change in the collective magnetization of the MSS conditioned on the state of the qubit using only local interactions between the two. The CNOT gate, controlled by the qubit, q, on its nearby spin within the MSS, s, $CNOT = |0\rangle\langle 0|_q \otimes \mathbb{1}_s + |1\rangle\langle 1|_q \otimes \sigma_x^s$, changes the magnetization of the MSS locally conditioned on the state of the qubit and evolving under zero-quantum flip-flop Hamiltonian,

$$H_{XY} = \sum_{i,j;i<j} a_{ij}\left(\sigma_+^i\sigma_-^j + \sigma_-^i\sigma_+^j\right) \quad a_{ij} \propto \frac{1}{|\vec{r}_{ij}|^3} \tag{5.21}$$

[4] It needs either accessing individual spins in the MSS or synthesizing N-body interaction among all the spins.

passes on this change to the rest of the spins in the MSS while preserving the total magnetization. These two processes are repeated r times to create a macroscopic effect. The Hamiltonian H_{XY} is widely used in QST proposals usually with only nearest-neighbor interactions, $a_{ij} = 0$ for $|i - j| \neq 1$. Here we consider all-to-all interactions with the coefficients a_{ij} proportional to inverse cube of the distance between the two spins, consistent with the magnetic dipolar interaction among the spins in the MSS. The important feature of H_{XY} is that it only redistributes the magnetization among the spins while preserving the collective magnetization of the MSS. The collective magnetization of the MSS varies only conditioned on the state of the qubit by the CNOT gate. Hence, in each repetition, the total magnetization of the MSS either is preserved or varies by $\Delta m_z \in [-1, 1]$, depending on the qubit's state.

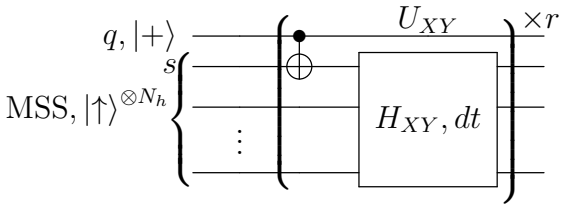

Figure 5.6: Magnification process based on repetitive interaction between the external qubit and its nearby spin from the MSS intervened by internal evolution of the MSS under the magnetization preserving H_{XY} Hamiltonian

With an initial superposition state of the qubit, $|+\rangle = \frac{1}{\sqrt{2}}(|0\rangle + |1\rangle)$, and polarized state of the MSS, $|\uparrow\rangle^{\otimes N_h}$, the general output state for the circuit 5.6 is,

$$\left|\phi^{XY}(dt, r)\right\rangle_{q,MSS} = \frac{1}{\sqrt{2}}\left(|0\rangle_q |\uparrow\rangle^{\otimes N_h} + |1\rangle_q \left|\psi_1^{XY}(dt, r)\right\rangle\right). \tag{5.22}$$

For appropriate choice of the evolution time, dt, and large enough repetitions, $r \propto N_h$, the state $\left|\psi_1^{XY}(dt, r)\right\rangle$ is macroscopically distinct from the state $|\uparrow\rangle^{\otimes N_h}$ upon collective magnetization measurement along z. Figure 5.7 shows the simulation results of the magnetization spectra of these two states for a MSS in a 1D spin chain geometry with number of repetitions $r = 2N_h$ and $dt = \pi/a_{12}$, where $a_{12} = a_{ii+1}$ is the nearest neighbor interaction strength of the Hamiltonian in Eq. (5.21) [5]. The spectrum of the polarized state $|\uparrow\rangle^{\otimes N_h}$ is a peak at $m_z = N_h/2$; whereas, the spectrum of the state $\left|\psi_1^{XY}\right\rangle$ is distributed around $m_z = 0$ and has nonzero values for $m_z = N_h/2, N_h/2 - 2, ..., -N_h/2$.

To characterize the spectrum of the state $\left|\psi_1^{XY}\right\rangle$, we simulate the mean and the standard deviation (SD) of its distribution as a function of the number of repetitions, r, with $dt =$

[5] All the numerical simulations are conducted using the open source "Expokit" software package [87]

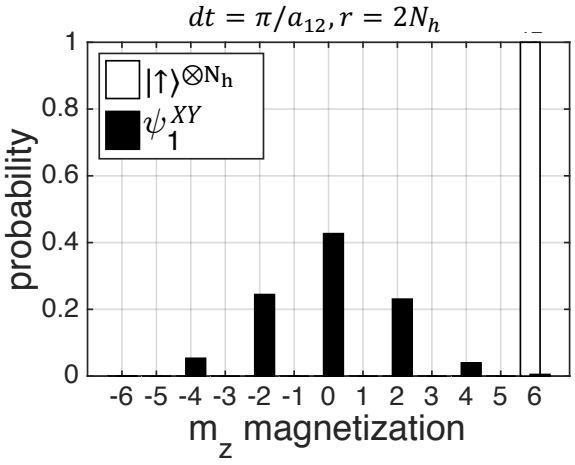

Figure 5.7: The distinct magnetization spectra of the MSS's states, $|\uparrow\rangle^{\otimes N_h}$ and $\left|\psi_1^{XY}\right\rangle$ correlated to $|0\rangle$ and $|1\rangle$ states of the target qubit simulated based on the circuit in Fig. 5.6 with $dt = \pi/a_{12}$ and $r = 2N_h$ for $N_h = 12$ spins in a 1D chain geometry.

π/a_{12} for up to $N_h = 20$ spins. As figure 5.8 shows, after a transient time the mean of the spectrum of $\left|\psi_1^{XY}\right\rangle$ approaches zero and its SD approaches $\sqrt{N_h}/2$, which are the same as the mean and the SD of a fully mixed state with N_h spins, $(\mathbb{1}_2/2)^{\otimes N_h}$, or an equal superposition state, $\left((|0\rangle + |1\rangle)/\sqrt{2}\right)^{\otimes N_h}$ [6]. This result can be extrapolated to larger systems; the mean and the SD of the spectrum of $\left|\psi_1^{XY}\right\rangle$ are expected to be ≈ 0 and $\approx \sqrt{N_h}/2$, respectively. On the other hand, the spectrum of $|\uparrow\rangle^{\otimes N_h}$ is focused at $N_h/2$. As a result, the macroscopic distinctness between the states $\left|\psi_1^{XY}\right\rangle$ and $|\uparrow\rangle^{\otimes N_h}$ scales as $\sqrt{N_h}$,

$$\frac{\langle J_z\rangle_0^{XY} - \langle J_z\rangle_1^{XY}}{(\Delta J_z)_0^{XY} + (\Delta J_z)_1^{XY}} \approx \frac{N_h/2 - 0}{0 + \sqrt{N_h}/2} \propto \sqrt{N_h} \tag{5.23}$$

It should be mentioned that the two states are not necessarily orthogonal; nevertheless, for the proper choices of dt and r their overlap is small. Thus, for a large enough MSS, $\sqrt{N_h} \gg 1$, and with appropriate dt and r the state in Eq. (5.22) is a micro-macro entangled state.

The introduced procedure provides a reasonable process for creating a micro-macro

[6] One difference is that the spectrum of the state $\left|\psi_1^{XY}(t)\right\rangle$ has nonzero values for every other magnetization whereas the spectrum of a fully mixed state or $\left((|0\rangle + |1\rangle)/\sqrt{2}\right)^{\otimes N_h}$ state includes all magnetization. But what is important is the extend of the two spectra which is quantified by their mean and SD and is similar for the two cases

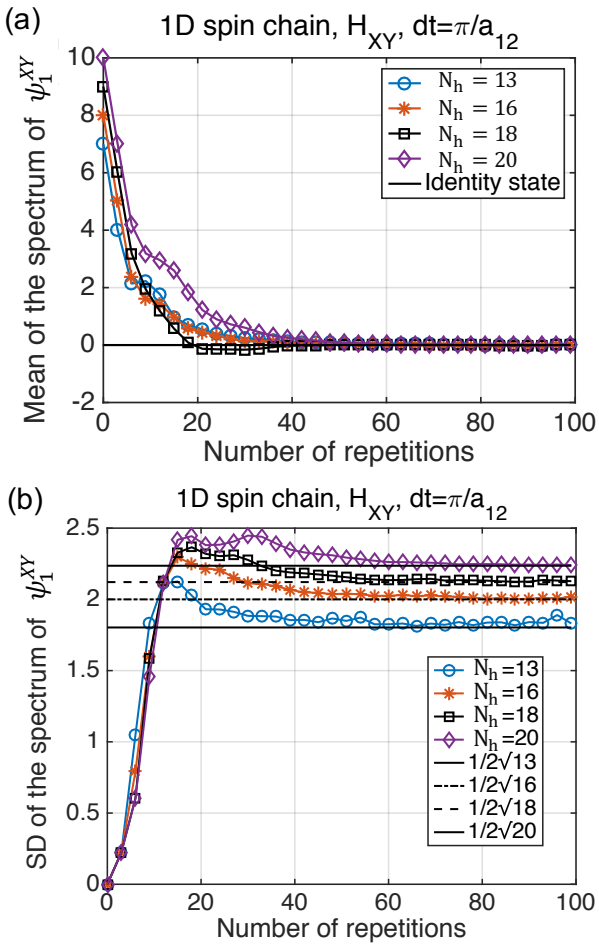

Figure 5.8: (a) The mean and (b) the standard deviation (SD) of the magnetization spectrum of $\left|\psi_1^{XY}\right\rangle$ as a function of the number of repetitions for $N_h = 13, 15, 16, 18$ qubits. After a transient time both the mean and the SD of the spectrum approach those of the identity state with the same size.

entangled state using only local interactions. However, it is hard to implement experimentally in a spin system with dipolar coupling. It needs the XY Hamiltonian which can not be synthesized out of the natural dipole-dipole interaction using collective rotations

[78]. Moreover, the number of the CNOT gates between the target qubit and the MSS is proportional to the number of spins in the MSS which is challenging for large systems.

Next, we will introduce a different procedure that requires only a one-time interaction between the qubit and the MSS. It also uses a Hamiltonian that can be engineered from the dipolar coupling using only collective control.

5.4.2 One-time interaction

Here we show that the circuit in Fig. 5.9 coherently magnifies the state of the target qubit in the collective magnetization of the MSS and creates a micro-macro entangled state using only one CNOT gate. The internal dynamics of the MSS is governed by the reversible grade-raising Hamiltonian,

$$H_{2GR} = \sum_{i,j;i<j} a_{ij} \left(\sigma_+^i \sigma_+^j + \sigma_-^i \sigma_-^j\right) \quad a_{ij} \propto \frac{1}{|\vec{r}_{ij}|^3} \tag{5.24}$$

which is a well known Hamiltonian within the nuclear magnetic resonance (NMR) community. Both $\pm H_{2GR}$ can be synthesized out of the naturally occurring magnetic dipole-dipole interaction at high field by applying appropriate sequences of collective rotations [88].

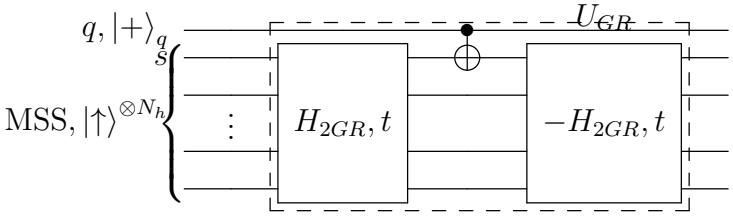

Figure 5.9: This circuit creates micro-macro entanglement between the target qubit and the MSS with a one-time interaction between the two and using experimentally available control.

The circuit in Fig. 5.9 works as follows. First, evolution under the grade-raising Hamiltonian correlates the spins in the MSS. For long enough evolution times a globally correlated state is created; specifically the spin of the MSS that is in contact with the

[7]Synthesis of XY Hamiltonian out of dipolar coupling needs $\pi-$pulses on every other qubit [25]. Depending on the geometry it might be achieved using field gradients.

[8]Secular dipolar-dipole interaction, H_{dip} in Eq. (5.1), preserves the collective magnetization similar to H_{XY}; but according to our simulations replacing H_{XY} by H_{dip} in the circuit in Fig. 5.6 does not yield the desired response

external target qubit becomes correlated with the rest of the spins in the MSS. Next, the CNOT gate controlled by target qubit, q, on its nearby spin in the MSS, s, perturbs the state of the MSS [9]. This local conditional gate has a global conditional effect due to correlations established in the MSS prior to its local interaction with the target qubit. Finally, applying the reverse of the first gate makes this global conditional effect observable in the collective magnetization spectrum of the MSS along the quantization axis. The unperturbed state of the MSS returns back to the initial polarized state $|\uparrow\rangle^{\otimes N}$ while the perturbed one evolves to a state with a *very* different collective magnetization.

The state of the target qubit and the MSS after the evolution follows the general form of a micro-macro entangled state in Eq. (5.5) with $|\psi_0^i\rangle = |\uparrow\rangle^{\otimes N_h}$ and $|\psi_1^i\rangle = \left|\psi_1^{GR}\right\rangle$,

$$\left|\phi^{GR}(t)\right\rangle_{q,MSS} = \frac{1}{\sqrt{2}}\left(|0\rangle_q |\uparrow\rangle^{\otimes N_h} + |1\rangle_q \left|\psi_1^{GR}(t)\right\rangle\right). \tag{5.25}$$

The states $\left|\psi_1^{GR}(t)\right\rangle$ and $|\uparrow\rangle^{\otimes N_h}$ are not only orthogonal but also macroscopically distinct given that the evolution time, t, is long enough.

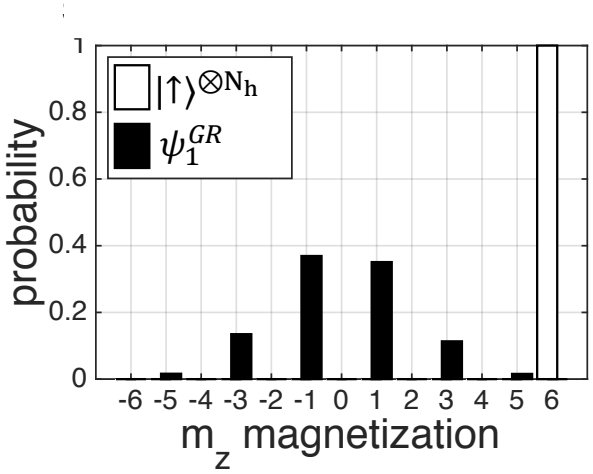

Figure 5.10: The distinct magnetization spectra of the MSS's states, $|\uparrow\rangle^{\otimes N_h}$ and $\left|\psi_1^{GR}\right\rangle$ correlated to $|0\rangle$ and $|1\rangle$ states of the target qubit simulated based on the circuit in Fig. 5.9 with $t = 2\pi N_h/a_{12}$ for $N_h = 12$ spins in a 1D chain geometry.

Figure 5.10 shows the separation in the collective magnetization spectra of the states $|\uparrow\rangle^{\otimes N_h}$ and $\left|\psi_1^{GR}(t)\right\rangle$ simulated for a MSS in a 1D chain geometry with $N_h = 12$ spins and

[9] Controlled-Z gate has similar effect.

evolution time $t = 2\pi N_h/a_{12}$, where a_{12} is the nearest neighbor coupling strength of the grade-raising Hamiltonian represented in Eq. (5.24). Figure 5.11 displays the mean and the SD of the magnetization spectrum of the state $\left|\psi_1^{GR}\right\rangle$ as a function of the normalized evolution time, t/N_h, for up to $N_h = 20$ spins. After a transient time, the mean of the spectrum approaches zero and the SD approaches $\sqrt{N_h}/2$ similar to the steady-state behaviour of the state $\left|\psi_1^{XY}\right\rangle$. Thus, the macroscopic distinctness of the states $\left|\psi_1^{GR}\right\rangle$ and $|\uparrow\rangle^{\otimes N_h}$, upon collective J_z measurement, scales as $\sqrt{N_h}$,

$$\frac{\langle J_z\rangle_0^{GR} - \langle J_z\rangle_1^{GR}}{(\Delta J_z)_0^{GR} + (\Delta J_z)_1^{GR}} \approx \frac{N_h/2 - 0}{0 + \sqrt{N_h}/2} \propto \sqrt{N_h} \tag{5.26}$$

After applying the introduced magnification process on both target qubits and their nearby halves of the MSS, the states of the whole MSS correlated with different states of the target qubits are: $\left|\psi_{00}^{GR}\right\rangle = |\uparrow\rangle^{\otimes N}$, $\left|\psi_{01}^{GR}\right\rangle = |\uparrow\rangle^{\otimes N_L}\left|\psi_1^{R,GR}\right\rangle$, $\left|\psi_{10}^{GR}\right\rangle = \left|\psi_1^{L,GR}\right\rangle|\uparrow\rangle^{\otimes N_R}$ and $\left|\psi_{11}^{GR}\right\rangle = \left|\psi_1^{L,GR}\right\rangle\left|\psi_1^{R,GR}\right\rangle$. According to the relations in Eq. (5.10), the mean and the SD of the collective magnetization spectra of these states scale as,

$$\begin{aligned}
\langle J_z\rangle_{00}^{GR} &\approx \frac{N}{2},\ (\Delta J_z)_{00}^{GR} \approx 0 \\
\langle J_z\rangle_{01}^{GR} &\approx \langle J_z\rangle_{01}^{GR} \approx \frac{N}{4},\ (\Delta J_z)_{01}^{GR} \approx (\Delta J_z)_{10}^{GR} \approx \frac{\sqrt{N/2}}{2} \\
\langle J_z\rangle_{11}^{GR} &\approx 0,\ (\Delta J_z)_{11}^{GR} \approx \frac{\sqrt{N}}{2}
\end{aligned} \tag{5.27}$$

where N is the size of the whole MSS and $N_L \approx N_R \approx N_h \approx N/2$. Macroscopic distinctness of the states $\left|\psi_{01}^{GR}\right\rangle$ and $\left|\psi_{10}^{GR}\right\rangle$ from both of the states $\left|\psi_{00}^{GR}\right\rangle$ and $\left|\psi_{11}^{GR}\right\rangle$ imposes a lower bound on the size of the MSS,

$$\frac{N}{4} \gg \left(\frac{\sqrt{N/2}}{2} + \frac{\sqrt{N}}{2}\right) \Rightarrow N \gg 12 \tag{5.28}$$

Comparing to the circuit based on XY Hamiltonian, the coherent control elements of this circuit meshes better with the experimentally available tools. It needs only one CNOT gate. Additionally, the grade-raising Hamiltonian can be synthesized from dipolar interaction with only collective pulses in contrast to the XY Hamiltonian that requires both collective pulses and rotations on every other spin [25]. Thus, in the rest of this chapter we will consider the circuit in Fig. 5.9, based on the grade-raising Hamiltonian as the magnification process.

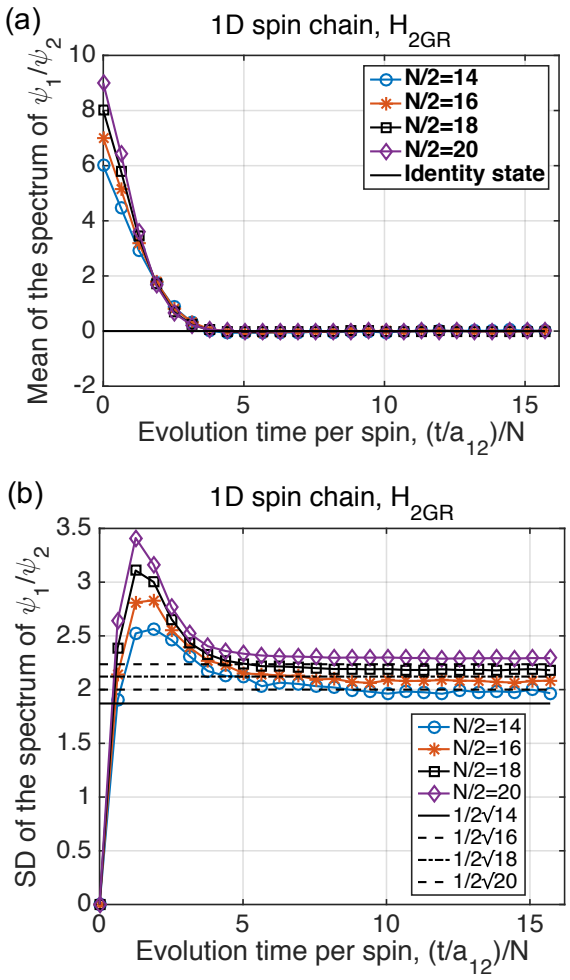

Figure 5.11: (a) The mean and (b) the SD of the magnetization spectrum of $\left|\psi_1^{GR}\right\rangle$ as a function of the normalized evolution time for MSSs with $N_h = 12, 16, 18, 20$ spins. After a transient time both the mean and the SD of the spectrum approach those of the identity state with the same size.

5.4.3 Dimensionality

The simulations in section 5.4.2 were all set in a 1D geometry. Here, generating micro-macro entanglement between a target qubit and a MSS that has a 2D structure is studied.

Figure 5.12 compares (a) the mean and (b) the SD of the spectrum of $\left|\psi_1^{GR}\right\rangle$ simulated for $N_h = 20$ spins when in a 1D chain versus 2 by 10 and 4 by 5 2D lattices. The asymptotic

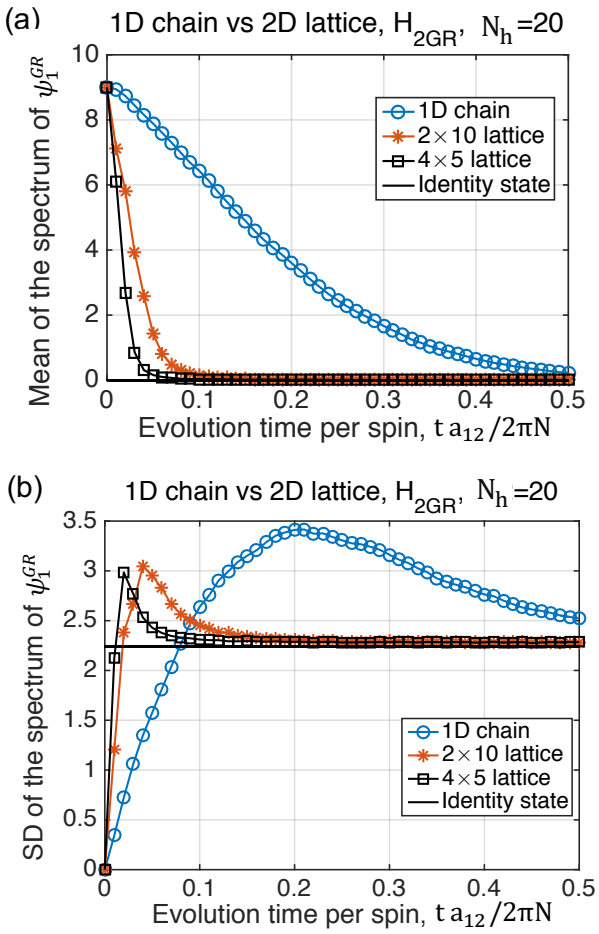

Figure 5.12: Comparing (a) the mean and (b) the SD of $\left|\psi_1^{GR}\right\rangle$ with the circuit in Fig. 5.9 for a 1D chain and 2D lattices. 2D lattice structures have much shorter transient times than a 1D chain with the same number of spins but the steady state responses are similar.

behaviours of 2D lattices are similar to that of a 1D chain; however, the transition times of the 2D structures are much shorter meaning that the information flows much faster. One simple explanation for this difference is that information flows over just one path in a 1D structure compared to multiple paths in 2D (or 3D) structures. One-directional information flow is crucial in quantum state transfer proposals; in contrast, our method relies on amplification of the qubit's state in the whole system rather than propagation of information in a specific direction. Therefore, it benefits from faster response in 2D (and

3D) structures.

To conclude, all the previous steady-state results apply to higher dimensions with an essential advantage of shorter transient times and faster responses.

5.4.4 Magnification time

An important consideration moving forward is determining the magnification process's time. Of particular interest is how the magnification time scales with the size of the MSS and what its relation is to the dimension of the MSS. This question is in general hard to answer because it depends on the many-body dynamics of the MSS. Nevertheless, we have some clues to the answer. We have shown that the dimension of the MSS significantly affects the response time. The magnification process has a much shorter transient time if the MSS has a 2D structure, compared to a 1D chain of the same size. Moreover, as depicted in Fig. 5.13, the long range magnetic dipole interaction entails shorter transient times compared with truncating to only nearest-neighbor (NN) interactions. Furthermore, comparing the SD vs normalized time for different numbers of spins in a 1D chain in Fig. 5.11 shows that as the size of the MSS increases, the peak is shifted towards shorter normalized times; indicating that the transient time has a sub-linear relation with the size of the MSS even in a 1D geometry.

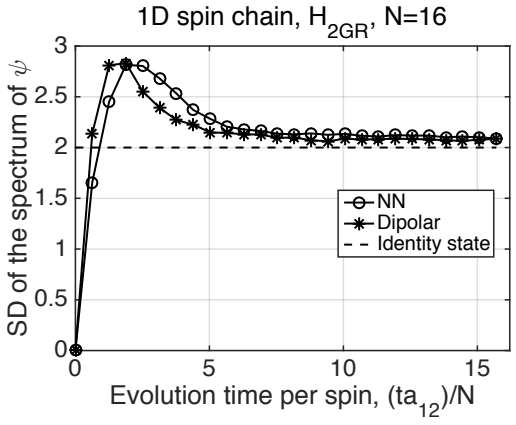

Figure 5.13: Comparing the transient times for MSSs with NN coupling and long range dipolar coupling. Information flows faster in a system with full dipolar compared to truncating to only NN interactions.

The magnification time in our protocol is closely related to the rate of information

flow in a system with dipolar coupling. In 1972, Lieb and Robinson showed that there is a constant group velocity for the flow of information in a system with local interactions, e.g., nearest-neighbor interactions (or exponentially decaying interaction strength), known as the Lieb-Robinson bound [89]. Our results show that the dynamics of MSS violates the Lieb-Robinson bound, a finding consistent with long-range dipolar interaction in the system. Recently, numerous attempts have been made to find the rate of information flow in systems with long-range interactions decaying with power law, $a_{ij} \propto \frac{1}{r_{ij}^{\alpha}}$ [90, 91, 92, 93, 94, 95, 96]. Based on these studies, different relations between the magnification time and the size of the MSS are expected depending on the MSS's dimension. It has been shown that the correlation times for a system with power-law interaction, $a_{ij} \propto \frac{1}{r_{ij}^{\alpha}}$, grow as $T \propto r^{\zeta}$, with $\frac{1}{\zeta} = 1 + \frac{1+D}{\alpha-2D}$ when $\alpha > 2D$ [96]. Thus, for a 1D chain, the magnification time is expected to scale as $t_{mag}^{1D} \propto l^{\frac{1}{3}} \propto N_h^{\frac{1}{3}}$ where l is the length of the spin chain. For 2D and 3D lattices with dipolar coupling, no bound tighter than an exponential information flow is found [90]. We also know that the information flow is faster in 2D and 3D structures than in 1D chains. Thus, in 2D and 3D structures the respective range of the magnification times are expected to be $(\sim log(l) \propto log(\sqrt{N_h})) \leq t_{mag}^{2D} < (\sim l^{\frac{1}{3}} \propto N_h^{\frac{1}{6}})$ and $(\sim log(l) \propto log(\sqrt[3]{N_h})) \leq t_{mag}^{3D} < (\sim l^{\frac{1}{3}} \propto N_h^{\frac{1}{9}})$. It is worth mentioning that recently an algorithm has been proposed that saturates the logarithmic bound for a 3D structure with dipolar coupling. It needs $t \propto \log(r)$ to transfer a state through a system with $\frac{1}{r^{\alpha}}$ interaction if $\alpha = D$ [97].

5.5 Measurement and Fidelity

The requirements of an ideal measurement procedure were discussed in section 5.3. Here we estimate the fidelity of the target qubits' post-selected entangled state using the magnification process introduced in section 5.4.2 and a collective measurement on the MSS through a two-level apparatus.

The measurement model is based on the general collective two-outcome POVM on a mesoscopic system suggested chapter 4. Any two outcome collective POVM can be parametrized with a phase function $\theta(m_z)$,

$$\begin{aligned} E_0 &= \sum_{m_z} \cos^2(\theta(m_z))\Pi^N(m_z) \\ E_1 &= \mathbb{1} - E_0 = \sum_{m_z} \sin^2(\theta(m_z))\Pi^N(m_z) \end{aligned} \tag{5.29}$$

Such a measurement is equivalent to a projective measurement on a two-level apparatus system after it interacts with the MSS according to the interaction gate [41, 40],

$$U_M = \sum_{m_z=-\frac{N}{2}}^{\frac{N}{2}} \Pi^N(m_z) \otimes e^{-i\theta(m_z)\sigma_y^a} \tag{5.30}$$

Linear collective interaction between the MSS and the apparatus qubit, $H_M = gJ_z \otimes \sigma_y$, conveniently creates U_M with a phase function proportional to the collective magnetization, $\theta(m_z) \propto m_z$. See Fig. 5.14. In this measurement process, the state of the MSS is updated according to Eq. (5.18), with the measurement operators,

$$\begin{aligned} M_0 &= \sum_{m_z} \cos(\theta(m_z))\Pi^N(m_z) \\ M_1 &= i\sum_{m_z} \sin(\theta(m_z))\Pi^N(m_z) \end{aligned} \tag{5.31}$$

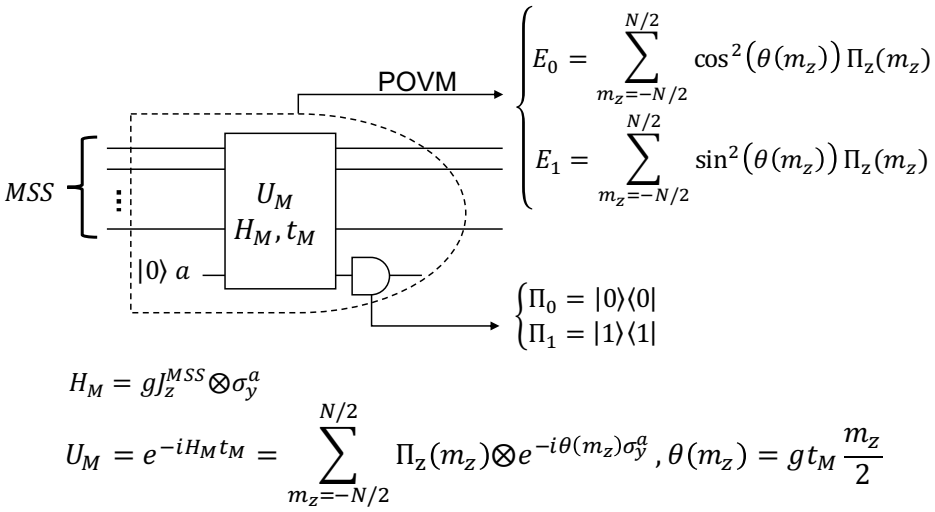

Figure 5.14: Two outcome POVM on a MSS implemented through an apparatus qubit.

In order to select $\left|\psi_{01}^{GR}\right\rangle$ and $\left|\psi_{10}^{GR}\right\rangle$ over $\left|\psi_{00}^{GR}\right\rangle$ and $\left|\psi_{11}^{GR}\right\rangle$, the linear phase function is chosen to be $\theta(m_z) = \frac{2\pi}{N} m_z$. Figure 5.15 depicts the corresponding expansion coefficients of the POVM operators and the fidelity of the target qubits' state with the maximally entangled state $|m_0\rangle$, upon measurement, post-selection on outcome 1 and disentangling

from the MSS. The fidelity increases with the size of the MSS and asymptotically approaches its maximum value, one. This increase has two origins. First, the macroscopic distinctness between the states $\{|\psi_{01}^{GR}\rangle, |\psi_{10}^{GR}\rangle\}$ and $\{|\psi_{00}^{GR}\rangle, |\psi_{11}^{GR}\rangle\}$ grows with the size of the MSS. Second, for larger MSSs, the measurement coefficients become closer to uniform distribution over the expansion of the spectrum of $|\psi_{01}^{GR}\rangle$ and $|\psi_{10}^{GR}\rangle$; thus these states get less distorted by the measurement and the following disentangling gate will restore more coherence between the qubits' states $|01\rangle_q$ and $|10\rangle_q$. It should be mentioned that we have simulated an ideal noise-free process. In practice, the fidelity is not expected to increase with the size of the MSS, indefinitely. Including noise effect imposes an upper bound on size of the MSS, since in general larger MSS are more sensitive to noise.

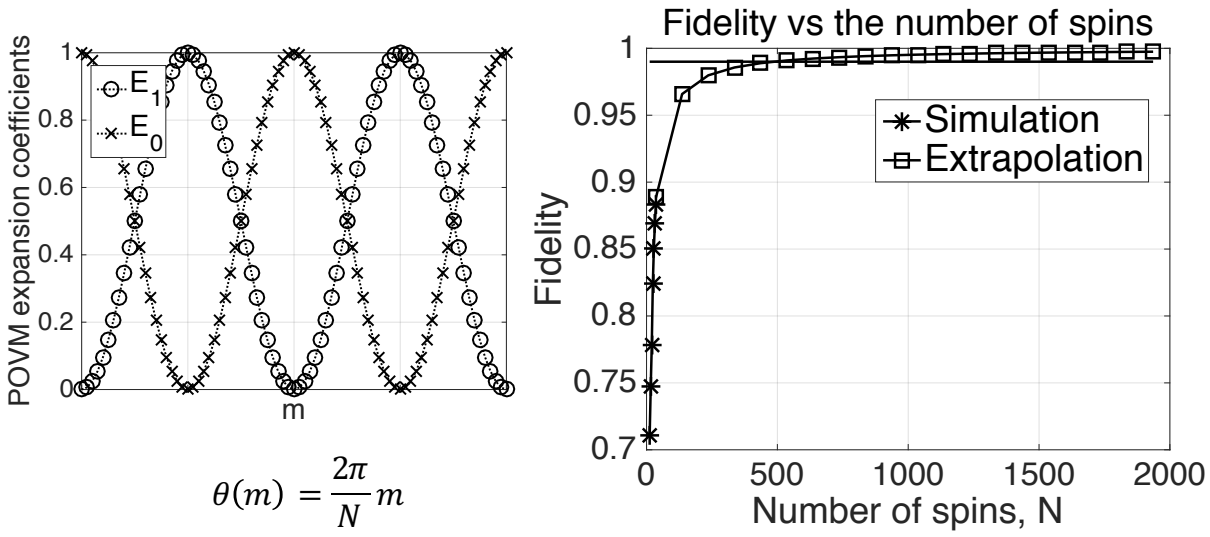

Figure 5.15: (a) The expansion coefficients of the two POVM operators based on the measurement procedure shown in Fig. 5.14 with $\theta(m_z) = \frac{2\pi}{N} m_z$, chosen to distinguish between $\{|\psi_{01}^{GR}\rangle, |\psi_{10}^{GR}\rangle\}$ and $\{|\psi_{00}^{GR}\rangle, |\psi_{11}^{GR}\rangle\}$ with highest probability. (b) The corresponding fidelity of the entangled state of the target qubits with the maximally entangled state $|m_0\rangle$, after applying the measurement in (a) on the MSS, post-selecting on outcome 1 and disentangling from the MSS. The fidelity is computed based on simulation of the spectra of the states $\{|\psi_{01}^{GR}\rangle, |\psi_{10}^{GR}\rangle, |\psi_{00}^{GR}\rangle, |\psi_{11}^{GR}\rangle\}$ for $N = 12, 16, 20, 24, 28, 32, 36$ spins and extrapolation of their spectra according to binomial distribution for larger systems.

Figure 5.15 shows that the fidelity, $F_{m_0}(\rho_q)$,exceeds 0.5 and the target qubits are entangled for all simulated sizes of the MSS, although the assumed measurement model is not an ideal measurement procedure. Moreover, for $N \geq 24$, the fidelity is greater than

0.78, enough to violate the CHSH inequality [69, 44].

5.6 Mixed initial state

So far, a pure polarized state, $|\uparrow\rangle^{\otimes N}$, has been considered as the initial state of the MSS. In this section, we prove robustness of the introduced indirect joint measurement procedure to limited initial polarization of the MSS. In particular, we will show that micro-macro entanglement between each target qubit and its nearby half of the MSS and the subsequent bipartite entanglement of the non-interacting target qubits are robust to deviations of the MSS's initial state from fully polarized state; when the MSS is initially in the experimentally relevant mixed state,

$$\begin{aligned} \rho_{in}(N,\epsilon) &= \left(\frac{\mathbb{1}+(1-\epsilon)\sigma_z}{2}\right)^{\otimes N} \\ &= \left((1-\frac{\epsilon}{2})\,|\uparrow\rangle\langle\uparrow| + \frac{\epsilon}{2}\,|\downarrow\rangle\langle\downarrow|\right)^{\otimes N} \end{aligned} \tag{5.32}$$

The polarization parameter, ϵ, ranges from 0, for a fully polarized pure state, to 1, for the maximally mixed state. We are particularly interested in highly polarized states, i.e., ϵ close to 0.

The magnification gate in Fig. 5.9 can be written as,

$$U_{GR} = |0\rangle\langle 0|_q \otimes \mathbb{1} + |1\rangle\langle 1|_q \otimes V_1 \tag{5.33}$$

with $V_1\,|\uparrow\rangle^{\otimes N_h} = \left|\psi_1^{GR}\right\rangle$. The state of one target qubit and its nearby half of the MSS after applying gate U_{GR} to the initial state $|+\rangle\langle+| \otimes \rho_{in}(N_h,\epsilon)$ is,

$$\begin{aligned} \rho_{q,MSS}^{GR} &= \frac{1}{2}\Big(|0\rangle\langle 0|_q \otimes \rho_{in} + |1\rangle\langle 1|_q \otimes (V_1\rho_{in}V_1^\dagger) \\ &+ |0\rangle\langle 1|_q \otimes (\rho_{in}V_1^\dagger) + |1\rangle\langle 0|_q \otimes (V_1\rho_{in})\Big) \end{aligned} \tag{5.34}$$

Micro-macro entanglement of state $\rho_{q,MSS}^{GR}$ requires bipartite entanglement between the qubit and the MSS and macroscopic distinctness between the state $\rho_0^{GR} = \rho_{in}$ and $\rho_1^{GR} = V_1\rho_{in}V_1^\dagger$. We investigate how these two characteristics change when the initial state of the MSS deviates from the ideal polarized state. Direct verification of bipartite entanglement between a microscopic and a mesoscopic system experimentally is a challenging task

[98, 99]. Nevertheless, it can be simulated for small sizes of the mesoscopic system. A computable measure of bipartite entanglement for a general state, ρ_{AB}, regardless of the size of each party and the purity of the overall state, is negativity, which is defined as the sum of the absolute values of the negative eigenvalues of the partially transposed density matrix, $\rho_{AB}^{T_A}$, [46]

$$\mathrm{Neg}(\rho_{AB}) := \sum_i |\lambda_i| \tag{5.35}$$

Negativity ranges from zero for separable states to 0.5 for maximally entangled states [10]. This measure is specifically helpful in quantifying bipartite entanglement of a mixed state, when one or both of the parties have more than two levels; where, other computable measures for mixed state entanglement such as concurrence can not be applied. A related measure is logarithmic negativity, defined as,

$$\mathrm{Lneg}(\rho_{AB}) := \log_2 ||\rho_{AB}^{T_A}||_1 = \log_2(2\mathrm{Neg}(\rho_{AB}) + 1) \tag{5.36}$$

where $||\rho_{AB}^{T_A}||_1$ is the trace norm of the partially transposed density matrix, $\rho_{AB}^{T_A}$. Logarithmic negativity ranges from 0, for separable states, to 1, for maximally entangled states [46].

Figure 5.16 shows logarithmic negativity of the bipartite entangled state of the qubit and the MSS, $\rho_{q,MSS}^{GR}$, as a function of the polarization parameter, ϵ, simulated for different sizes of the MSS up to 10 spins. We are particularly interested in highly polarized states, where ϵ is close to 0. For the fully polarized initial state ($\epsilon = 0$), the state $\rho_{q,MSS}^{GR}$ is maximally entangled as already discussed. The entanglement reduces with decrease in the polarization (increase in ϵ) with a slow initial pace. The larger the MSS, the slower the initial drop in entanglement, i.e. for larger MSS, bipartite entanglement of state $\rho_{q,MSS}^{GR}$ is more robust to polarization reduction of the MSS's initial state.

Macroscopic distinctness between the states ρ_0^{GR} and ρ_1^{GR} can be quantified according to Eq. (5.6). The collective magnetization spectrum of the state $\rho_0^{GR} = \rho_{in}(N_h, \epsilon)$ is a shifted [11] binomial distribution with the probability of success $p = 1 - \epsilon/2$, and number of trials N_h. Its mean and SD are $\langle J_z \rangle_0^{GR}(\epsilon) = (1-\epsilon)N_h/2$ and $(\Delta J_z)_0^{GR}(\epsilon) = \sqrt{N_h \frac{\epsilon}{2}(1-\frac{\epsilon}{2})}$.

The mean and SD of the spectrum of state $\rho_1^{GR} = V_1 \rho_{in} V_1^\dagger$ are known for the two extreme cases; $\epsilon = 0$ and $\epsilon = 1$. It was shown that with a polarized initial state, $\epsilon = 0$, the mean of the spectrum is $\langle J_z \rangle_1^{GR}(\epsilon = 0) \approx 0$ and its SD scales as $(\Delta J_z)_1^{GR}(\epsilon = 0) \approx \sqrt{N_h}/2$.

[10] Based on the PPT criteria **cite** all separable states have zero negativity but not all entangled states have nonzero negativity except for 2×2 and 2×3 systems. In other words nonzero negativity guarantees entanglement but there are entangled states with zero negativity.

[11] The distribution ranges from $-N_h/2$ to $N_h/2$ rather than 0 to N_h.

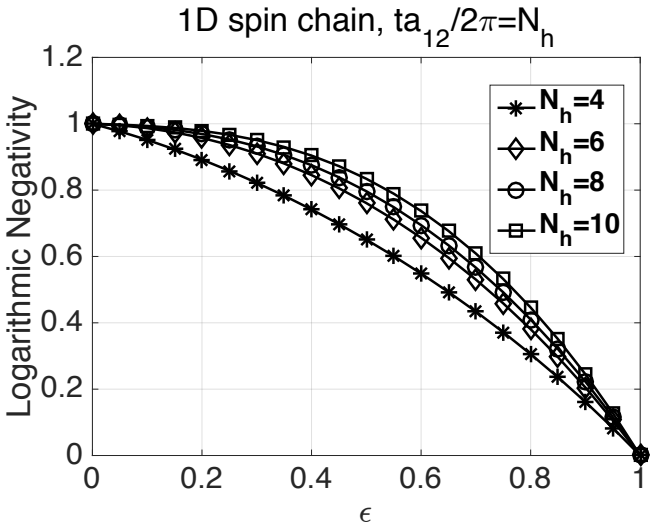

Figure 5.16: Entanglement between one target qubit and its nearby half of the MSS as a function of deviation of the initial state of the MSS from fully polarized state simulated for different sizes of the MSS. For larger MSSs, bipartite entanglement between the target qubit and the MSS is more robust to polarization reduction.

On the other side of the range, when $\epsilon = 1$, the initial state, ρ_{in}, is a fully mixed state; thus ρ_1^{GR} is also a fully mixed state and the mean and SD of its spectrum are, $\langle J_z \rangle_1^{GR}(\epsilon = 1) = 0$ and $(\Delta J_z)_1^{GR}(\epsilon = 1) = \sqrt{N_h}/2$. Similar mean and SD for the two extreme cases suggests the same scaling for all other polarizations, $0 < \epsilon < 1$. Simulation results for different polarization with $N_h = 12$ spins, shown in Fig. 5.17, confirms this prediction. Thus, the mean and SD of the spectrum of ρ_1^{GR} are $\langle J_z \rangle_1^{GR}(\epsilon) \approx 0$ and $(\Delta J_z)_1^{GR}(\epsilon) \approx \sqrt{N_h}/2$, for all initial polarizations. Consequently, the macroscopic distinctness between the states ρ_0^{GR} and ρ_1^{GR} requires that,

$$\frac{\langle J_z \rangle_0^{GR}(\epsilon) - \langle J_z \rangle_1^{GR}(\epsilon)}{(\Delta J_z)_0^{GR}(\epsilon) + (\Delta J_z)_1^{GR}(\epsilon)} \approx \frac{(1-\epsilon)N_h/2 - 0}{\sqrt{\epsilon(2-\epsilon)}\sqrt{N_h}/2 + \sqrt{N_h}/2} \gg 1 \tag{5.37}$$

For $0 \leq \epsilon \leq 1$, the maximum of $\sqrt{\epsilon(2-\epsilon)}$ is 1 at $\epsilon = 1$ and the above relation is lower bounded by,

$$\frac{\langle J_z \rangle_0^{GR}(\epsilon) - \langle J_z \rangle_1^{GR}(\epsilon)}{(\Delta J_z)_0^{GR}(\epsilon) + (\Delta J_z)_1^{GR}(\epsilon)} > \frac{(1-\epsilon)N_h/2}{\sqrt{N_h}} \propto \frac{1-\epsilon}{2}\sqrt{N_h} \tag{5.38}$$

Thus, $\frac{1-\epsilon}{2}\sqrt{N_h} \gg 1$ assures macroscopic distinctness between the states ρ_0^{GR} and ρ_1^{GR}. This condition along with robustness of entanglement to decreases in polarization, shown in Fig.

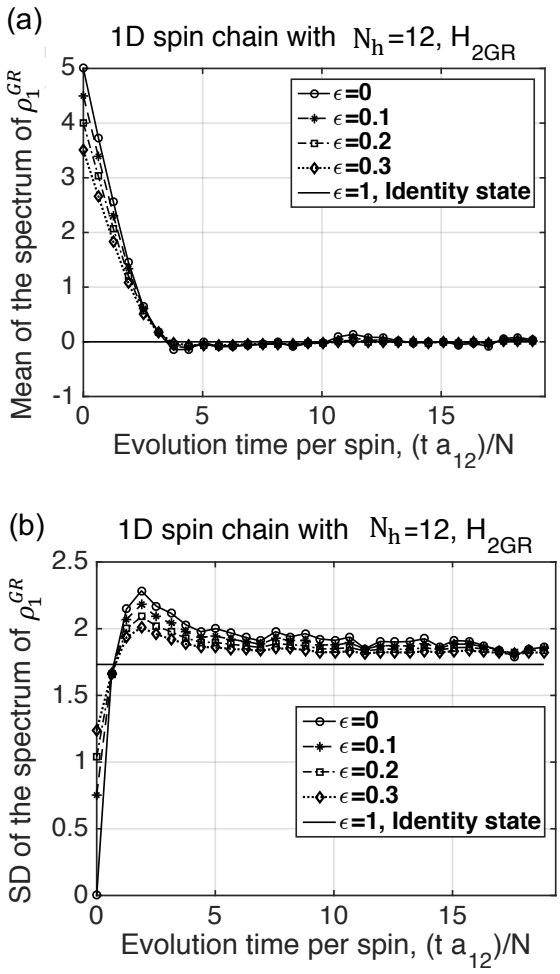

Figure 5.17: (a) The mean and (b) the SD of the spectrum of ρ_1^{GR} as a function of time simulated with $N_h = 12$ spins in a 1D chain for different initial polarization of the MSS.

5.16, prove that the micro-macro entanglement between each target qubit and its nearby half of the MSS is robust to polarization loss when ϵ is close to 0 and $N_h(1-\epsilon)^2 \gg 4$.

Two copies of the state in Eq. (5.34) represent the state of the two non-interacting

target qubits and the uncoupled halves of the intermediate MSS,

$$\begin{aligned}\rho_{q,MSS} &= \frac{1}{4}\Big(|00\rangle\langle 00|_q \otimes \rho_{00}^{GR} + |01\rangle\langle 01|_q \otimes \rho_{01}^{GR} \\ &+ |10\rangle\langle 10|_q \otimes \rho_{10}^{GR} + |11\rangle\langle 11|_q \otimes \rho_{11}^{GR} \\ &+ |01\rangle\langle 10|_q \otimes (\rho_{in}^{L} V_1^{L\dagger}) \otimes (V_1^{R} \rho_{in}^{R}) \\ &+ |10\rangle\langle 01|_q \otimes (V_1^{L} \rho_{in}^{L}) \otimes (\rho_{in}^{R} V_1^{R\dagger}) \\ &+ \text{other off-diagonal terms}\Big) \end{aligned} \tag{5.39}$$

where $\rho_{ij}^{GR} = \rho_i^{GR} \otimes \rho_j^{GR}$ for $i, j = 0, 1$. The normalized state of the target qubits after the measurement, post-selection on zero magnetization and disentangling from the MSS is,

$$\rho_q = \mathrm{Tr}_{MSS}\left(U_{GR}^{L\dagger} \otimes U_{GR}^{R\dagger} \frac{(\mathbb{1} \otimes M_1)\rho_{q,MSS}(\mathbb{1} \otimes M_1^\dagger)}{\mathrm{Tr}(E_1 \rho_{q,MSS})} U_{GR}^{L} \otimes U_{GR}^{R}\right) \tag{5.40}$$

The measurement on the MSS and post-selection, $\mathbb{1} \otimes M_1$, defined in Eq. (5.31), selects ρ_{01}^{GR} and ρ_{10}^{GR}, correlated with $|01\rangle_q$ and $|10\rangle_q$ states of the qubits, and the disentangling gate, $U_{GR}^{L\dagger} \otimes U_{GR}^{R\dagger}$, restores the coherence between the target qubits.

Success of the measurement process relies on distinguishability of the states ρ_{01}^{GR} and ρ_{10}^{GR} from the states ρ_{00}^{GR} and ρ_{11}^{GR}, which requires,

$$\begin{aligned}\frac{N}{4}(1-\epsilon) &\gg \left(\frac{\sqrt{N}}{2}\sqrt{\frac{1+\epsilon(2-\epsilon)}{2}} + \frac{\sqrt{N}}{2}\right) \sim \sqrt{N} \\ &\Rightarrow \quad N(1-\epsilon)^2 \gg 16 \end{aligned} \tag{5.41}$$

Restoring the coherence between the states $|01\rangle_q$ and $|10\rangle_q$ requires each qubit to be entangled with its nearby half of the MSS prior to the measurement on the MSS.

The target qubits' state can be expanded in the computational basis as,

$$\rho_q = \sum_{i,j,k,l=0}^{1} c_{ij,kl} \, |ij\rangle\langle kl| \tag{5.42}$$

with the normalization condition $c_{00,00} + c_{01,01} + c_{10,10} + c_{11,11} = 1$. The amplitude of the states $|01\rangle_q$ and $|10\rangle_q$ ($c_{01,01}$ and $c_{10,10}$) and the coherence between them ($c_{01,10}$ and $c_{10,01}$) equally contribute to the fidelity of the target qubits' state with the maximally entangled

state $|m_0\rangle = \frac{1}{\sqrt{2}}(|01\rangle + |10\rangle)$,

$$\begin{aligned} F_{m_0}(\rho_q) &= \frac{c_{01,01} + c_{10,10} + c_{01,10} + c_{10,01}}{2} \\ &= c_{01,01} + c_{01,10} = c_{01,01}\left(1 + \frac{c_{01,10}}{c_{01,01}}\right) \end{aligned} \tag{5.43}$$

where $0 \leq c_{01,10} \leq c_{01,01} \leq 0.5$ and the second line follows the equalities: $c_{01,01} = c_{10,10}$ and $c_{01,10} = c_{10,01}$ that hold assuming identical states on the two qubits and their nearby halves of the MSS.

Equation 5.43 shows that reduction of the fidelity, as the polarization decreases, originates from two sources: leakage from the subspace spanned by $\{|01\rangle_q, |10\rangle_q\}$ to the subspace spanned by $\{|00\rangle_q, |11\rangle_q\}$ and loss of coherence between the states $|01\rangle_q$ and $|10\rangle_q$, which are associated to losing macroscopic distinctness and bipartite entanglement in the micro-macro entangled state in Eq. (5.34), respectively.

Figure 5.18 shows (a) the fidelity in Eq. 5.43, (b) the population in $\{|01\rangle_q, |10\rangle_q\}$ subspace $(c_{01,01} + c_{10,10})$ and (c) the coherence between the states $|01\rangle_q$ and $|10\rangle_q$ relative to the population $(c_{01,10}/c_{01,01})$, simulated as a function of ϵ for MSSs with $N = 8, 12, 16, 20$ spins. In these simulations, the measurement model of section 5.5 is used with the measurement parameter $\theta(m_z) = \frac{2\pi}{N(1-\epsilon)} m_z$, modified as a function of the polarization such that the measurement operator M_1 selects ρ_{01}^{GR} and ρ_{10}^{GR} over ρ_{00}^{GR} and ρ_{11}^{GR} with the highest probability.

These plots show that for the simulated sizes of the MSS, the fidelities drop fast with decrease in the polarization, as a result of the fast decreases in the populations in $\{|01\rangle_q, |10\rangle_q\}$ subspace. The coherence losses happen at a slow rate consistent with the slow entanglement losses in the corresponding micro-macro entangled states, depicted in Fig. 5.16.

Fast decreases in the populations, observed in Fig. 5.18(b), are not generic effects and result from the small sizes of the simulated systems, that do not satisfy the distinguishability condition: $N(1-\epsilon)^2 \gg 16$. For large enough systems, $N \gg 16$, the population drops with a slow rate as ϵ grows, up to a point where the macroscopic distinctness condition is not satisfied, $\epsilon \approx 1 - \frac{8}{\sqrt{N}}$, as shown in Fig. 5.19. Thus, the population in $\{|01\rangle_q, |10\rangle_q\}$ subspace is close to 1 when $N(1-\epsilon)^2 \gg 16$. In addition, as figure 5.18(c) shows, the larger the MSS, the slower the rate of the coherence loss. Thus, for large MSSs, $N(1-\epsilon)^2 \gg 16$, both population in $\{|01\rangle_q, |10\rangle_q\}$ subspace and coherence between the states $|01\rangle_q$ and $|10\rangle_q$, and consequently the fidelity, $F_{m_0}(\rho_q)$, are robust to decrease in polarization of the MSS's initial state.

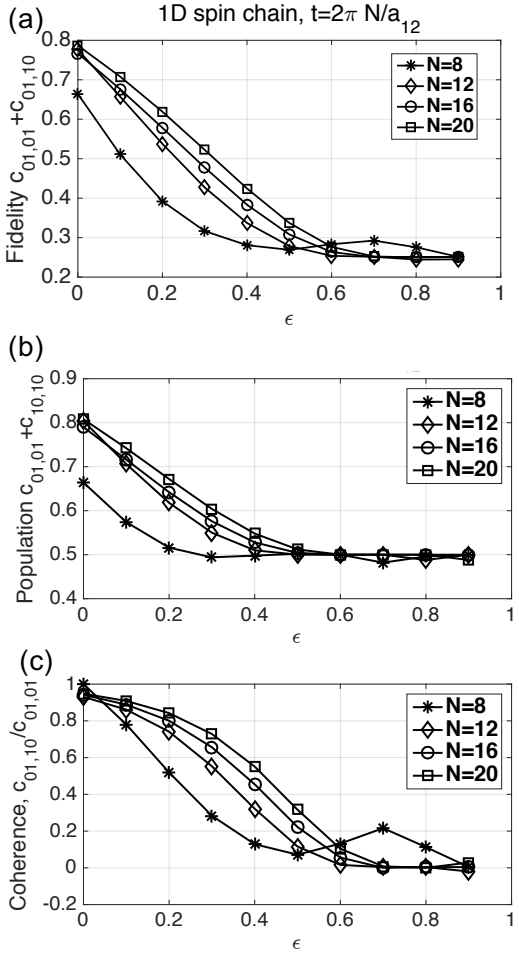

Figure 5.18: Simulation results of (a) the fidelity (b) the population (the diagonal terms of the density matrix) and (c) the coherence (the off-diagonal terms of the density matrix relative to diagonal terms) of the target qubits' states as a function of initial polarization of the MSS for small number of spins. Slow initial drop in the coherence follows robustness in the bipartite entanglement between each qubit and its nearby half of the MSS to polarization reduction. Fast decrease in the population and the fidelity results from small sizes of the simulated system that do not satisfy macroscopic distinctness condition.

In conclusion, bipartite entanglement between the target qubits is robust to deviation of the initial state of the MSS from the fully polarized state, as long as $N(1-\epsilon)^2 \gg 16$. With a fixed measurement resolution limited initial polarization of the MSS needs to be

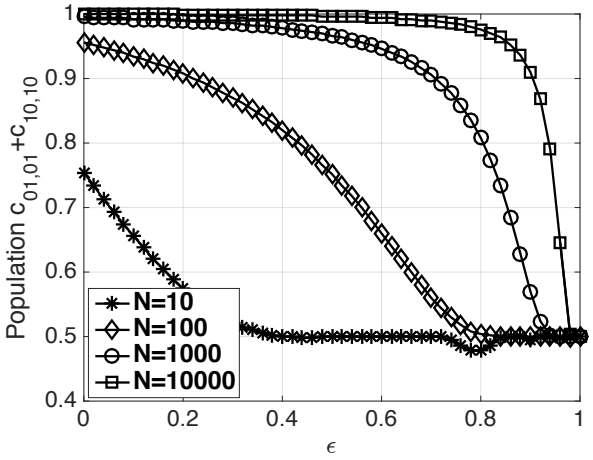

Figure 5.19: Simulation of diagonal terms of the qubits' state, $c_{01,01} + c_{10,10}$, based on the extrapolation of the spectra of $\rho_{00}, \rho_{01}, \rho_{10}$ and ρ_{11} according to the binomial distribution and using the measurement model of section 5.5 with $\theta(m) = \frac{2\pi}{N(1-\epsilon)}$.

compensated for by enlarging the MSS, $N_\epsilon = N_{\epsilon=0}/(1-\epsilon)$.

5.7 Sensitivity to noise

A common feature of micro-macro entangled states and more generally macroscopic superposition states is their sensitivity to noise [100]; to the extent that the rate of coherence loss has been suggested as a measure of the macroscopicity of quantum superposition states [101, 102]. This section discusses sensitivity of the micro-macro entangled state $\left|\phi^{GR}\right\rangle_{q,MSS}$, in Eq. (5.25) and bipartite entanglement of the target qubits to single particle loss[12].

Among the two characteristics of micro-macro entanglement, namely microscopic distinctness and bipartite entanglement, macroscopic distinctness is, by definition, robust to single particle loss. The states of the MSS associated with $|0\rangle_q$ and $|1\rangle_q$ states of the qubit differ by many spin flips; thus, single particle loss does not significantly affect their distinctness.

[12]Particle loss is a common noise in photonic systems. For a spin system, in which particles are preserved, loss of a single spin models a generalized amplitude damping channel on the spin with an arbitrary fixed point and the damping probability of one.

Before studying the sensitivity of bipartite entanglement of the state $\left|\phi^{GR}\right\rangle_{q,MSS}$ to particle loss, we first analyse a class of symmetric entangled states between the target qubit and the MSS,

$$|S_k\rangle_{q,MSS} = \frac{1}{\sqrt{2}}\left(|0\rangle_q \otimes |\uparrow\rangle^{\otimes N_h} + |1\rangle_q \otimes |D_k\rangle\right) \tag{5.44}$$

The parameter k ranges from 1 to N_h, and $|D_k\rangle$ is the symmetric pure state with k spins $|\downarrow\rangle$ and $N_h - k$ spins $|\uparrow\rangle$,

$$|D_k\rangle = \frac{1}{\sqrt{\binom{N_h}{k}}} \sum_{i=1}^{\binom{N_h}{k}} P_i(|\downarrow\rangle^{\otimes k} |\uparrow\rangle^{\otimes N_h - k}) \tag{5.45}$$

where P_i is the permutation operator and the summation is over all permutations. State $|D_k\rangle$ is an eigenstate of the collective magnetization operator, J_z, with the eigenvalue $m_z = \frac{N_h - 2k}{2}$; hence, the (macroscopic) distinctness between the states $|\uparrow\rangle^{\otimes N_h}$ and $|D_k\rangle$ is proportional to k and for $k \gg 1$, $|S_k\rangle_{q,MSS}$ is a micro-macro entangled state. We show that sensitivity of bipartite entanglement between the qubit and the MSS in state $|S_k\rangle_{q,MSS}$ to single particle loss increases with k. Thus, there is a trade off between macroscopic distinctness of a micro-macro entangled state and robustness of its bipartite entanglement to particle loss.

The state of the target qubit and the MSS after loss of any single particle is,

$$\begin{aligned}
\rho^k_{q,MSS-1} &= p^k_\uparrow \left|\psi^k_\uparrow\right\rangle\left\langle\psi^k_\uparrow\right| + p^k_\downarrow \left|\psi^k_\downarrow\right\rangle\left\langle\psi^k_\downarrow\right| \qquad (5.46)\\
\sqrt{p^k_\uparrow}\left|\psi^k_\uparrow\right\rangle &= \frac{1}{\sqrt{2}}|0\rangle_q \otimes |\uparrow\rangle^{\otimes N_h - 1} \\
&+ \frac{1}{\sqrt{2}\sqrt{\binom{N_h}{k}}}|1\rangle_q \otimes \sum_{i=1}^{\binom{N_h-1}{k}} P_i(|\downarrow\rangle^{\otimes k} |\uparrow\rangle^{\otimes N_h - k - 1}) \\
\sqrt{p^k_\downarrow}\left|\psi^k_\downarrow\right\rangle &= \frac{1}{\sqrt{2}\sqrt{\binom{N_h}{k}}}|1\rangle_q \otimes \sum_{i=1}^{\binom{N_h-1}{k-1}} P_i(|\downarrow\rangle^{\otimes k-1} |\uparrow\rangle^{\otimes N_h - k})
\end{aligned}$$

where the states $\left|\psi^k_\uparrow\right\rangle$ and $\left|\psi^k_\downarrow\right\rangle$ are normalized and orthogonal to each other and $p^k_\uparrow + p^k_\downarrow = 1$. The entanglement of projection between the target qubit and the MSS in state $\rho^k_{q,MSS-1}$ is defined as [45],

$$E_p(\rho^k_{q,MSS-1}) = p^k_\uparrow E(\left|\psi^k_\uparrow\right\rangle) + p^k_\downarrow E(\left|\psi^k_\downarrow\right\rangle) \tag{5.47}$$

where $E(|\psi_{AB}\rangle)$ is the von Neumann entropy of the pure bipartite state $|\psi_{AB}\rangle$, defined as $E(|\psi_{AB}\rangle) = -\mathrm{Tr}[\rho_A \log_2(\rho_A)]$ with $\rho_A = \mathrm{Tr}_B(\rho_{AB})$. Entanglement of projection ranges between 0 to 1 and is an upper bound for entanglement of formation [50, 103].

State $\left|\psi_{\downarrow}^{k}\right\rangle$ is a separable state ,thus $E(\psi_{\downarrow}^{k}) = 0$. The von Neumann entropy of state $\left|\psi_{\uparrow}^{k}\right\rangle$ is,

$$E(\left|\psi_{\uparrow}^{k}\right\rangle) = \frac{1}{1+r_\uparrow}\log_2(\frac{1}{1+r_\uparrow}) + \frac{r_\uparrow}{1+r_\uparrow}\log_2(\frac{r_\uparrow}{1+r_\uparrow}) \tag{5.48}$$

where $r_\uparrow(k) = \binom{N_h-1}{k}/\binom{N_h}{k} = 1 - \frac{k}{N_h}$ is the probability of finding one spin $|\uparrow\rangle$ in the state $|D_k\rangle$ of the MSS, and ranges from $r_\uparrow = 0$, for $k = N_h$, to $r_\uparrow = 1 - \frac{1}{N_h}$, for $k = 1$. The entanglement of projection of state $\rho_{q,MSS-1}^{k}$, according to Eq. (5.47), is,

$$\begin{aligned} E_p(\rho_{q,MSS-1}^{k}) &= \\ E_p^r(r_\uparrow) &:= -\frac{1+r_\uparrow}{2}\left(\frac{1}{1+r_\uparrow}\log_2(\frac{1}{1+r_\uparrow})\right. \\ &+ \left.\frac{r_\uparrow}{1+r_\uparrow}\log_2(\frac{r_\uparrow}{1+r_\uparrow})\right) \end{aligned} \tag{5.49}$$

Note that $E_p(\rho_{q,MSS-1}^{k})$ depends on the ratio k/N_h and not on k and N_h, independently.

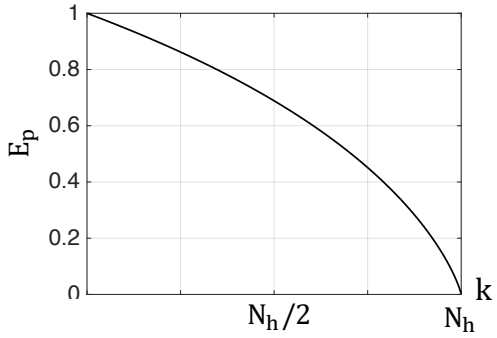

Figure 5.20: Entanglement of projection of the symmetric bipartite entangled state $|S_k\rangle_{q,MSS}$ upon single particle loss as a function of macroscopic distinctness between $|\uparrow\rangle^{N_h}$ and $|D_k\rangle$. The more macroscopically distinct the states $|\uparrow\rangle^{N_h}$ and $|D_k\rangle$ are, the more fragile the bipartite entanglement of $|S_k\rangle_{q,MSS}$ is.

Figure 5.20 plots $E_p(\rho_{q,MSS-1}^{k})$ as a function of the macroscopic distinctness, k. The bipartite entanglement between the target qubit and the MSS becomes more fragile to

particle loss as the macroscopic distinctness in state $|S_k\rangle_{q,MSS}$ increases. At the limit of maximum macroscopic distinctness, $|D_{N_h}\rangle = |\downarrow\rangle^{\otimes N_h}$, $|S_k\rangle_{q,MSS}$ represents an overall GHZ state, and no entanglement will remain after loss of one particle from the MSS.

The entangled state of interest, $\left|\phi^{GR}(t)\right\rangle_{q,MSS}$ in Eq. (5.25), follows a similar form to state $|S_k\rangle_{q,MSS}$ in Eq. 5.44 except that $|D_k\rangle$ is replaced by $\left|\psi_1^{GR}(t)\right\rangle$. The state $\left|\psi_1^{GR}(t)\right\rangle$ is not necessarily symmetric; thus, to quantify the sensitivity of state $\left|\phi^{GR}(t)\right\rangle_{q,MSS}$ to single particle loss, we average the entanglement of projection upon losing each of the spins in the MSS, assuming that all spins have equal probabilities of being lost.

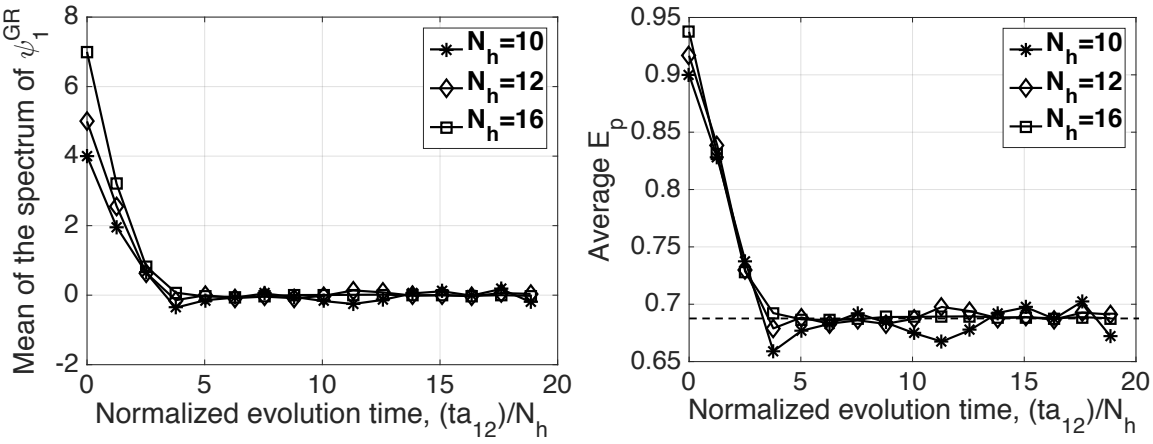

Figure 5.21: (a) The mean of the spectrum of state $\left|\psi_1^{GR}(t)\right\rangle$ as a measure of macroscopic distinctness between $\left|\psi_1^{GR}(t)\right\rangle$ and $|\uparrow\rangle^{N_h}$. (b) The entanglement of projection of the state $\left|\phi^{GR}(t)\right\rangle_{q,MSS}$ upon single spin loss as a function of time. Bipartite entanglement of state $\left|\phi^{GR}(t)\right\rangle_{q,MSS}$ upon single particle loss reduces with increase in the macroscopic distinctness between $\left|\psi_1^{GR}(t)\right\rangle$ and $|\uparrow\rangle^{N_h}$ until it reaches the asymptotic value 2/3. This asymptotic value is similar for all sizes of the MSS and corresponds to difference in the mean of the collective J_z magnetization, $\langle J_z\rangle_0^{GR} - \langle J_z\rangle_1^{GR} \sim \frac{1}{2}N_h/2$, similar to symmetric bipartite entangled state $|S_k\rangle_{q,MSS}$ with $k = N_h/2$.

Figure 5.21 shows simulation results for the mean of the spectrum of state $\left|\psi_1^{GR}(t)\right\rangle$ and the entanglement of projection of state $\left|\phi^{GR}(t)\right\rangle_{q,MSS}$ upon single particle loss as a function of the evolution time for different sizes of MSS. As evolution time increases, the mean of the spectrum of state $\left|\psi_1^{GR}(t)\right\rangle$ decreases and macroscopic distinctness in the state $\left|\phi^{GR}(t)\right\rangle_{q,MSS}$ and its sensitivity to particle loss increase. For long evolution times,

the probability of finding any of the spins in the MSS in state $|\uparrow\rangle$ is close to 1/2. Thus, the asymptotic value of the average of entanglement of projection is,

$$\sum_{j=1}^{N_h} E_p(\mathrm{Tr}_j(\left|\phi^{GR}(t)\right\rangle\left\langle\phi^{GR}(t)\right|)) \approx E_p^r(r_\uparrow = 1/2) = \frac{2}{3} \tag{5.50}$$

Decrease in bipartite entanglement of the micro-macro entangled state $\left|\phi^{GR}\right\rangle$, upon particle loss, is reflected in the fidelity of the target qubits' entangled state. Even with an ideal measurement on the MSS and post-selection, that perfectly selects the $\{|01\rangle_q, |10\rangle_q\}$ subspace of the qubits over the $\{|00\rangle_q, |11\rangle_q\}$ subspace, the fidelity can not be greater than $F_{\max} = c_{01,01}^{\max} + c_{01,10}^{\max} = 1/2 + 1/4 = 3/4$ (See section 5.7.1). This upper bound follows the reduced coherence between $|01\rangle_q$ and $|10\rangle_q$ in the state of the qubits, even when the population is preserved.

Fragility of the micro-macro entangled state and bipartite entanglement of the target qubits to particle loss illustrates the importance of shorter transient time with a MSS that has a 2D or 3D structure compared to a 1D chain, demonstrated in section 5.4. Since any loss in the MSS results in a reduction of bipartite entanglement between the target qubits, the overall experiment time needs to be much shorter than T_1 divided by the number of spins in the MSS, $t_{exp} \ll \frac{T_1}{N_h}$.

5.7.1 Upper bound on Fidelity upon single particle loss

The sensitivity of the micro-macro entangled states and bipartite entanglement between the target qubits to spin loss in the MSS was discussed in section 5.7. In particular, it was specified that the upper bound on the fidelity of the target qubits' state with the maximally entangled state $|m_0\rangle = \frac{1}{\sqrt{2}}(|01\rangle_q + |10\rangle_q)$, upon single particle loss, reduces from one to 3/4 and this decrease solely originates from reduction of the coherence between $|01\rangle_q$ and $|10\rangle_q$ states. In this section, we prove this upper bound on the fidelity.

The state of the target qubits and the MSS after the magnification process is: $\left|\phi^{GR}\right\rangle_L \otimes \left|\phi^{GR}\right\rangle_R$ where $\left|\phi^{GR}\right\rangle_i = \frac{1}{\sqrt{2}}(|0\rangle_{q_i} |\uparrow\rangle^{\otimes N_h} + |1\rangle_{q_i} \left|\psi_1^{GR}\right\rangle_i$ with $i = L, R$ is the state of each qubit and its nearby half of the MSS. Let's consider that the state of one spin from the MSS with index $\mathfrak{a}$ is lost and is replaced by a state $\rho_\mathfrak{a}$. This particle loss process corresponds to a generalized amplitude damping map with the fixed point $\rho_\mathfrak{a}$ and the damping probability of one on spin $\mathfrak{a}$. Without loss of generality, we assume the lost spin is in the left half of

the MSS, $\mathfrak{a} \leq N/2$. The state $\left|\psi_1^{GR}\right\rangle_L$ can be expanded in the basis $\{|\uparrow\rangle_\mathfrak{a}, |\downarrow\rangle_\mathfrak{a}\}$ of spin $\mathfrak{a}$ as,

$$\left|\psi_1^{GR}\right\rangle_L = \alpha_\mathfrak{a} \left|\psi_\alpha^\mathfrak{a}\right\rangle |\uparrow\rangle_\mathfrak{a} + \beta_\mathfrak{a} \left|\psi_\beta^\mathfrak{a}\right\rangle |\downarrow\rangle_\mathfrak{a} \tag{5.51}$$

where $\alpha_\mathfrak{a} \left|\psi_\alpha^\mathfrak{a}\right\rangle = (\langle\uparrow|_\mathfrak{a} \otimes \mathbb{1}_{N_h-1}) \left|\psi_1^{GR}\right\rangle_L$, $\beta_\mathfrak{a} \left|\psi_\beta^\mathfrak{a}\right\rangle = (\langle\downarrow|_\mathfrak{a} \otimes \mathbb{1}_{N_h-1}) \left|\psi_1^{GR}\right\rangle_L$, and $|\alpha_\mathfrak{a}|^2 + |\beta_\mathfrak{a}|^2 = 1$ following the normalization of state $\left|\psi_1^{GR}\right\rangle_L$. After particle loss the state of the target qubit q_L and its nearby half of the MSS will be,

$$\rho^{GR}_{q_L, MSS_L} = \left(p_\uparrow \left|\psi_\uparrow^\mathfrak{a}\right\rangle\left\langle\psi_\uparrow^\mathfrak{a}\right| + p_\downarrow \left|\psi_\downarrow^\mathfrak{a}\right\rangle\left\langle\psi_\downarrow^\mathfrak{a}\right|\right) \otimes \rho_\mathfrak{a} \tag{5.52}$$

where the states $\left|\psi_\uparrow^\mathfrak{a}\right\rangle$ and $\left|\psi_\downarrow^\mathfrak{a}\right\rangle$ are,

$$\begin{aligned}
\sqrt{p_\uparrow}\left|\psi_\uparrow^\mathfrak{a}\right\rangle &= \frac{1}{\sqrt{2}}\left(|0\rangle_{q_L} |\uparrow\rangle^{\otimes N_h - 1} + |1\rangle_{q_L} \left(\alpha_\mathfrak{a} \left|\psi_\alpha^\mathfrak{a}\right\rangle\right)\right) \\
\sqrt{p_\downarrow}\left|\psi_\downarrow^\mathfrak{a}\right\rangle &= \frac{|1\rangle_{q_L}}{\sqrt{2}} \beta_\mathfrak{a} \left|\psi_\beta^\mathfrak{a}\right\rangle
\end{aligned} \tag{5.53}$$

An ideal measurement that perfectly selects the states of the MSS correlated to zero magnetization of the qubits over the states of the MSS correlated to ± 1 magnetizations of the qubits, updates the state $\rho^{GR}_{q_L, MSS_L} \otimes \left|\phi^{GR}\right\rangle\left\langle\phi^{GR}\right|_R$ of the target qubits and the MSS to the state,

$$\begin{aligned}
\rho_{q_L q_R, MSS} &= \frac{1}{2}\Big(|01\rangle\langle 01| \otimes (|\uparrow\rangle\langle\uparrow|^{\otimes N_h - 1} \otimes \rho_\mathfrak{a}) \otimes \left|\psi_1^{GR}\right\rangle\left\langle\psi_1^{GR}\right|_R \\
&+ (|10\rangle\langle 10| \otimes ((|\alpha_\mathfrak{a}|^2 \left|\psi_\alpha^\mathfrak{a}\right\rangle\left\langle\psi_\alpha^\mathfrak{a}\right| + |\beta_\mathfrak{a}|^2 \left|\psi_\beta^\mathfrak{a}\right\rangle\left\langle\psi_\beta^\mathfrak{a}\right|) \otimes \rho_\mathfrak{a}) \otimes |\uparrow\rangle\langle\uparrow|^{\otimes N_h} \\
&+ |01\rangle\langle 10| \otimes (\alpha_\mathfrak{a}^\star |\uparrow\rangle^{N_h - 1} \langle\psi_\alpha^\mathfrak{a}| \otimes \rho_\mathfrak{a}) \otimes \left|\psi_1^{GR}\right\rangle_R \langle\uparrow|^{\otimes N_h} \\
&+ |10\rangle\langle 01| \otimes (\alpha_\mathfrak{a} \left|\psi_\alpha^\mathfrak{a}\right\rangle \langle\uparrow|^{N_h - 1} \otimes \rho_\mathfrak{a}) \otimes |\uparrow\rangle^{\otimes N_h} \left\langle\psi_1^{GR}\right|_R\Big)
\end{aligned}$$

Note that the off-diagonal terms of the qubits are scaled with $\alpha_\mathfrak{a}$ and $\alpha_\mathfrak{a}^\star$. This state is a correlated state between the target qubits and the MSS. The following disentangling gate needs to restore the coherence between the target qubits. The maximum retrievable coherence between the target qubits is $|\alpha_\mathfrak{a}|^2$ that corresponds to the state $\rho_\mathfrak{a} = |\uparrow\rangle\langle\uparrow|$. With this choice of the $\rho_\mathfrak{a}$, after applying the disentangling gate and tracing over the MSS, the target qubits' state will be,

$$\rho_{q_L q_R} = \frac{1}{2}\left(|01\rangle\langle 01| + |01\rangle\langle 01| + |\alpha_\mathfrak{a}|^2 |01\rangle\langle 10| + |\alpha_\mathfrak{a}|^2 |10\rangle\langle 01|\right) \tag{5.54}$$

The fidelity of this state with the maximally entangled triplet zero state is $F^\mathfrak{a}_{\max} = (1 + |\alpha_\mathfrak{a}|^2)/2$ where $|\alpha_\mathfrak{a}|^2$ can be interpreted as the probability of finding spin $\mathfrak{a}$ in state $|\uparrow\rangle_\mathfrak{a}$ when

the MSS is in state $\left|\psi_1^{GR}\right\rangle_L$. We know that the mean of the collective magnetization spectrum of state $\left|\psi_1^{GR}\right\rangle_L$ is zero, which is mathematically equivalent to $\sum_{\mathfrak{a}} |\alpha_{\mathfrak{a}}|^2 = \sum_{\mathfrak{a}} |\beta_{\mathfrak{a}}|^2$. Combining with the normalization condition $|\alpha_{\mathfrak{a}}| + |\beta_{\mathfrak{a}}| = 1$, the average of maximum fidelity upon loss of each particle in the MSS is,

$$F_{\max} := \frac{1}{N} \sum_{\mathfrak{a}} F_{\max}^{\mathfrak{a}} = \frac{1}{2} + \frac{\sum_{\mathfrak{a}} |\alpha_{\mathfrak{a}}|}{2N} = \frac{1}{2} + \frac{1}{4} = \frac{3}{4} \tag{5.55}$$

This relation completes the proof for the upper bound on the fidelity of the target qubits' state.

Based on the dynamics that create state $\left|\psi_1^{GR}\right\rangle_L$, the magnetization is expected to be distributed uniformly among the spins in the MSS, thus $|\alpha_{\mathfrak{a}}|^2$ is anticipated to be close to 1/2 for all spins and the maximum fidelity upon loss of any spin is expected to be $F_{\max}^{\mathfrak{a}} \approx 3/4$.

5.8 Discussion and Conclusion

We analyzed the resources required for entangling two uncoupled spin qubits through an intermediate mesoscopic spin system by indirect joint magnetization measurement. In contrast to direct joint measurement, that needs a high-resolution apparatus capable of detecting a single qubit flip to entangle two qubits, indirect joint measurement benefits from coherent magnification of the target spin qubits' state in the collective magnetization of the MSS and only requires a low-resolution collective measurement on the MSS. This work complements the ongoing efforts in using mesoscopic systems as coherent control elements in coupling separated qubits [14, 19] [20, 21, 22, 23, 24, 25, 26, 27, 28, 29].

A MSS consisting of two non-interacting halves, each coupled to one of the target qubits, was identified as a practically helpful geometry, that allows implementing the coherent magnification process with experimentally available control tools; namely local interaction between each target qubit and the MSS, naturally occurring dipolar coupling among the spins in each half of the MSS and collective rotations on the MSS. It was demonstrated that the requirements on the pre-measurement state of the target qubits and the MSS, entirely fulfill the specifications of micro-macro entanglement between each target qubit and its nearby half of the MSS. It has been shown that direct experimental demonstration of micro-macro entanglement is challenging [98, 99]. Verification of bipartite entanglement between the target qubits provides a means of proving micro-macro entanglement between each target qubit and half of the MSS in the pre-measurement state.

The numerical simulations showed that available internal dipolar interaction and collective control can be used to prepare each half of the MSS in a globally correlated state, such that a one-time interaction between each target qubit and a nearby spin within the MSS suffices to magnify the qubit's state in the collective magnetization of the MSS and create a micro-macro entangled state. The time scale of the magnification process was discussed. In particular, it was demonstrated that, with long-range dipolar coupling in the MSS, the magnification time scales sub-linear with the size of the MSS regardless of the dimension of its structure. Moreover, it was shown that the magnification time is much shorter with a MSS in 2D and 3D lattices compared to a 1D spin chain.

It was shown that a low-resolution collective magnetization measurement on the MSS capable of detecting only $(1-\epsilon)N/4$ spin flips, where N is the number of spins in the MSS and $1-\epsilon$ is the polarization of each spin, suffices to distinguish between the states of the MSS correlated with different magnetizations of the target qubits. The measurement must also probabilistically project the state of the MSS into the subspace associated with zero magnetization of the target qubits, with minimum disturbance.

Different scenarios can be considered for implementing such a measurement. When a linearly-polarized photon passes through a magnetic material, its polarization rotates depending on the magnetic moment of the medium, according to the Faraday rotation effect. The Faraday effect follows the required collective dynamics and has been proposed as a means for implementing a quantum non-demolition measurement on an ensemble of spins [104]. Strong coupling to a superconducting cavity may provide another means for implementing a collective measurement on the MSS that follows the required state-update-rule. Measurement through a cavity in the dispersive regime has been used to entangle two superconducting qubits [59, 61] where an incoming photon is transmitted through or reflected from the cavity depending on the joint state of the qubits. In these experiments, couplings between the superconducting qubits and the cavities are so strong that a single qubit flip results in a detectable shift in the resonance frequency of the cavity. Couplings between spin qubits and superconducting cavities are too weak to enable direct joint measurement of two spin qubits. Correlating different states of the spin qubits with macroscopically distinct states of the MSS can in principle compensate for this weak coupling since the shift in the resonance frequency of the cavity corresponding to different states of the qubits scales proportionally to the size of the MSS. See Fig. 5.22. Faraday rotation and state-dependent shift of a cavity's resonance frequency are examples of two phenomena that potentially enable measurements that are collective and update the MSS's state according to the measurement outcome. Evaluating the details of the measurements based on these phenomena [13] and their resolution need to be further explored.

[13] As an example, coupling of a spin ensemble with a cavity in the dispersive regime introduces indirect

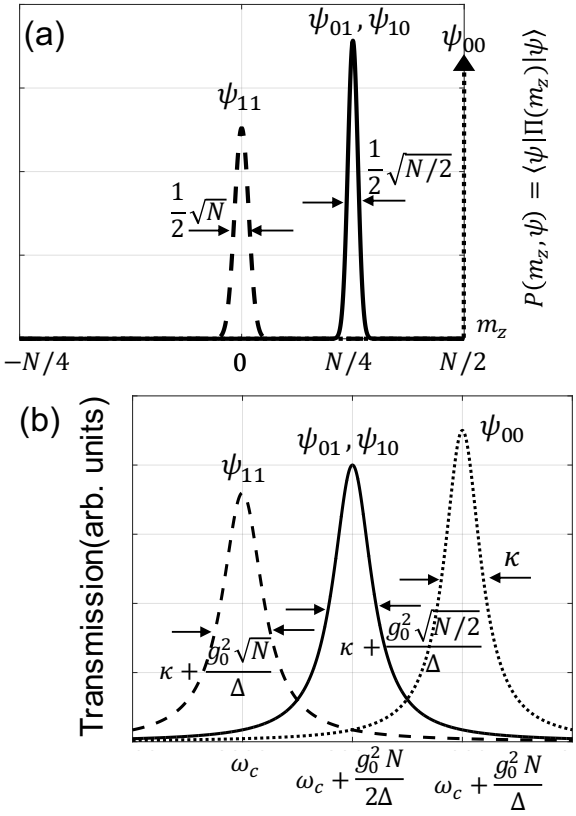

Figure 5.22: (a) The spectra of the MSS's states correlated to different states of the target qubits. (b) The expected transmission probability of a photon through a cavity coupled to the MSS in its dispersive regime. The unloaded resonance frequency of the cavity is ω_c, g_o is the coupling strength between a single spin in the MSS and the cavity, κ is the cavity loss and Δ is the difference between the resonance frequency of the cavity and the spin system. The resolution of the measurement is high enough if the three peaks corresponding to different states of the MSS can be resolved, $\frac{g_0^2 N}{2\Delta} > \kappa + \frac{g_0^2\sqrt{N}}{\Delta}$.

Indirect joint measurement through a MSS was shown to be robust to limited initial polarization of the MSS as long as $N(1-\epsilon)^2 \gg 16$ and the measurement resolution is high enough to detect $(1-\epsilon)N/4$ spin flips. Thermal polarization of an ensemble of electron

interaction between the spins mediated through the cavity. Effect of such interactions on the measurement needs to be explored.

spins is close to one at low temperatures and high magnetic fields (e.g. $T \approx 1$K and $B \approx 7$T). Hyperpolarization of nuclear spins may be achieved through dynamic nuclear magnetization processes that transfer polarization from electron spins to nuclear spins [105, 106].

The process of entangling non-interacting qubits by indirect joint measurement is inevitably sensitive to noise in the MSS. It was shown that single particle loss in the MSS reduces the upper bound on the fidelity of the target qubits' state with the intended maximally entangled state from 1 to 3/4. Thus, creating highly entangled target qubits requires the relaxation time of the MSS to be long compared to the number of spins in the MSS times experiment time, $T_1 \gg N t_{exp}$.

Different factors compete in determining the practical size of the MSS. The number of spins in the MSS needs to be large enough to satisfy the macroscopic distinctness condition, $N_1 \gg 16/(1-\epsilon)^2$, and the distinguishability criteria according to the resolution of the measurement, $N_2 > 4\Delta m/(1-\epsilon)$, where Δm is the minimum number of spin flips the measurement apparatus can detect. The overall lower bound on the size of the MSS is $N_{min} = \max(\min(N_1), \min(N_2))$. Upper bound on the size of the MSS is imposed by the fragility of the micro-macro entangled state between the target qubits and the MSS and as a result the fragility of the bipartite entanglement of the target qubits to noise, $N_{max} \ll T_1/t_{exp}$.

To summarize, among the required resources, the control tools are available, highly polarized initial states of the MSS and long T_1 relaxation times are feasible at low temperatures. The bottleneck is implementing a collective measurement on the many-body state of the MSS that follows the required state-update-rule; namely probabilistic selection of the states of the MSS correlated to zero magnetization of the qubits over the states of the MSS correlated to ± 1 magnetizations of the qubits with minimum disturbance to the selected states.

Chapter 6

Conclusion and Future Works

One of the main challenges in building complex quantum systems is connecting separated qubits. Mesoscopic systems are particularly attractive candidates for this purpose due to their local coupling to the qubits, their extension in space and their collective quantum characteristics. In this thesis, we analyzed creating quantum correlations between separated quantum systems through an intermediate mesoscopic system from a new perspective. We introduced novel techniques for entangling two non-interacting qubits by measuring their joint state through the mesoscopic system. These scenarios were used to quantitatively evaluate the resources needed for using a mesoscopic system to entangle uncoupled qubits.

First, we introduced a simple idealized method that facilitates entangling the qubits by implementing two successive projective measurements on the mesoscopic system, including and excluding two spins in the mesoscopic system that are locally coupled to the target qubits. The success of this procedure relies entirely on the high-resolution collective measurements on the mesoscopic system and it has little requirements on the other resources, e.g. any initial state of the mesoscopic system is acceptable. Nevertheless, this method does not take advantage of the large number of particles in the mesoscopic system.

Next, we proposed a general technique for implementing an indirect joint measurement on the target qubits through the mesoscopic system. In contrast to the previous method, indirect joint measurement benefits from the large number of particles in the mesoscopic system to magnify the state of the qubits, and thus needs only a coarse-grained collective measurement on the mesoscopic system to create post-selected bipartite entanglement between the target qubits. This method was designed to require only local interaction between each target qubit and the mesoscopic system. It is robust to imperfect prepa-

ration of the mesoscopic system. The measurement and post-selection on the mesoscopic system only need to detect a large number of spin flips (on the order of the number of particles in the mesoscopic system), and they must update the mesoscopic spin system's state according to the measurement outcome with minimum disturbance to the selected state.

Lastly, we evaluated the resources needed for implementing the indirect joint measurement procedure using a mesoscopic system consisting of dipolarly coupled spin-1/2 particles. A mesoscopic spin system with two non-interacting halves, each coupled to one of the target qubits was proved to provide a useful geometry that allows implementing the magnification process with the experimentally available control tools; including collective external control of the mesoscopic system, internal dipolar interaction between the spins in each half of the mesoscopic system and local coupling between each target qubit and the mesoscopic system. We showed that the general conditions on the amplified state of target qubits and the mesoscopic system perfectly matches the specifications of micro-macro entanglement between each target qubit and its nearby half of the mesoscopic system, in this geometry. This equivalence brought clarity and accuracy in evaluating the requirements for implementing indirect joint measurement and quantifying the sensitivity of this method to the experimental imperfections. In particular, bipartite entanglement between the target qubits was shown to be robust to imperfect preparation of the mesoscopic system following the robustness of micro-macro entanglement. Moreover, the sensitivity of the target qubits' entanglement to noise was estimated based on the fragility of the micro-macro entangled states and was shown to be consistent with simulation results for small sizes of the mesoscopic system.

This thesis complements the ongoing studies on the collective quantum dynamics of mesoscopic systems and brings new insights into the opportunities that these many-body systems provide for entangling separated quantum systems. We expect our work to motivate future experiments and ultimately lead to developing technologies that can be integrated into quantum processors and quantum measurement devices.

The presented study can be expanded in different directions both towards more comprehensive theoretical analyses and towards future experiments. On the theory side, an immediate extension of the indirect joint measurement technique, that eliminates the challenging step of the measurement and post-selection on the mesoscopic system, is to investigate entangling the target qubits by first, creating micro-macro entanglement between one qubit and the mesoscopic system, then flipping the state of the second qubit conditioned on the state of the mesoscopic system. This approach can be viewed as generating an indirect CNOT gate between the two non-interacting qubits mediated through the mesoscopic system where the first qubit is the control qubit and the second qubit is the target

qubit. Flipping the target qubit conditioned on the state of the mesoscopic system can be conversely seen as measuring the state of the mesoscopic system by the target qubit. The target qubit is coupled locally to the mesoscopic system; thus, this measurement is a local measurement as opposed to the collective measurement on the mesoscopic system in indirect joint measurement scheme. It will be interesting to estimate the resources needed for implementing this protocol as well as its success probability, and compare the results to the indirect joint measurement scheme.

We demonstrated that micro-macro entanglement plays a crucial role in entangling two non-interacting qubits through an intermediate mesoscopic spin system. Here, we briefly discuss opportunities for creation and verification of micro-macro entanglement using the electron spin of a nitrogen-vacancy (NV^-) center in diamond as the qubit and phosphorous nuclear spins doped in a silicon crystal as the mesoscopic system. The goal is not to propose an experiment but to show that experimental opportunities and theoretical questions are close to each other.

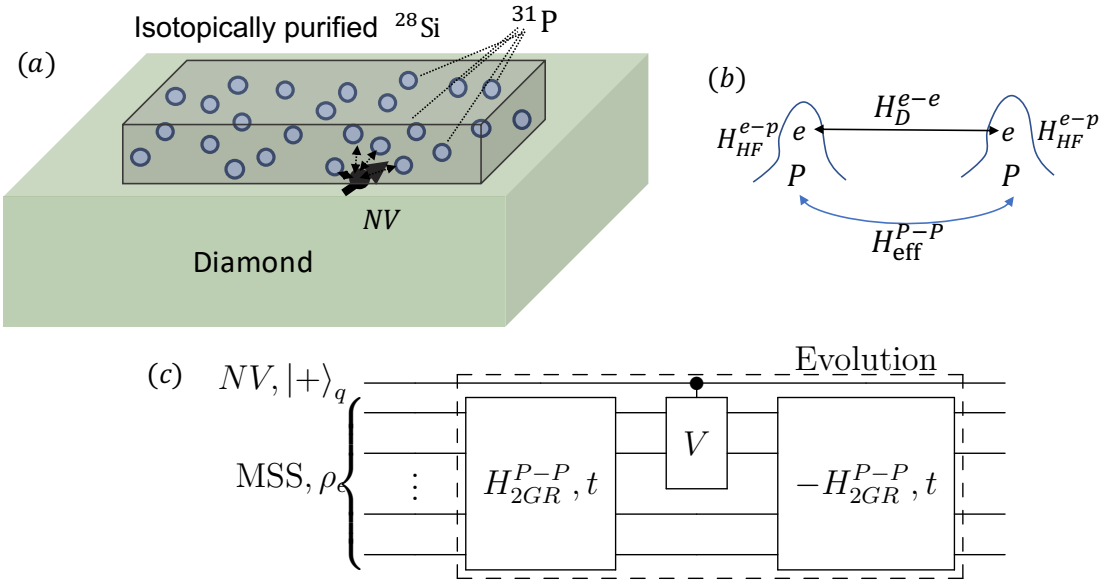

Figure 6.1: (a) A schematic of the spin systems. (b) Effective interaction between the phosphorous spins mediated through their nearby electron spins. (c) A quantum circuit for creating micro-macro entanglement between the NV qubit and the mesoscopic phosphorous spin system based on the method discussed in section 5.4.2.

Figure 6.1(a) shows a schematic of the spin configuration. The electron spin of an

NV^- center close to the diamond surface is considered as the microscopic system. The electronic structure of an NV^- center effectively forms a three level, spin 1 electron. In zero external field, the $|\pm 1\rangle$ levels are degenerate and separated from the $|0\rangle$ level by a zero-field splitting of 2.87 GHz. Introducing an external field along the NV axis removes the degeneracy between the $|\pm 1\rangle$ manifolds, and two levels of this three-level system (e.g. $|0\rangle$ and $|1\rangle$) can be treated as a qubit. The NV qubit can be initialized in the $|0\rangle$ state and measured along the zero-field splitting through optically detected magnetic resonance [107].

An isotropically purified ^{28}Si sample enriched with ^{31}P is attached to the surface of the diamond and the phosphorous nuclear spins form the mesoscopic system. Each phosphorous spin is accompanied by a donor electron. At low temperatures (less than ~ 35K) the wave-function of the electron is localized around the phosphorous and the two spins are coupled via a strong hyperfine coupling (~ 117 MHz). A powerful feature of this hybrid (electron-nuclear spin) system is that it benefits from long coherence times of the nuclear spins while high polarization and strong interactions can be achieved through the electron spins. At low temperatures (~ 100 mK) and high magnetic fields (~ 7 T) the thermal polarization of the electron spins is effectively 100%. Fast hyperpolarization of phosphorous nuclear spins has been demonstrated by transferring this polarization to nuclear spins [105, 106].

A layout of the quantum circuit, based on the *one-time interaction* approach discussed in section 5.4.2, is depicted in figure 6.1(c). Evolution of the mesoscopic phosphorous system under the grade-raising internal Hamiltonian needs to create a globally correlated state among the phosphorous spins, so that the local conditional gate, $|0\rangle\langle 0|_q \otimes \mathbb{1}_N + |1\rangle\langle 1|_q \otimes V_k \otimes \mathbb{1}_{N-k}$, has a global conditional effect. The grade-raising Hamiltonian can be engineered from the dipolar coupling using collective pulses. However, direct dipolar coupling between the phosphorous nuclear spins is negligible even at highest concentrations ($\sim$ mHz at $\sim 10^{16}/\text{cm}^3$). The dipolar coupling between the electron spins is six orders of magnitude stronger ($\sim 1 - 10$kHz at $\sim 10^{16}/\text{cm}^3$) due to their larger gyromagnetic ratio. An effective strong interaction between the nuclear spins of phosphorous can be mediated through the electron spins. This indirect coupling can be engineered using the electron-nuclear hyperfine coupling and coherent control on both electron and nuclear spins [108]. Local interaction between the NV and the nearby phosphorous spins also needs to be mediated through their corresponding electrons. The experiment needs to be done within the relaxation times of both the NV and the mesoscopic system. The coherence time of the phosphorous spins is extremely long at sub-Kelvin temperatures. The coherence time of the NV electron spin can be extended using a nearby nuclear spin as a memory [109, 110].

To verify micro-macro entanglement both entanglement between the qubit and the

mesoscopic system and macroscopic distinctness between magnetization of the states of the mesoscopic system correlated with different states of the qubit need to be confirmed. We discuss a set of measurements to achieve these.

Macroscopic distinctness and correlation in one direction can be verified by measuring both the qubit and the mesoscopic system along the quantization axis. The first step would be to measure the NV by a single shot projective measurement along the quantization axis ($\Pi_0 = |0\rangle\langle 0|, \Pi_1 = |1\rangle\langle 1|$). Such a measurement collapses the state of the mesoscopic system along with the state of the NV. Repetitive measurement scheme through a nearby carbon spin can be used to increase the visibility of the signal in this measurement [111]. Next the mean or the standard deviation of magnetization of the mesoscopic system along the z-axis should be measured using a coarse-grained collective measurement e.g. inductive measurement of the phosphorous spins. Observing different outcomes depending on the outcome of the measurement on the qubit, proves macroscopic distinctness between the states of the mesoscopic system correlated with the $|0\rangle_q$ and $|1\rangle_q$ states of the qubit. It also proves correlation between the qubit and the mesoscopic system along the z-axis. Direct inductive measurement of the phosphorous spins' magnetization needs a large number of spins ($\sim 10^{11-12}$); if measured through the electron spins this number can be reduced by three orders of magnitude ($\sim 10^{8-9}$). A more physically viable approach is to measure the mesoscopic system's magnetization by observing the mean-field seen by the NV. Observing different mean-fields depending on the outcome of projective measurement on the NV confirms correlation between the state of the microscopic and the mesoscopic systems along the quantization axis; however this measurement is a local measurement and can not specify the extend of correlation, thus it is generally not enough to prove macroscopic distinctness.

Proving correlation in one direction is not enough for demonstrating entanglement since it can not discern an entangled state,

$$|\phi\rangle_{q,MSS} = \frac{1}{\sqrt{2}}\left(|0\rangle_q |\psi_0\rangle + |1\rangle_q |\psi_1\rangle\right).$$

from a classically correlated state,

$$\rho_{q,MSS} = \frac{1}{2}(|0\rangle\langle 0|_q \otimes \rho_0 + |1\rangle\langle 1|_q \otimes \rho_1)$$

A spin counting experiments, depicted in figure 6.2, can distinguish between the above entangled and classically correlated states by measuring only the qubit. It can also verify the extend of correlation between the qubit and the mesoscopic system, and thus prove

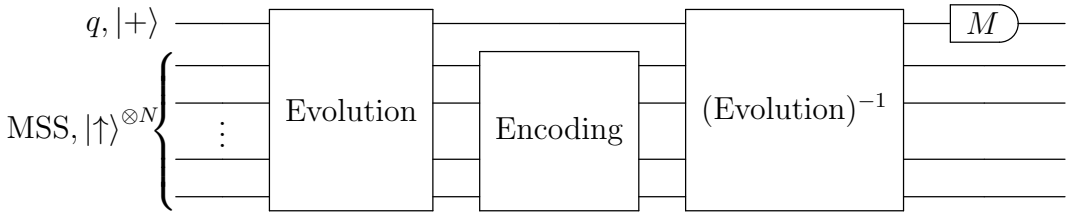

Figure 6.2: A schematic of the spin counting experiment. This circuit measures the coherence and the extend of correlation between the qubit and the mesoscopic system, by measuring only the qubit.

macroscopic distinctness when direct measurement on the mesoscopic system is not available.

The evolution step, shown in figure 6.1(c), ideally prepares the micro-macro entangled state, $|\phi\rangle_{q,MSS} = \frac{1}{\sqrt{2}}\left(|0\rangle_q |\psi_0\rangle + |1\rangle_q |\psi_1\rangle\right)$. The encoding step applies a collective rotation along the quantization axis $e^{i\theta J_z}$ on the mesoscopic system,

$$\begin{aligned} e^{i\theta J_z}|\phi\rangle_{q,MSS} &\approx \frac{1}{\sqrt{2}}\left(|0\rangle_q e^{i\theta\langle J_z\rangle_0}|\psi_0\rangle + |1\rangle_q e^{i\theta\langle J_z\rangle_1}|\psi_1\rangle\right) \\ &= \frac{e^{i\theta\langle J_z\rangle_0}}{\sqrt{2}}\left(|0\rangle_q |\psi_0\rangle + e^{i\theta(\langle J_z\rangle_1 - \langle J_z\rangle_0)}|1\rangle_q |\psi_1\rangle\right) \end{aligned}$$

where $\langle J_z\rangle_i = \mathrm{Tr}(|\psi_i\rangle\langle\psi_i| J_z)$ for $i = 0, 1$. The relative phase in the above superposition state is proportional to the difference in the average magnetization of the states $|\psi_0\rangle$ and $|\psi_1\rangle$. By reversing the evolution, this phase appears on the superposition state of the qubit only and can be detected by measuring the qubit in the transverse plane. Repeating this measurement for different angles and taking the Fourier transform with respect to θ reveals $\langle J_z\rangle_1 - \langle J_z\rangle_0$. If the evolution step prepares a classical mixture instead, $\rho = \frac{1}{2}(|0\rangle\langle 0| \otimes \rho_0 + |1\rangle\langle 1| \otimes \rho_1)$, the encoding step results in,

$$\begin{aligned} e^{i\theta J_z}(\rho_{q,MSS})e^{-i\theta J_z} &\approx \frac{1}{2}(|0\rangle\langle 0|_q \otimes e^{i\theta\langle J_z\rangle_0}\rho_0 e^{-i\theta\langle J_z\rangle_0} + |1\rangle\langle 1|_q \otimes e^{i\theta\langle J_z\rangle_1}\rho_1 e^{-i\theta\langle J_z\rangle_1}) \\ &= \frac{1}{2}(|0\rangle\langle 0|_q \otimes \rho_0 + |1\rangle\langle 1|_q \otimes \rho_1) = \rho_{q,MSS} \end{aligned}$$

Thus, even if the states ρ_0 and ρ_1 have macroscopically distinct magnetization spectra, the result of the spin counting experiment is independent of θ since no coherence between the two states exists.

The demonstration of micro-macro entanglement in solid-state is yet to be realized. But as outlined above, the different components have already been achieved or are in reach

within the current or near future technologies. One main challenge is combining them all together. It remains to explore whether the discussed set of measurements are enough to rigorously prove entanglement between the mesoscopic system and the qubit. If yes, what are the conditions? If no, what other measurements are required?

We investigated procedures for creating micro-macro entanglement in spin systems and provided a list of measures for verifying their validity. Our analysis paves the way towards observing this extended quantum phenomena in solid-state. We also showed that producing micro-macro entangled states between a qubit and a mesoscopic system provides a new tool for information transfer and quantum control which may be used to connect separated quantum systems. Fabrication and control of mesoscopic systems are practically viable since atomic precision is not required. By illustrating their potential application in quantum control, our study opens new avenues towards using mesoscopic spin systems in large scale quantum architectures.

References

[1] T. D. Ladd, F. Jelezko, R. Laflamme, Y. Nakamura, C. Monroe, and J. L. O'Brien, "Quantum computers," *Nature*, vol. 464, p. 45, Mar 2010. Review Article.

[2] F. Jelezko, T. Gaebel, I. Popa, A. Gruber, and J. Wrachtrup, "Observation of coherent oscillations in a single electron spin," *Phys. Rev. Lett.*, vol. 92, p. 076401, Feb 2004.

[3] J. Harrison, M. Sellars, and N. Manson, "Measurement of the optically induced spin polarisation of n-v centres in diamond," *Diamond and Related Materials*, vol. 15, no. 4, pp. 586 – 588, 2006. Diamond 2005.

[4] M. V. G. Dutt, L. Childress, L. Jiang, E. Togan, J. Maze, F. Jelezko, A. S. Zibrov, P. R. Hemmer, and M. D. Lukin, "Quantum register based on individual electronic and nuclear spin qubits in diamond," *Science*, vol. 316, no. 5829, pp. 1312–1316, 2007.

[5] C. Wang, C. Kurtsiefer, H. Weinfurter, and B. Burchard, "Single photon emission from SiV centres in diamond produced by ion implantation," *Journal of Physics B: Atomic, Molecular and Optical Physics*, vol. 39, pp. 37–41, dec 2005.

[6] J. L. O'Brien, S. R. Schofield, M. Y. Simmons, R. G. Clark, A. S. Dzurak, N. J. Curson, B. E. Kane, N. S. McAlpine, M. E. Hawley, and G. W. Brown, "Towards the fabrication of phosphorus qubits for a silicon quantum computer," *Phys. Rev. B*, vol. 64, p. 161401, Sep 2001.

[7] M. Arndt, "Mesoscopic quantum phenomena," in *Compendium of Quantum Physics* (D. Greenberger, K. Hentschel, and F. Weinert, eds.), pp. 379–384, Berlin, Heidelberg: Springer Berlin Heidelberg, 2009.

[8] Y. Murayama, *Mesoscopic Systems: Fundamentals and Applications*. Verlag Berlin, Germany: Wiley-VCH, 2001.

[9] Y. Imry, *Introduction to Mesoscopic Physics*. Oxford University Press, second ed., 2002.

[10] Y. Imry, "Mesoscopic physics and the fundamentals of quantum mechanics," *Physica Scripta*, vol. T76, no. 1, p. 171, 1998.

[11] T. Ando, Y. Arakawa, K. Furuya, S. Komiyama, and H. Nakashima, *Mesoscopic Physics and Electronics*. Springer, 1998.

[12] Y. Yamamoto and A. Imamoglu, *Mesoscopic Quantum Optics*. John Wiley and Sons, Inc., 1999.

[13] A. J. Leggett, B. Ruggiero, and P. Silvestrini, *Quantum Computing and Quantum Bits in Mesoscopic Systems*. Springer US, 2004.

[14] Sørensen, Anders S. and van der Wal, Caspar H. and Childress, Lilian I. and Lukin, Mikhail D., "Capacitive Coupling of Atomic Systems to Mesoscopic Conductors," *Phys. Rev. Lett.*, vol. 92, p. 063601, Feb 2004.

[15] L. Trifunovic, O. Dial, M. Trif, J. R. Wootton, R. Abebe, A. Yacoby, and D. Loss, "Long-distance spin-spin coupling via floating gates," *Phys. Rev. X*, vol. 2, p. 011006, Jan 2012.

[16] M. Serina, C. Kloeffel, and D. Loss, "Long-range interaction between charge and spin qubits in quantum dots," *Phys. Rev. B*, vol. 95, p. 245422, Jun 2017.

[17] G. Yang, C.-H. Hsu, P. Stano, J. Klinovaja, and D. Loss, "Long-distance entanglement of spin qubits via quantum hall edge states," *Phys. Rev. B*, vol. 93, p. 075301, Feb 2016.

[18] S. J. Elman, S. D. Bartlett, and A. C. Doherty, "Long-range entanglement for spin qubits via quantum hall edge modes," *Phys. Rev. B*, vol. 96, p. 115407, Sep 2017.

[19] L. Trifunovic, F. L. Pedrocchi, and D. Loss, "Long-distance entanglement of spin qubits via ferromagnet," *Phys. Rev. X*, vol. 3, p. 041023, Dec 2013.

[20] S. Bose, "Quantum communication through an unmodulated spin chain," *Phys. Rev. Lett.*, vol. 91, p. 207901, Nov 2003.

[21] M. Christandl, N. Datta, A. Ekert, and A. J. Landahl, "Perfect state transfer in quantum spin networks," *Phys. Rev. Lett.*, vol. 92, p. 187902, May 2004.

[22] A. Kay, "Perfect state transfer: Beyond nearest-neighbor couplings," *Phys. Rev. A*, vol. 73, p. 032306, Mar 2006.

[23] M. Avellino, A. J. Fisher, and S. Bose, "Quantum communication in spin systems with long-range interactions," *Phys. Rev. A*, vol. 74, p. 012321, Jul 2006.

[24] D. Burgarth, V. Giovannetti, and S. Bose, "Optimal quantum-chain communication by end gates," *Phys. Rev. A*, vol. 75, p. 062327, Jun 2007.

[25] P. Cappellaro, C. Ramanathan, and D. G. Cory, "Simulations of information transport in spin chains," *Phys. Rev. Lett.*, vol. 99, p. 250506, Dec 2007.

[26] C. Di Franco, M. Paternostro, and M. S. Kim, "Perfect state transfer on a spin chain without state initialization," *Phys. Rev. Lett.*, vol. 101, p. 230502, Dec 2008.

[27] C. Ramanathan, P. Cappellaro, L. Viola, and D. G. Cory, "Experimental characterization of coherent magnetization transport in a one-dimensional spin system," *New Journal of Physics*, vol. 13, no. 10, p. 103015, 2011.

[28] P. Cappellaro, L. Viola, and C. Ramanathan, "Coherent-state transfer via highly mixed quantum spin chains," *Phys. Rev. A*, vol. 83, p. 032304, Mar 2011.

[29] A. Ajoy and P. Cappellaro, "Perfect quantum transport in arbitrary spin networks," *Phys. Rev. B*, vol. 87, p. 064303, Feb 2013.

[30] C. H. Bennett, G. Brassard, C. Crépeau, R. Jozsa, A. Peres, and W. K. Wootters, "Teleporting an unknown quantum state via dual classical and einstein-podolsky-rosen channels," *Phys. Rev. Lett.*, vol. 70, pp. 1895–1899, Mar 1993.

[31] D. Bouwmeester, J.-W. Pan, K. Mattle, M. Eibl, H. Weinfurter, and A. Zeilinger, "Experimental quantum teleportation," *Nature*, vol. 390, no. 6660, pp. 575–579, 1997.

[32] C. H. Bennett and D. P. DiVincenzo, "Quantum information and computation," *Nature*, vol. 404, p. 247, Mar 2000.

[33] D. Gottesman and I. L. Chuang, "Demonstrating the viability of universal quantum computation using teleportation and single-qubit operations," *Nature*, vol. 402, no. 6760, pp. 390–393, 1999.

[34] E. Gallopoulos and Y. Saad, "Efficient solution of parabolic equations by krylov approximation methods," *SIAM Journal on Scientific and Statistical Computing*, vol. 13, no. 5, pp. 1236–1264, 1992.

[35] M. S. Mirkamali and D. G. Cory, "Using a mesoscopic system to generate entanglement," October 2017. US Patent 9792558.

[36] M. S. Mirkamali, D. G. Cory, and J. Emerson, "Entanglement of two noninteracting qubits via a mesoscopic system," *Phys. Rev. A*, vol. 98, p. 042327, Oct 2018.

[37] M. A. Nielsen and I. L. Chuang, *Quantum Computation and Quantum Information*. Cambridge University Press, Cambridge, England, 2000.

[38] J. Emerson, "Lecture notes in open quantum systems," March 2017.

[39] R. Horodecki, P. Horodecki, M. Horodecki, and K. Horodecki, "Quantum entanglement," *Rev. Mod. Phys.*, vol. 81, pp. 865–942, Jun 2009.

[40] M. A. Neumark, "On a representation of additive operator set functions," *C. R. (Dokl.) Acad. Sci. URSS*, vol. 41, pp. 359–361, 1943.

[41] J. von Neumann, *Mathematische Grundlagen der Quantenmechanik*. Springer Verlag, Berlin, 1932. [English translation (by R. Beyer): Mathematical Foundations of Quantum Mechanics (Princeton University Press, Princeton 1955)].

[42] P. Horodecki, R.and Horodecki, "Quantum redundancies and local realism," *Physics Letters A*, vol. 194, no. 3, pp. 147 – 152, 1994.

[43] C. H. Bennett, H. J. Bernstein, S. Popescu, and B. Schumacher, "Concentrating partial entanglement by local operations," *Phys. Rev. A*, vol. 53, pp. 2046–2052, Apr 1996.

[44] C. H. Bennett, G. Brassard, S. Popescu, B. Schumacher, J. A. Smolin, and W. K. Wootters, "Purification of noisy entanglement and faithful teleportation via noisy channels," *Phys. Rev. Lett.*, vol. 76, pp. 722–725, Jan 1996.

[45] R. Garisto and L. Hardy, "Entanglement of projection and a new class of quantum erasers," *Phys. Rev. A*, vol. 60, pp. 827–831, Aug 1999.

[46] G. Vidal and R. F. Werner, "Computable measure of entanglement," *Phys. Rev. A*, vol. 65, p. 032314, Feb 2002.

[47] M. B. Plenio and S. Virmani, "An introduction to entanglement measures.." arXiv:quant-ph/0504163v3, 2006.

[48] A. Peres, "Separability criterion for density matrices," *Phys. Rev. Lett.*, vol. 77, pp. 1413–1415, Aug 1996.

[49] M. Horodecki, P. Horodecki, and R. Horodecki, "Separability of mixed states: necessary and sufficient conditions," *Physics Letters A*, vol. 223, no. 1, pp. 1 – 8, 1996.

[50] S. Hill and W. K. Wootters, "Entanglement of a pair of quantum bits," *Phys. Rev. Lett.*, vol. 78, pp. 5022–5025, Jun 1997.

[51] P. Cappellaro, C. Ramanathan, and D. G. Cory, "Dynamics and control of a quasi-one-dimensional spin system," *Phys. Rev. A*, vol. 76, p. 032317, Sep 2007.

[52] G. Giedke, J. M. Taylor, D. D'Alessandro, M. D. Lukin, and A. Imamoğlu, "Quantum measurement of a mesoscopic spin ensemble," *Phys. Rev. A*, vol. 74, p. 032316, Sep 2006.

[53] R. Ruskov and A. N. Korotkov, "Entanglement of solid-state qubits by measurement," *Phys. Rev. B*, vol. 67, p. 241305, Jun 2003.

[54] B. Trauzettel, A. N. Jordan, C. W. J. Beenakker, and M. Büttiker, "Parity meter for charge qubits: An efficient quantum entangler," *Phys. Rev. B*, vol. 73, p. 235331, Jun 2006.

[55] N. S. Williams and A. N. Jordan, "Entanglement genesis under continuous parity measurement," *Phys. Rev. A*, vol. 78, p. 062322, Dec 2008.

[56] Lalumière, Kevin and Gambetta, J. M. and Blais, Alexandre, "Tunable joint measurements in the dispersive regime of cavity QED," *Phys. Rev. A*, vol. 81, p. 040301, Apr 2010.

[57] L. Tornberg and G. Johansson, "High-fidelity feedback-assisted parity measurement in circuit QED," *Phys. Rev. A*, vol. 82, p. 012329, Jul 2010.

[58] G. Haack, H. Förster, and M. Büttiker, "Parity detection and entanglement with a Mach-Zehnder interferometer," *Phys. Rev. B*, vol. 82, p. 155303, Oct 2010.

[59] D. Riste, M. Dukalski, C. A. Watson, G. de Lange, M. J. Tiggelman, Y. M. Blanter, K. W. Lehnert, R. N. Schouten, and L. DiCarlo, "Deterministic entanglement of superconducting qubits by parity measurement and feedback," *Nature*, vol. 502, pp. 350–354, Oct 2013.

[60] O.-P. Saira, J. P. Groen, J. Cramer, M. Meretska, G. de Lange, and L. DiCarlo, "Entanglement Genesis by Ancilla-Based Parity Measurement in 2D Circuit QED," *Phys. Rev. Lett.*, vol. 112, p. 070502, Feb 2014.

[61] N. Roch, M. E. Schwartz, F. Motzoi, C. Macklin, R. Vijay, A. W. Eddins, A. N. Korotkov, K. B. Whaley, M. Sarovar, and I. Siddiqi, "Observation of measurement-induced entanglement and quantum trajectories of remote superconducting qubits," *Phys. Rev. Lett.*, vol. 112, p. 170501, Apr 2014.

[62] A. Chantasri, M. E. Kimchi-Schwartz, N. Roch, I. Siddiqi, and A. N. Jordan, "Quantum trajectories and their statistics for remotely entangled quantum bits," *Phys. Rev. X*, vol. 6, p. 041052, Dec 2016.

[63] W. Pfaff, T. H. Taminiau, L. Robledo, H. Bernien, M. Markham, D. J. Twitchen, and R. Hanson, "Demonstration of entanglement-by-measurement of solid-state qubits," *Nat Phys*, vol. 9, pp. 29–33, Jan 2013.

[64] P. Cappellaro, J. Emerson, N. Boulant, C. Ramanathan, S. Lloyd, and D. G. Cory, "Entanglement assisted metrology," *Phys. Rev. Lett.*, vol. 94, p. 020502, Jan 2005.

[65] J. Appel, P. J. Windpassinger, D. Oblak, U. B. Hoff, N. Kjærgaard, and E. S. Polzik, "Mesoscopic atomic entanglement for precision measurements beyond the standard quantum limit," *Proceedings of the National Academy of Sciences*, vol. 106, no. 27, pp. 10960–10965, 2009.

[66] M. D. Lukin, M. Fleischhauer, R. Cote, L. M. Duan, D. Jaksch, J. I. Cirac, and P. Zoller, "Dipole blockade and quantum information processing in mesoscopic atomic ensembles," *Phys. Rev. Lett.*, vol. 87, p. 037901, Jun 2001.

[67] J. M. Taylor, A. Imamoglu, and M. D. Lukin, "Controlling a Mesoscopic Spin Environment by Quantum Bit Manipulation," *Phys. Rev. Lett.*, vol. 91, p. 246802, Dec 2003.

[68] J. M. Taylor, C. M. Marcus, and M. D. Lukin, "Long-Lived Memory for Mesoscopic Quantum Bits," *Phys. Rev. Lett.*, vol. 90, p. 206803, May 2003.

[69] J. F. Clauser, M. A. Horne, A. Shimony, and R. A. Holt, "Proposed experiment to test local hidden-variable theories," *Phys. Rev. Lett.*, vol. 23, pp. 880–884, Oct 1969.

[70] M. Benito, M. J. A. Schuetz, J. I. Cirac, G. Platero, and G. Giedke, "Dissipative long-range entanglement generation between electronic spins," *Phys. Rev. B*, vol. 94, p. 115404, Sep 2016.

[71] P. Szumniak, J. Pawłowski, S. Bednarek, and D. Loss, "Long-distance entanglement of soliton spin qubits in gated nanowires," *Phys. Rev. B*, vol. 92, p. 035403, Jul 2015.

[72] M. Friesen, A. Biswas, X. Hu, and D. Lidar, "Efficient multiqubit entanglement via a spin bus," *Phys. Rev. Lett.*, vol. 98, p. 230503, Jun 2007.

[73] U. L. Andersen and J. S. Neergaard-Nielsen, "Heralded generation of a micro-macro entangled state," *Phys. Rev. A*, vol. 88, p. 022337, Aug 2013.

[74] A. I. Lvovsky, R. Ghobadi, A. Chandra, A. S. Prasad, and C. Simon, "Observation of micromacro entanglement of light," *Nature Physics*, vol. 9, p. 541, July 2013.

[75] A. J. Leggett, "Testing the limits of quantum mechanics: motivation, state of play, prospects," *Journal of Physics: Condensed Matter*, vol. 14, no. 15, p. R415, 2002.

[76] E. Schrödinger, "Die gegenwärtige situation in der quantenmechanik," *Naturwissenschaften*, vol. 23, pp. 807–812, Nov 1935.

[77] W. H. Zurek, "Decoherence and the transition from quantum to classical – revisited." arXiv:quant-ph/0306072, 2003.

[78] M. Brune, E. Hagley, J. Dreyer, X. Maître, A. Maali, C. Wunderlich, J. M. Raimond, and S. Haroche, "Observing the progressive decoherence of the "meter" in a quantum measurement," *Phys. Rev. Lett.*, vol. 77, pp. 4887–4890, Dec 1996.

[79] S. Haroche, "Entanglement, mesoscopic superpositions and decoherence studies with atoms and photons in a cavity," *Physica Scripta*, vol. 1998, no. T76, p. 159, 1998.

[80] B. Vlastakis, G. Kirchmair, Z. Leghtas, S. E. Nigg, L. Frunzio, S. M. Girvin, M. Mirrahimi, M. H. Devoret, and R. J. Schoelkopf, "Deterministically encoding quantum information using 100-photon schrödinger cat states," *Science*, vol. 342, no. 6158, pp. 607–610, 2013.

[81] N. Bruno, A. Martin, P. Sekatski, N. Sangouard, R. T. Thew, and N. Gisin, "Displacement of entanglement back and forth between the micro and macro domains," *Nature Physics*, vol. 9, p. 545, July 2013.

[82] C. Monroe, D. M. Meekhof, B. E. King, and D. J. Wineland, "A "schrödinger cat" superposition state of an atom," *Science*, vol. 272, no. 5265, pp. 1131–1136, 1996.

[83] K. G. Johnson, J. D. Wong-Campos, B. Neyenhuis, J. Mizrahi, and C. Monroe, "Ultrafast creation of large schrdinger cat states of an atom," *Nature Communications*, vol. 8, p. 697, 2017.

[84] N. Y. Yao, L. Jiang, A. V. Gorshkov, Z.-X. Gong, A. Zhai, L.-M. Duan, and M. D. Lukin, "Robust quantum state transfer in random unpolarized spin chains," *Phys. Rev. Lett.*, vol. 106, p. 040505, Jan 2011.

[85] P. Jordan and E. Wigner, "Über das paulische äquivalenzverbot," *Zeitschrift für Physik*, vol. 47, pp. 631–651, Sep 1928.

[86] M. Żukowski, A. Zeilinger, M. A. Horne, and A. K. Ekert, ""event-ready-detectors" bell experiment via entanglement swapping," *Phys. Rev. Lett.*, vol. 71, pp. 4287–4290, Dec 1993.

[87] R. B. Sidje, "Expokit: A software package for computing matrix exponentials," *ACM Trans. Math. Softw.*, vol. 24, pp. 130–156, Mar. 1998.

[88] W. S. Warren, S. Sinton, D. P. Weitekamp, and A. Pines, "Selective excitation of multiple-quantum coherence in nuclear magnetic resonance," *Phys. Rev. Lett.*, vol. 43, pp. 1791–1794, Dec 1979.

[89] E. H. Lieb and D. W. Robinson, "The finite group velocity of quantum spin systems," *Communications in Mathematical Physics*, vol. 28, pp. 251–257, Sep 1972.

[90] M. B. Hastings and T. Koma, "Spectral gap and exponential decay of correlations," *Communications in Mathematical Physics*, vol. 265, pp. 781–804, Aug 2006.

[91] P. Hauke and L. Tagliacozzo, "Spread of correlations in long-range interacting quantum systems," *Phys. Rev. Lett.*, vol. 111, p. 207202, Nov 2013.

[92] Z.-X. Gong, M. Foss-Feig, S. Michalakis, and A. V. Gorshkov, "Persistence of locality in systems with power-law interactions," *Phys. Rev. Lett.*, vol. 113, p. 030602, Jul 2014.

[93] K. R. A. Hazzard, M. van den Worm, M. Foss-Feig, S. R. Manmana, E. G. Dalla Torre, T. Pfau, M. Kastner, and A. M. Rey, "Quantum correlations and entanglement in far-from-equilibrium spin systems," *Phys. Rev. A*, vol. 90, p. 063622, Dec 2014.

[94] P. Jurcevic, B. P. Lanyon, P. Hauke, C. Hempel, P. Zoller, R. Blatt, and C. F. Roos, "Quasiparticle engineering and entanglement propagation in a quantum many-body system," *Nature*, vol. 511, pp. 202–205, July 2014.

[95] P. Richerme, Z.-X. Gong, A. Lee, C. Senko, J. Smith, M. Foss-Feig, S. Michalakis, A. V. Gorshkov, and C. Monroe, "Non-local propagation of correlations in quantum systems with long-range interactions," *Nature*, vol. 511, pp. 198–201, July 2014.

[96] M. Foss-Feig, Z.-X. Gong, C. W. Clark, and A. V. Gorshkov, "Nearly linear light cones in long-range interacting quantum systems," *Phys. Rev. Lett.*, vol. 114, p. 157201, Apr 2015.

[97] Z. Eldredge, Z.-X. Gong, J. T. Young, A. H. Moosavian, M. Foss-Feig, and A. V. Gorshkov, "Fast quantum state transfer and entanglement renormalization using long-range interactions," *Phys. Rev. Lett.*, vol. 119, p. 170503, Oct 2017.

[98] P. Sekatski, N. Gisin, and N. Sangouard, "How difficult is it to prove the quantumness of macroscropic states?," *Phys. Rev. Lett.*, vol. 113, p. 090403, Aug 2014.

[99] T. Wang, R. Ghobadi, S. Raeisi, and C. Simon, "Precision requirements for observing macroscopic quantum effects," *Phys. Rev. A*, vol. 88, p. 062114, Dec 2013.

[100] F. Fröwis, P. Sekatski, W. Dür, N. Gisin, and N. Sangouard, "Macroscopic quantum states: Measures, fragility, and implementations," *Rev. Mod. Phys.*, vol. 90, p. 025004, May 2018.

[101] W. Dür, C. Simon, and J. I. Cirac, "Effective size of certain macroscopic quantum superpositions," *Phys. Rev. Lett.*, vol. 89, p. 210402, Oct 2002.

[102] H. Kwon, C.-Y. Park, K. C. Tan, and H. Jeong, "Disturbance-based measure of macroscopic coherence," *New Journal of Physics*, vol. 19, no. 4, p. 043024, 2017.

[103] W. K. Wootters, "Entanglement of formation of an arbitrary state of two qubits," *Phys. Rev. Lett.*, vol. 80, pp. 2245–2248, Mar 1998.

[104] Y. Takahashi, K. Honda, N. Tanaka, K. Toyoda, K. Ishikawa, and T. Yabuzaki, "Quantum nondemolition measurement of spin via the paramagnetic faraday rotation," *Phys. Rev. A*, vol. 60, pp. 4974–4979, Dec 1999.

[105] D. R. McCamey, J. van Tol, G. W. Morley, and C. Boehme, "Fast nuclear spin hyperpolarization of phosphorus in silicon," *Phys. Rev. Lett.*, vol. 102, p. 027601, Jan 2009.

[106] P. Gumann, O. Patange, C. Ramanathan, H. Haas, O. Moussa, M. L. W. Thewalt, H. Riemann, N. V. Abrosimov, P. Becker, H.-J. Pohl, K. M. Itoh, and D. G. Cory, "Inductive measurement of optically hyperpolarized phosphorous donor nuclei in an isotopically enriched silicon-28 crystal," *Phys. Rev. Lett.*, vol. 113, p. 267604, Dec 2014.

[107] Patange, Om, "On an instrument for the coherent investigation of nitrogen-vacancy centres in diamond," 2013.

[108] C. P. Slichter, *Principles of magnetic resonance*. Springer, 1962.

[109] G. D. Fuchs, G. Burkard, P. V. Klimov, and D. D. Awschalom, "A quantum memory intrinsic to single nitrogen-vacancy centres in diamond," *Nature Physics*, vol. 7, p. 789, Jun 2011. Article.

[110] P. C. Maurer, G. Kucsko, C. Latta, L. Jiang, N. Y. Yao, S. D. Bennett, F. Pastawski, D. Hunger, N. Chisholm, M. Markham, D. J. Twitchen, J. I. Cirac, and M. D. Lukin, "Room-temperature quantum bit memory exceeding one second," *Science*, vol. 336, no. 6086, pp. 1283–1286, 2012.

[111] L. Jiang, J. S. Hodges, J. R. Maze, P. Maurer, J. M. Taylor, D. G. Cory, P. R. Hemmer, R. L. Walsworth, A. Yacoby, A. S. Zibrov, and M. D. Lukin, "Repetitive readout of a single electronic spin via quantum logic with nuclear spin ancillae," *Science*, vol. 326, no. 5950, pp. 267–272, 2009.